TU
VIENNA

TECHNISCHE
UNIVERSITÄT
WIEN

VIENNA
UNIVERSITY OF
TECHNOLOGY

D I P L O M A R B E I T

Nonstationary Autoregressive Modeling for Epileptic Seizure Propagation Analysis

ausgeführt am
Institut für Wirtschaftsmathematik
der Technischen Universität Wien

unter der Leitung von
o.Univ.Prof. Dr. Manfred Deistler

in Kooperation mit
Austrian Research Centers GmbH – ARC

von

ANDREAS GRAEF
Flemingstraße 6
4600 Wels

Wien, Oktober 2008

Statutory Declaration

I hereby certify that all work presented in this diploma thesis is my own, no other than the sources and aids referred to were used and that all parts which have been adopted either literally or in a general manner from other sources have been indicated accordingly.

Furthermore I permit Austrian Research Centers GmbH - ARC to use any of my work included in this diploma thesis for their purposes.

Vienna, October 2008

Andreas Graef

Abstract

In this diploma thesis I present a novel method for the characterization of coupling effects in instationary multichannel invasive EEG (ECoG). It allows for the visualization of the spatio-temporal evolution of synchronization effects which are characteristic for epileptic seizures. In contrast to numerous existing methods no channel pre-selection is required in order to obtain stable results, which is crucial for clinical application, e.g. in the pre-surgical evaluation in epilepsy monitoring units.

The presented method is based on a linear spatio-temporal regression that is performed for each output signal separately. Hereby, a channel selection algorithm determines an optimal spatial neighborhood before the regression is computed, whereas the constant temporal model order is fixed by simulations. Adaptive estimation is done by means of the recursive least-squares (RLS) algorithm in order to cope with the instationarity of the biosignal, which is statistically analyzed. Besides an analysis of the regression quality of RLS in comparison to ordinary-least squares (OLS) estimation, the properties of the RLS algorithm are examined.

Based on variances a novel measure termed extrinsic-to-intrinsic-power-ratio (EIPR) is introduced, which is physiologically meaningful and valuable. The visualization of the spatio-temporal evolution of this measure allows to track the propagation of the seizure.

The results of the described method are in excellent accordance with descriptions from clinical experts.

Acknowledgment

ii

Summary

In this diploma thesis we present a novel method for epileptic seizure propagation analysis, which allows to track the spatio-temporal evolution of the seizure focus.

We start this work with a medical introduction in chapter 1. After a view on medical generalities in the field of epilepsy we discuss pathophysiological fundamentals and the course of the disease, followed by clinical symptomatology. As we deal with temporal lobe epilepsy, we complete this chapter with a short characterization of this type of seizures.

In chapter 2 we give a short overview on alternative approaches in literature. We present common frequency domain-based dependency measures, which could be used instead of our measure termed EIPR. This chapter is concluded by an outlook on graphical modeling.

In chapter 3 we present the main idea of our novel method: We set up a linear autoregressive model which does not depend on manual channel preselection. Dynamic channel selection is automatically done during the computation by a channel selection algorithm.

Furthermore, using the variances of intrinsic and extrinsic model coefficients, we introduce a novel dependency measure termed extrinsic-to-intrinsic-power-ratio (EIPR). We interpret high values of EIPR, which result from strong extrinsic contributions, as indication for epileptic activity. Plotting the evolution of EIPR in a spatio-temporal map allows us to track the propagation of the epileptic seizure.

In chapter 4 we discuss possible implementations for estimating the coefficients of the autoregressive model. MMSE regression is presented as a first choice, needing a number of mathematical assumptions – notably short-term stationarity – which are not necessarily fulfilled by ECoG recordings.

We therefore refine the approach by introducing recursive least-squares estimation (RLS). This self-adaptive algorithm is capable of dealing with insta-tionarity in the ECoG signal better, allowing us to omit assumptions on signal stationarity.

In chapter 5 we finally discuss results obtained from one patient by means of OLS and RLS regression. In the case of RLS regression, the results show good statistical properties (regression fit, absence of residual autocorrelation). The

good spatial and temporal correlation of EIPR with epileptic activity reveals its characterization as a physiologically meaningful dependency measure.

Penalizing the past of the intrinsic channel by introducing a dead time degrades the statistical properties, but puts more focus on extrinsic channels. Thanks to this restriction, plotting the evolution of EIPR in a spatio-temporal map gives a clear indication of epileptic seizure propagation. Hereby, values of EIPR below a manually set threshold are omitted. The resulting indication of the seizure propagation is in perfect accordance with the findings of clinicians who visually inspected the raw ECoG recordings.

Contents

List of Figures

List of Tables

List of Algorithms

Chapter 1

Introduction

As the reader might rather have a mathematical or technical background, but not necessarily a medical one, this first chapter is intended to acquire the basic knowledge needed: It starts with a short overview of the medical background of epileptic seizures. We will then clarify the aim of epileptic seizure propagation, why clinicians might need it and how we want to help them by setting up a mathematical model. At the end of this chapter we will have a look at alternative approaches which can be found in literature.

If the reader is not familiar with common medical expressions, he is recommended to consult the standard medical dictionary [Wol05][1] whenever necessary.

1.1 Medical background

We are going to start at the very beginning of epileptic seizure analysis by asking: What is seizure disorder? Understanding the pathophysiological fundamentals of epilepsy will then lead us to the classification of epileptic seizures and more specifically to temporal lobe epilepsy, as data used in this work come from patients suffering from this specific form of the disease.

This short overview is compiled from [Her99] and [Bau01], which both provide a more exhaustive source for the interested reader. If needed, additional explanations on the biology of the human brain and the basic biochemical functionality of neurons can be found in [NMW02].

1.1.1 Generalities

Epilepsy is one of the most common serious neurological disorders: Its prevalence of 0.5 to 1% and its cumulative incidence (the probability of contracting epilepsy until the age of 80) of 4% make it nearly as prevalent as, for example, diabetes.

---

[1]A standard German medical dictionary would be [Gru04].

In industrial nations the relative incidence of seizure disorders lies around 24 to 53 per 10,000 inhabitants per year, and in developing countries the number of incidences is even two or three times higher.

Several factors influence the incidence of epilepsy:

Age In industrial nations we observe two maxima: The first peak lies in the first months of life, followed by a strong decline after the first year. Until the age of 10 years we observe a plateau, afterwards another decrease leads to a minimum in adulthood. The second maximum appears after the age of 70.

Sex Men are slightly more affected than women.

Socioeconomical status and race The socioeconomical status is a reciprocal factor: the better the status, the smaller the incidence. Race also seems to play a certain role, as blacks apparently tend to contract epilepsy more often than whites.

1.1.2   Definition of epilepsy and epileptic seizure

Clinicians clearly differentiate between an *epileptic seizure* and the disease termed *epilepsy* itself:

Epileptic seizure is the clinical manifestation of excessive, hyper-synchronous discharges of neurons in the cerebral cortex. The clinical symptomatology depends on the function of the affected neuronal assembly and can comprise disorder of advanced brain functions, limitation of consciousness, abnormal sensory or psychical perceptions, motor disorders or generalized spasms.

Epilepsy is, as a chronic disease, a heterogeneous group of affections with various syndromes and different causes, but one common characteristic: *recurrent, unprovoked seizures.*

Therefore doctors speak of epilepsy when unprovoked seizures appear in repetition. *Not considered* are

- isolated, unprovoked seizures

- acute symptomatic seizures when patients suffer from an acute affection of the central nervous system (infections, traumata, cerebrovascular diseases), as in this case an immediate activator can be identified

- febrile seizures, which are, by definition, acute symptomatic seizures, but form their own subgroup due to their specific characteristics (age, genetic predisposition).

1.1.3 Pathophysiological fundamentals

Epilepsy is not caused by a single mechanism, but by several factors: Necessary conditions for epilepsy are, on the one hand, the genetic disposition, and on the other hand realization factors like infections, infantile damage of the brain or metabolism disorders. However, science has not found any uniform explanation yet, but only explains epileptic seizures as excessive neuronal discharges due to increased excitation or a decrease of inhibitory mechanisms.

At the time of interictal spikes in EEG signals, cell membrane depolarizations with high amplitudes are observed together with a series of high-frequency action potentials. This period of change is usually terminated by hyper-polarization. This electrical phenomenon is termed *paroxysmal depolarization shift* (PDS)[2], and many researchers consider it to be the basic electro-physiological cellular phenomenon for focal interictal discharges. During a seizure, PDS is replaced by a continuing depolarization leading to a change of the ional surrounding environment, which causes transmembrale electric currents. The resulting hyper-synchronization is pathological and disturbs the normal processing of information.

During long-lasting epileptic activities three factors play a major role:

Imbalance between inhibition and excitation contributes to the excessive discharge: The chemical balance of post-synaptical neuro-transmitters is disturbed, and therefore information is not correctly forwarded from one neuron to another.

Pacemaker cells activate themselves in an auto-rhythmic way independently of synaptic control.

Synchronization mechanisms affect large neuronal collectives: Synaptic and non synaptic effects have a positive feedback and therefore lead to a synchronization. Depending on the place of the focal excitation further regions of the cortex are affected. The localization of the primary focus and the extent of the secondary propagation determine the different types of seizures.[3]

It is exactly these synchronization affects which we need for exploiting our mathematical model. By estimating the dependencies between different positions on the cortex we try to predict the propagation of the seizure. An outlook on this approach is given later in this chapter in section 1.3.

Epileptogenesis is summarized in figure 1.1.[4]

---

[2]Discovered 1964 by Matsumoto and Ajmono-Marsan.
[3]For their classification see subsection 1.1.5.
[4]Adapted from [Her99].
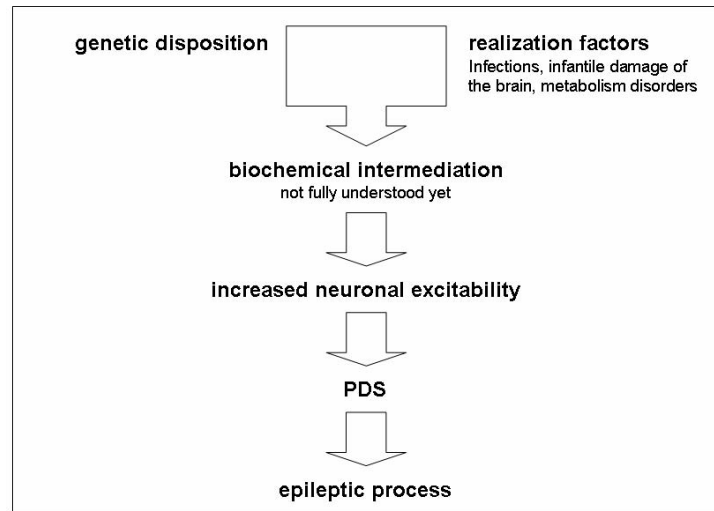
Figure 1.1: ***Epileptogenesis.*** *Epileptic activity is triggered by genetic disposition and realization factors via a biochemical intermediation.*

1.1.4   Course of disease

Before considering the classification of epileptic seizures in the next subsection 1.1.5, we are going to have a quick look at the different courses of epilepsy which can occur:

Complete remission After initial seizures patients have seizure freedom with complete remission, even on a long-term basis without medicamentous therapy.

Partial remission After the initial seizure patients have seizure freedom, but it comes to a relapse, for example in many cases when the medicamentous therapy is abandoned.

No remission Seizures regularly occur with short-term or even missing remissions.

1.1.5   Clinical symptomatology

In 1981, the *Commission on Classification and Terminology of the International League against Epilepsy* proposed a classification of epileptic seizures, which is still in use.

1.1.5.1   Focal (partial) seizures

Focal seizures have their initial focus in only one part of one cerebral hemisphere. They are classified into:

Seizures with simple signs (= full preservation of consciousness) may lead to motoric, sensory (prickling, flashes, humming, ...) or vegetative symptoms (paleness, sweating, ...). Mental symptoms, however, appear more often during complex partial seizures.

Seizures with complex signs (= limitation of consciousness) may have limitation of consciousness from the seizure onset on or only successively.

Secondary generalized seizures start with an initial focus and develop into generalized seizures.

1.1.5.2 Generalized seizures

Generalized seizures initially involve more than a minimal part of both cerebral hemispheres.
They are classified into:

Absences have the common characteristic of limitations of consciousness with the patient suddenly pausing right in his action.

Myoclonic seizures imply sudden, short and involuntary muscle convulsions. These convulsions can either be caused by muscle contractions (positive myoclonus) or by loss of muscle tonus (negative myoclonus).

Clonic seizures start with loss of tonus or tonic spasms which might cause the patient to fall to the ground. This phase is followed by recurrent clonic convulsions.

Tonic seizures imply a sudden, strong increase of muscle tonus (partially or globally). These seizures, lasting from 5 to 20s, may lead to downfall and apnoe (with immediate postictal respiration onset).

Tonic-clonic seizures are the historically called "Grand Mal" seizures (with spasms, downfalls, limitations of consciousness). Possible myoclonic convulsions are followed by a tonic and then a clonic phase. The whole seizure lasts between one and two minutes and is followed by postictal unconsciousness.

Atonic seizures are characterized by a sudden short-term loss of tonus (partially or globally, with the latter leading to downfall).

1.1.5.3 Not-classifiable seizures

Seizures which can not be classified due to missing data or because they do not fit any of the categories above are termed *not-classifiable*.

1.1.6   Temporal lobe epilepsy

This subsection is dedicated to the most common form of focal epilepsy: temporal lobe epilepsy. All data used in this work come from patients suffering from this form of focal epilepsy[5], where we want to track the propagation of the seizure from its initial focus.

Temporal lobe epilepsy occurs, as its name already says, in the temporal lobe, *lobus temporalis*, which is one of the 4 lobes of the cortex:

- Frontal lobe, *lobus frontalis*

- Parietal lobe, *lobus parietalis*

- Occipital lobe, *lobus occipitalis*

- Temporal lobe, *lobus temporalis*

The temporal lobe is located at both sides of the brain and contains the primary auditory cortex, Wernicke's area (responsible for speech comprehension) and structures important for the memory function of the brain (declarative memory, working memory). Figure 1.2[6] shows its position in the human brain in green.
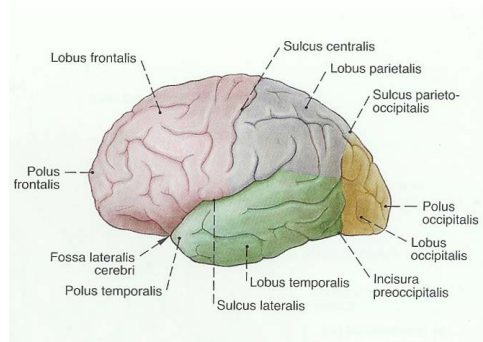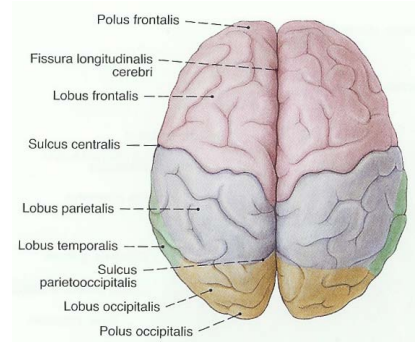
Figure 1.2 (a)   Figure 1.2 (b)

Figure 1.2:   *Temporal lobe.* *Lateral view on the temporal lobe (in green) in figure 1.2 (a) and medial view in figure 1.2 (b).*

Note that focal epilepsy can occur in all four lobes, but due to the reasons mentioned above we only describe temporal lobe epilepsy here.

90% of all patients suffering from temporal lobe epilepsy report aurae at the beginning of the seizure. They are typically epigastric (reported as an "ascending feeling" from the stomach region) or affective (angst), in rare cases mental (déjà-vu, jamais-vu, hallucinations). These aurae remain either isolated, or the seizure develops into a focal complex one.

---

[5]In some of our cases, seizures develop into the secondary generalized form.
[6]Source: [PP04].

In case of a focal complex temporal epileptic seizure, which normally lasts between one and two minutes, the typical sequence of symptoms is as follows:

1. Aurae, typically epigastric or affective

2. Limitation of consciousness without major motor disorders ("motion-less-stare")
   Patients pause right in their action, stare motionlessly into space with their eyes wide open and do not react on address.

3. Oro-alimentary automatisms: chewing, smacking, swallowing or gnashing one's teeth.

4. Repetitive automatisms of the hand: wiping or gesticulating

5. Glances in all directions

6. Movements of the whole body

7. Long-lasting postictal disorientation, confusion and speech disorder

The recommended therapy follows the three-step-schema defining the treatment of focal epilepsy:

1. Medicamentous mono-therapy

2. In case of failure medicamentous combination therapy

3. If seizure control has still not been established by the administration of drugs, the patient is termed *therapy refractory.* In this case, the possibility of an *epilepsy surgical intervention* has to be clarified.

1.2 The aim of epileptic seizure propagation

Before it comes to an epilepsy surgical intervention, the patient undergoes a permanent long-lasting presurgical examination (mostly one week) in which the clinicians try to identify the regions affected by epileptic seizures and determine important areas, i.e the one for speech recognition. As the surgical intervention is not reversible and might have severe consequences, the precedent examination demands the highest precision possible and is therefore conducted in two steps.

Electroencephalography (EEG) is first used to border the possibly affected brain regions. This wide-spread technique delivers plots of the temporal evolution of the electric cortical activity, usually recorded by 19 electrodes placed on the head of the patient.[7] These electrodes are adjusted according to the 20-10-schema, which is shown in figure 1.3 on page 8.[8]
    Clinicians then manually inspect the EEG recordings. By explaining the

---

[7]Up to 128 electrodes can be used for EEG analysis.
[8]Source: [EH02]. In figure 1.3 N denotes the position of the nose, A_1 and A_2 the location of the ears.
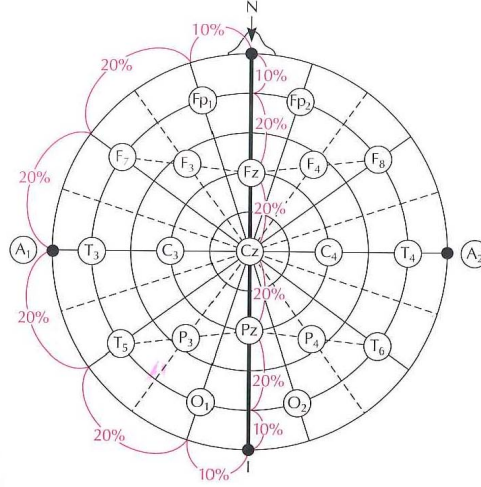
Figure 1.3: *20-10-schema for EEG electrodes placement. Connection lines NI and A_1A_2 are equally divided into 10-20-20-20-20-10%. Semi-circles NA_1I and NA_2I are similarly split into 10-20-20-20-20-10%.*

visible wave forms and spikes they try to deduce a first estimation of the focus and the propagation of the epileptic seizure.[9]

In order to give an example how a typical ictal EEG recording looks like, figure 1.4[10] shows the EEG signals from a patient suffering from temporal lobe epilepsy.

Figure 1.4: ***EEG recordings***. *Ictal data obtained from a patient suffering from temporal lobe epilepsy.*

Electrocorticography (ECoG) is used afterwards, if necessary, to identify the position of the epileptic foci in a more precise way. Electrodes consisting of a metal ribbon are placed directly on regions of the exposed surface

---

[9]The interpretation of EEG signals, which itself is a vast field of science, is described in detail in [EH02] and [THRK08].

[10]Source: [THRK08].

of the brain which had been identified by EEG before. The invasive character of this method has the advantage that the number of artefacts in the obtained signal is reduced and that the local resolution is increased to less than one centimeter. However, as the skullcap has to be opened, ECoG is only applied in special cases like intrasurgical monitoring or examination before epilepsy surgical interventions.

Figure 1.5[11] shows a surgeon's draft of the implemented electrodes and an x-ray control picture. The slightly curved metal ribbons are visible in white just above the eye holes.
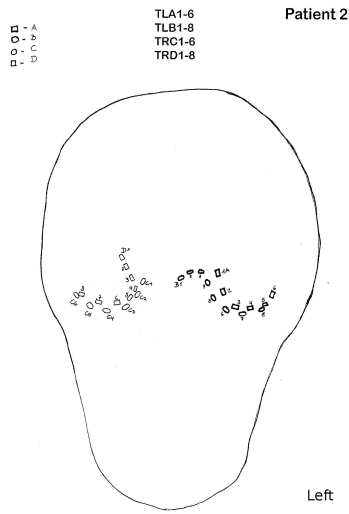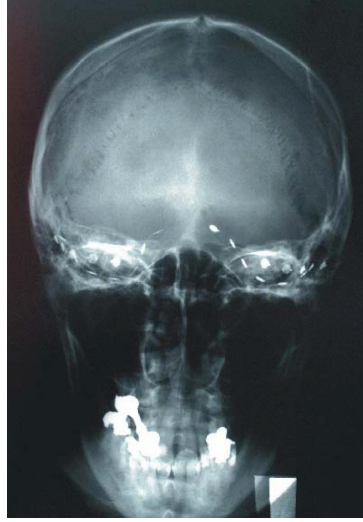
Figure 1.5 (a)   Figure 1.5 (b)

Figure 1.5: *Implemented ECoG electrodes. Electrode positions are marked in figure 1.5 (a), and the X-ray control picture 1.5 (b) reveals the electrode bands in white.*

A two-minute-recording of EcoG signals obtained from this patient (using the electrode configuration shown in this draft) is presented below on page 10 in figure 1.6. This plot shows ECoG signals of 28 channels, recording time Oct. 17th, 2002 12:45:36 - 12:47:36 with epileptic seizure onset 15 seconds after the start. Channel 6 is the reference electrode and therefore constantly near zero.

The goals of epilepsy surgery are twofold. On the one hand the epileptogenic tissue has to be removed in order to abolish the seizures, but on the other hand essential brain regions have to be spared in order to avoid neurological deficits

---

[11]Source of all pictures and ECoG signals in this paragraph: C. Baumgartner: 2nd Neurological Department, General Hospital Hietzing with Neurological Center Rosenhuegel; 1130 Vienna, Austria.

17-Oct-2002 12:45:36 to 17-Oct-2002 12:47:36 - duration: 00 - 00:02:00
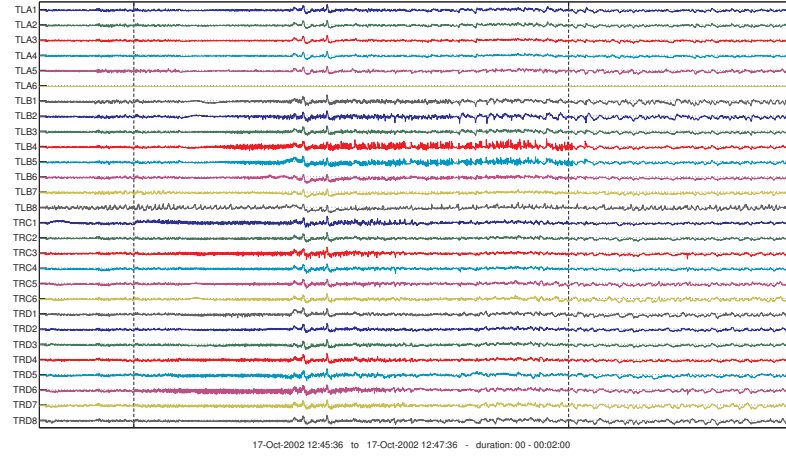
Figure 1.6: ***ECoG recordings during an epileptic seizure.*** *Seizure onset 15 seconds after recording start, begin and and end of seizure indicated by dashed lines.*

caused by the operation.[12] Thus, exact localization of the epileptogenic zone and of essential brain regions is crucial for the successful surgical treatment of seizures which can only be accomplished during a thorough presurgical examination. Especially in patients with seizures arising adjacent to essential brain regions, ECoG recordings with chronically indwelling sub-dural strip and grid electrodes or depth electrodes have to be applied.

However, the interpretation of the ECoG signals demands huge experience in ECoG signal analysis and is subject to the personal opinion of the neurologist. As the interpretation cannot or can only hardly be controlled, its quality only reveals after the surgical intervention.

Furthermore, the epileptogenic zone cannot be localized adequately in about 30-50% of patients. In these cases the patients cannot be offered a surgical therapy and the electrodes have to be removed without resective surgery. The major reasons for this failure are difficulties in the visual interpretation of the ECoG recordings due to rapid seizure spread.

Neurologists might therefore be interested in an automated tool which autonomously inspects the ECoG raw data and supports them by delivering an objective control prediction of the initial focus and the propagation of epileptic seizures.

Achieving this goal shall therefore be the motivation for this work. In the next section 1.3 we are going to give a brief overview of the method representing a first approach in the direction of the realization of the neurosurgical tool described above.

---

[12]Such brain regions are the primary motor and sensory cortex as well as brain areas supporting language and memory functions; compare [Lüd92].

If the reader is interested in a deeper understanding of presurgical diagnostics and surgical intervention, he will find a good introduction to these topics in chapters 16 and 17 of [Bau01] and in chapter 14 of [Her99].

1.3 Outlook on the problem resolution

A widely used approach to EEG/ECoG modeling is the use of autoregressive (AR) models due to their numerical simplicity: Only a linear system has to be solved in order to identify the model coefficients. However, numerical problems risk to arise in this step, as the considered system is highly correlated in time as well as in the cross-sectional dimension (the different channels).

In this work, we only use ECoG and not EEG raw data, because they have – as mentioned in section 1.2 – the advantage of a reduced number of artefacts which would complicate the algorithmic propagation analysis.

When considering ECoG recordings consisting of 28 channels,[13] and estimating them by means of autoregressive methods, we have to deal with the problem of high auto- and cross-correlation, as mentioned before. This makes it impossible to apply classical multivariate autoregressive models, as numerical problems would preponderate when solving the AR model.[14]

Accordingly we could imagine a manual preselection of only few channels, which are known to contribute in an important way. This would reduce the complexity of the system before we could afterwards successfully apply the AR model to this small set of time series. However, in our case, we do not want to allow preselection, as the system should work autonomously in clinics, and the importance of specific channels is not known by the doctors a priori, either. In fact, we have to deal with the exactly opposite situation: We want to assist surgeons in finding out which parts of the brain are involved in the seizure.

Therefore the approach to the analysis of epileptic seizure propagation chosen in this diploma thesis is the following:[15]

1. We define a (univariate) spatio-temporal regression model explaining each output signal by its own (intrinsic) present and past and the past of a set of extrinsic neighborhood channels. This model will be defined in section 3.2.

2. Before the regression is computed for each output signal, a channel selection algorithm determines the optimal spatial neighborhood set for this specific output channel. This algorithm assures the needed complexity reduction (without preselecting channels!) and is explained in section 3.3

---

[13]Up to 128 electrodes could be used for recording ECoG signals.

[14]The mentioned numerical problems are a direct consequence of the bad conditioning of the variance-covariance matrix Σ.

[15]The basic idea of this method is described in [HK07].

3. As we deal with instationary biosignals, we estimate the model coeffi-
   cients in an adaptive way by means of *recursive-least-squares (RLS)*. This
   algorithm is deduced in section 4.2.

4. Based on a linear decomposition of variances of the regression terms we in-
   troduce a novel measure termed *extrinsic-to-intrinsic-power-ratio (EIPR)*
   which is physiologically meaningful and valuable. Plotting its spatio-
   temporal evolution allows to track the seizure propagation in the brain.
   We will have a closer look at this approach and the characteristics of this
   measure in particular in section 3.4.

Chapter 2

Alternative approaches in literature

Before going into technical details and presenting results of our work, we want to have a quick look at alternative approaches in literature to which this short chapter is dedicated.

The main difference between the method described in this work and all others, which have been published by now, is our dropping of an initial channel preselection. This abandonment of any preselection is, as mentioned in section 1.3, realized by the introduction of a dynamic channel selection.[1]

2.1   Measures derived from parametric spectra

In this section we especially want to present one approach which can be found in numerous publications, like for example in [KKB04]: Its main idea is to fit an AR-model to preselected EEG/ECoG channels and then calculate frequency-domain dependencies, which are based on the estimated parametric spectra.

2.1.1   Estimation of parametric spectra

The approach described in this subsection is composed of the following steps:

1. Setting up of a *parametric model:* Using a channel preselection consisting of K channels, the (relevant) EEG/ECoG data can be represented as a vector $\mathbf{x}$ consisting of K signals recorded in time. At each moment n, we therefore have $\mathbf{x}[n] = (x_1[n], x_2[n], ...x_K[n])^T$.
We fit these data $\mathbf{x}[n]$ to a multivariate (K-dimensional) AR(p)-model expressed as

$$\mathbf{x}[n] = \sum_{s=1}^{p} \mathbf{A}_s \mathbf{x}[n-s] + \epsilon[n], \qquad (2.1)$$

---

[1] The channel selection algorithm is described in section 3.3.

where $\epsilon[n]$ represents K-dimensional zero-mean white noise with covariance matrix $\boldsymbol{\Sigma}_\epsilon$.

As a result, this step delivers p matrices $\widehat{\mathbf{A}}_s$, the estimated coefficients of the AR(p)-model.[2]

2. Estimation of *parametric spectra:* By transforming the model equation (2.1) from the time to the frequency domain and denoting the transformed vector-valued variables by capital letters, we get[3]

$$\mathbf{X}(f) = \sum_{s=1}^{p} \mathbf{A}_s \mathbf{X}(f) e^{-2i\pi f s} + \mathbf{E}(f)$$

$$\mathbf{X}(f)\left(1 - \sum_{s=1}^{p} \mathbf{A}_s e^{-2i\pi f s}\right) = \mathbf{E}(f).$$

Denoting the contents of the brackets by $\mathbf{A}(f)$, the equation reads[4]

$$\begin{aligned}
\mathbf{X}(f)\mathbf{A}(f) &= \mathbf{E}(f) \\
\mathbf{X}(f) &= \mathbf{A}(f)^{-1}\mathbf{E}(f) \\
\mathbf{X}(f) &= \mathbf{H}(f)\mathbf{E}(f).
\end{aligned} \qquad (2.2)$$

The matrix $\mathbf{H}(f)$ is termed the *transfer matrix* of the system. We can now easily calculate *power spectra* $\mathbf{S}(f)$ by evaluating

$$\mathbf{S}(f) = \mathbf{H}(f)\boldsymbol{\Sigma}_\mathbf{E}\mathbf{H}^H(f), \qquad (2.3)$$

where ^{H} denotes the conjugated transpose, and $\boldsymbol{\Sigma}_\mathbf{E}$ is the covariance matrix of the white noise $\mathbf{E}(f)$.

By inserting the estimated matrices $\widehat{\mathbf{A}}_s$ into (2.2), we obtain the desired estimated power spectra $\widehat{\mathbf{S}}(f)$.

3. Definition of *measures in the frequency domain:* In the last step, measures are derived from the estimated spectra.

We are going to have a closer look at the various possibilities of defining such characteristic numbers in the next subsection.

2.1.2 Measures in the frequency domain

Now we want to have a closer look at measures in the frequency domain, which can often be found in literature.

When examining a system on dependencies in the frequency domain, it would be obvious to have, first of all, a look at its coherence.

---

[2] Not to forget, the multivariate AR(p)-model has matricial coefficients: $\widehat{\mathbf{A}}_s \in \mathbb{R}^{K \times K}$.

[3] i is the imaginary unit.

[4] $A(f)$ is invertible.

Ordinary coherence is the analogon of correlation in the frequency domain and shows the coupling of two signals at a certain frequency. It is defined as

$$k_{ij}^2 = \frac{S_{ij}^2(f)}{S_{ii}(f)S_{jj}(f)} \qquad (2.4)$$

and is examined, for example, in [MSAW01].

Its huge disadvantage of being unable to distinguish between direct and indirect influence leads to the following improved definition:

Partial coherence, being the equivalent of partial correlation in the frequency domain, is a measure of the joint variance of two signals at a certain variance after the influence of all other signals has been removed. Its is defined as

$$\chi_{ij}^2(f) = \frac{M_{ij}^2(f)}{M_{ii}(f)M_{jj}(f)} , \qquad (2.5)$$

where M_{ij} is the minor of **S**, obtained by removing row i and column i from **S**.

However, as the explanatory power of coherence by itself is not satisfying enough, different publications now follow different approaches by defining various improved dependency measures in the frequency domain. As coherence, they all make use of the transfer matrix $\mathbf{H}(f)$ from (2.2) or its inverse $\mathbf{A}(f)$ and/or the power spectra $\mathbf{S}(f)$ from (2.3).

Directed transfer function (DTF) is proposed in [KB91] and [KDTB01] as a meaningful measure. It describes the ration between the *inflow* from channel j to channel i in respect to all inflows to channels i:

$$\gamma_{ij}^2(f) = \frac{|H_{ij}(f)|^2}{\sum_{m=1}^{k} |H_{im}(f)|^2} . \qquad (2.6)$$

The normalization condition

$$\sum_{n=1}^{k} \gamma_{in}^2(f) = 1$$

holds and implies $\gamma_{ij} \in [0,1]$. Values near 1 mean that most of the signal i comes from the channel j; values near 0 indicate that there is in fact no inflow from channel j.

Direct directed transfer function (dDTF) is introduced in [KMK$^+$03]. As an improvement of the directed transfer function it distinguishes between direct and indirect inflows.

It is defined as

$$\delta_{ij}(f) = \chi_{ij}(f)\eta_{ij}(f), \qquad (2.7)$$

where χ_{ij} is the partial coherence (2.5) and η_{ij} is the *full frequency directed*

transfer function (ffDTF)[5]

$$\eta_{ij}^2(f) = \frac{|H_{ij}(f)|^2}{\sum_f \sum_{m=1}^k |H_{im}(f)|^2} \cdot$$

The direct directed transfer function dDTF describes only direct relations: Values near 0 mean that there is either no flow from channel j to channel i or that intermediate channels are involved; values near 1 indicate that (only) the given channels i and j are related.

Directed coherence (DC) is presented in [BS01]. Is measures whether and how two structures are functionally connected. Unlike the ordinary coherence (2.4), DC examines the relative structural relationship by decomposing it into into feedforward and feedback aspects.
Its definition is

$$\overline{\gamma}_{ij}^2(f) = \frac{H_{ij}(f)^2}{S_{ii}(f)} \tag{2.8}$$

and therefore coincides with DTF (2.6), if $\mathbf{\Sigma} = \mathbf{I}_{K \times K}$.

Partial directed coherence (PDC) is as well proposed in [BS01] for describing direct causal relations between signals. It is defined as

$$\pi_{ij}^2(f) = \frac{A_{ij}^2(f)}{\sum_{m=1}^k A_{mj}^2(f)} \cdot \tag{2.9}$$

As the normalization in the denominator is inverse to the one of DTF (2.6), the appropriate normalization condition here yields

$$\sum_{n=1}^k \pi_{nj}^2(f) = 1$$

and implies $\pi_{ij} \in [0,1]$. Because of this normalization, π_{ij} measures the ratio between the outflow from channel j to channel i in respect to all *outflows* from source j − unlike DTF (2.6) describing the *inflows* to the destination i.
Similar to dDTF (2.7), large values of PDC indicate that there is a direct transmission from channel j to channel i; values close to 0 describe a lack of this relation.

2.1.3   Link to our approach

We want to state that our approach described in chapters 3 and 4 is fully compatible with the use of the frequency-domain measures defined above in subsection 2.1.2: In fact we *do* identify an AR-system as well - this is discussed in section 3.5.

---

[5]As the denominator of η_{ij} is independent of the frequency f, the spectral properties of ffDTF only depend on the outflow from channel j.

Instead of defining EIPR in the time-domain in section 3.4, we could calculate parametric spectra and derive the associated measures in the frequency domain (which we defined above in subsection 2.1.2).

2.1.4 Granger causality

Granger causality was introduced in 1969 by Granger.[6] It is a statistical concept of causality based on prediction: An observed time series $x_j[n]$ *"Granger-causes"* another series $x_i[n]$, if knowledge of $x_j[n]$'s past significantly improves prediction of $x_i[n]$.

In the basic case of a bivariate autoregressive model, *spectral Granger causality* is simply the non-normalized version of DTF:

$$I_{ij}^2(f) = |H_{ij}(f)|^2 = \frac{|A_{ij}(f)|^2}{|\mathbf{A}(f)|^2}.$$

[KDTB01] even shows an equivalence between spectral Granger causality and the non-normalized version of DTF in the multivariate case:[7]

$$I_{ij}^2(f) = \frac{|M_{ij}(f)|^2}{|\mathbf{A}(f)|^2}. \tag{2.10}$$

DTF (2.6) can therefore be interpreted in terms of Granger causality.

Furthermore, as stated in [BS01], PDC (2.9) provides a frequency-domain picture for Granger causality descriptions and can therefore be interpreted in the context of Granger causalities as well.

2.2 Graphical modeling

Finally, we also want to mention *graphical modeling*, which is a methodology to find dependencies between multivariate structures (e.g. by using the coupling indications described in subsection 2.1.2) and to visualize them in a graph: As [Dah00] explains, channels are represented by vertices and dependencies different from zero by edges. Therefore, this approach delivers an intuitive representation of coupling effects in multivariate time series. When using dependency measures, which only take direct couplings into consideration (but suppress indirect ones), one obviously obtains a graph which only shows direct relations.[8]

[Dah00], [DE03] and [Eic06] explain the theoretical background of graphical modeling and point out the intuitive graphical representation mentioned above.

---

[6]See [Gra69] for the original article.

[7]Consider $(i,j) = (2,1)$ without loss of generality. Based on the definition of matrix inversion, we then have

$$\text{non-normalized DTF} = |H_{21}(f)|^2 = \left|\left[\mathbf{A}^{-1}(f)\right]_{21}\right|^2 = \frac{|M_{12}(f)|^2}{|\mathbf{A}(f)|^2}.$$

[8]Compare [SWH+06] for a discussion on this distinction.

Although graphical interaction models have definitely become an important tool for analyzing multivariate data, we are not going to address the theoretical aspects of this approach in this diploma thesis, but refer the interested reader to the publications cited above.

Note however, for reasons of completeness, that we do use a graph by representing the novel EIPR dependencies in the spatio-temporal map in figure 5.24 – but without explicitly calling our visualization a graph. We do not use any theoretical results of graphical modeling, either.

Chapter 3

Method

Now that the readers has acquired the necessary medical background knowledge and got an idea of alternative approaches to seizure analysis, we are going to introduce our approach in this chapter.

In order to explain the basic method used for analyzing the propagation of epileptic seizures, we are first going to define our mathematical model, then present the channel selection algorithm and finally introduce the novel measure for coupling effects in multivariate time series termed *extrinsic-to-intrinsic-power ratio (EIPR)*.[1]

In this chapter we are going to hypothesize some properties of the time series considered in order to set up a purely mathematical model. It is obvious that these hypotheses will not be admissible when applying our method to ECoG data. However, we are not going to address this aspect here, but concentrate on the elaboration of the mathematical method. In return, we are going to discuss the arising problems and proposed solutions in chapter 4.

3.1   Terminology

Before coming to the technical part of this work, we first want to clarify some terminological questions. Although we have already used several terms intuitively in sections 1.3 and 2.1, we want to define them properly here, as this is needed in the oncoming mathematical context.

In the following analysis we are going to consider discrete real-valued time series of length T consisting of K components: $\mathbf{x}_t \in R^{T \times K}$ with $t = 1..T$. However, as this work is established in the context of neurological signal treatment, we are not always going to use the common mathematical terms. We adapt our notation to the standards in the field of neuroinformatics and signal processing:

---

[1] This chapter details the basic method which was initially elaborated by the business unit neuroinformatics at Austrian Research Centers GmbH and is described in the business area report [HK07].

3.1.1   Naming

We therefore agree on the following terminology:

Signal We call any discrete real-valued time series a *signal*.

Sample We call each value of the given signal at a certain time, $\mathbf{x}[n = n_0]$, a
sample. The index of the time axis is termed *sample index n*.
The resulting frequency is the *sampling frequency*:

$$f_s = \frac{\text{length of signal [in seconds]}}{\text{number of samples}} .$$

Channel We call each component of the signal a *channel*. The corresponding
index is termed *channel index k*.

3.1.2   Conventions

Furthermore, we make use of the following conventions:

Sample indices When describing a channel of the (time-discrete) signal $\mathbf{x} \in$
$\mathbb{R}^{T \times K}$ consisting of T samples and K channels, we write it in the form
$x_k[n]$, where k is the channel index and n the sample index.[2]
We sometimes simply call such a channel itself *signal* and specify the
channel index (in order to avoid confusions): x_k.

Stochastic symbols As usual, the mean is denoted by $\mathbb{E}$, variance by $\mathbb{V}$, the
variance-covariance-matrix by $\mathbf{\Sigma}$ and estimators by $\hat{\ }$.

3.1.3   Second-order-statistics

For the definition of second-order-statistics used in this work we limit ourselves
to the case of real-valued zero-mean stationary signals (which we are going to
deal with):

Cross-covariance function For any channel indices k, l and given lag $s \in \mathbb{Z}$,
the cross-covariance function of a signal $\mathbf{x} \in \mathbb{R}^{T \times K}$ is defined as

$$r_{x_k x_l}[s] \triangleq \mathbb{E}\left\{x_k[n + s]x_l[n]\right\} \in \mathbb{R}. \tag{3.1}$$

Autocovariance function is a particular case of the cross-covariance function
for $k = l$

$$r_{x_k}[s] \triangleq r_{x_k x_k}[s] = \mathbb{E}\left\{x_k[n + s]x_k[n]\right\} \in \mathbb{R}. \tag{3.2}$$

---

[2]Readers with a mathematical background would rather write, using common mathematical notation, x_n^k or even x_t^k.

Covariance function of a signal $\mathbf{x} \in \mathbb{R}^{T \times K}$ is a matrix function with K auto-covariances (3.2) on its main diagonal and the respective cross-covariances (3.1) on the other positions:

$$\mathbf{R_{xx}}[s] \triangleq \begin{pmatrix} r_{x_1 x_1}[s] & r_{x_1 x_2}[s] & \cdots & r_{x_1 x_K}[s] \\ r_{x_2 x_1}[s] & r_{x_2 x_2}[s] & & r_{x_2 x_K}[s] \\ \vdots & & \ddots & \vdots \\ r_{x_K x_1}[s] & r_{x_k x_2}[s] & \cdots & r_{x_K x_K}[s] \end{pmatrix} \in \mathbb{R}^{K \times K}. \qquad (3.3)$$

In case of a mono-channel signal, the covariance function is reduced to the one-dimensional autocovariance function.

Note that in our real-valued case the covariance function is symmetric and satisfies

$$\mathbf{R_{xx}}[-s] = \mathbf{R_{xx}}[+s]^T.$$

Covariance matrix of a multi-channel signal $\mathbf{x} \in \mathbb{R}^{T \times K}$ finally is the exhaustive representation of all linear dependencies. In our definition it contains all covariances of all lags $\{0...p-1\}$.[3]

It is a block-Toeplitz matrix with each block consisting of the covariance function (3.3) of the respective lag:

$$\mathbf{R}_{\mathbf{x},p} \triangleq \begin{pmatrix} \mathbf{R_{xx}}[0] & \mathbf{R_{xx}}[-1] & \cdots & \mathbf{R_{xx}}[-p+1] \\ \mathbf{R_{xx}}[1] & \mathbf{R_{xx}}[0] & & \mathbf{R_{xx}}[-p+2] \\ \vdots & & \ddots & \vdots \\ \mathbf{R_{xx}}[p-1] & \mathbf{R_{xx}}[p-2] & \cdots & \mathbf{R_{xx}}[0] \end{pmatrix} \in \mathbb{R}^{Kp \times Kp}.$$

$$(3.4)$$

In case of a mono-channel signal, all blocks are replaced by scalars, and the covariance matrix takes the simpler form

$$\mathbf{R}_{x,p} = \begin{pmatrix} r_x[0] & r_x[1] & \cdots & r_x[p-1] \\ r_x[1] & r_x[0] & & r_x[p-2] \\ \vdots & & \ddots & \vdots \\ r_x[p-1] & r_x[p-2] & \cdots & r_x[0] \end{pmatrix} \in \mathbb{R}^{p \times p}. \qquad (3.5)$$

Covariance vector In the univariate case, we also define the *covariance vector*, which is − unlike the univariate covariance matrix − the exhaustive representation of all linear dependencies of all lags $\{1...p\}$.

We denote it by

$$\mathbf{r}_{x,p} \triangleq \begin{pmatrix} r_x[1] \\ r_x[2] \\ \vdots \\ r_x[p] \end{pmatrix} \in \mathbb{R}^{p \times 1}. \qquad (3.6)$$

---

[3]Note that the covariance matrix can also be defined to contain all lags $\{0,...,p\}$ having the dimension $\mathbb{R}^{K(p+1) \times K(p+1)}$. However, for the identification of AR-systems, we only need covariances up to lag $p-1$.

Its multivariate generalization is

$$\mathbf{r}_{\mathbf{x},p} \triangleq \begin{pmatrix} \mathbf{R}_{\mathbf{xx}}[1] \\ \mathbf{R}_{\mathbf{xx}}[2] \\ \vdots \\ \mathbf{R}_{\mathbf{xx}}[p] \end{pmatrix} \in \mathbb{R}^{Kp \times K}. \tag{3.7}$$

Note that the formulae above define theoretical moments. When we use second-order-statistics estimated from data, we denote them by ˆ in order to underline the fact that we talk about empirical moments. In this case, the stochastic mean in all definitions above is replaced by the empiric one, as subsection 4.1.5 details.

3.2   Regression model

Given the conventions from 3.1, we demand the following signal properties of $\mathbf{x}[n]$ for our analysis:

Hypothesis 1: The signal $\mathbf{x}[n]$ is zero-mean: $\mathbb{E}\mathbf{x}[n] = \mathbf{0}$.

Hypothesis 2: The signal $\mathbf{x}[n]$ is stationary, it especially fulfills time-invariance of the covariance matrix $\mathbf{R}_{\mathbf{x},p}$.

3.2.1   Model definition

Taking these two hypotheses into consideration, we set up an autoregressive model for estimating model coefficients which we are going to use later for defining the EIPR in section 3.4.[4]

For each channel of the signal $x_k[n]$ we define a regressand by

$$\widehat{x}_k[n] \triangleq \dot{x}_k[n] + \vec{x}_k[n] \tag{3.8}$$

having a multivariate autoregressive model in mind:

$$\mathbf{x}[n] = \sum_{s>1} \mathbf{A}_s \mathbf{x}[n-s] + \epsilon[n], \tag{3.9}$$

where $\epsilon[n]$ is zero-mean white noise with covariance matrix $\mathbf{\Sigma}_\epsilon$.

We therefore explain a signal in (3.8) as the sum of an *intrinsic regression term* $\dot{x}_k[n]$ and an *extrinsic regression term* $\vec{x}_k[n]$:[5]

---

[4]The goal is *not* to estimate the original output signal, although we could easily do this. We reconstruct the original output signal in chapter 5 for control purposes only.

[5]Due to hypothesis 1 we do not include a scalar off set in (3.8).

- The intrinsic regression term describes its own past contribution of the channel x_k and is defined as

$$\dot{x}_k[n] \triangleq \sum_{s \in \mathbb{S}} a_{s;k,k} x_k[n-s], \qquad (3.10)$$

where $\mathbb{S}$ is a given *intrinsic lag index set* and $a_{s;k,k}$ the *intrinsic model coefficient* of channel k at lag s.

- The extrinsic regression term models past and present contributions of extrinsic channels and is defined as the sum of *partial extrinsic regression terms*:

$$\vec{x}_k[n] \triangleq \sum_{l \in \mathbb{L}_k} \vec{x}_{k,l}[n], \qquad (3.11)$$

where the channels contributing to $\vec{x}_k[n]$ are chosen according to an extrinsic channel set $\mathbb{L}_k$. This set is separately defined for the regression of each x_k[6] and built up by the channel selection algorithm in section 3.3.

The partial extrinsic regression terms in (3.11) are defined as

$$\vec{x}_{k,l}[n] \triangleq \sum_{q \in \mathbb{Q}} a_{q;k,l} x_l[n-q], \qquad (3.12)$$

where $\mathbb{Q}$ is a given *extrinsic lag index set* and $a_{q;k,l}$ the *extrinsic model coefficient* of the intrinsic channel k and the extrinsic channel l at lag q.

3.2.2 Remarks on the model

1. Although this general definition of the model would allow positive and negative lags and therefore a non-causal regression from both past and future (what [HK07] initially proposes), we limit it to the causal case corresponding to (3.9)[7] implying:

    - Channel k is only explained by its *intrinsic past*. We therefore set $\mathbb{S} = \{1, 2, ...s_S\}$ in (3.10) with s_S being the maximal intrinsic lag.

    - Channel k is only explained by the *extrinsic past* of neighborhood channels. We therefore set $\mathbb{Q} = \{1, 2, ...q_Q\}$ in (3.12) with q_Q being the maximal extrinsic lag.

2. Both intrinsic and extrinsic model coefficients in (3.10) and (3.12) do not depend on the sample index n, but only on the intrinsic and extrinsic lags s and q. We need hypothesis 2 for this simplifying time-invariant modeling.

---

[6]Naturally, different channels have different extrinsic channel sets, as the extrinsic contributions differ from one to another.

[7]Compare section 3.5.

3. Throughout the formulae, we use the following notation for describing directed dependencies: $\vec{x}_{k,l}[n]$ or $a_{q;k,l}$ means that we speak about the influence of channel l on channel k (at a certain sample index or lag).[8]

3.3   Channel selection

Choosing an appropriate extrinsic channel set $\mathbb{L}_k$ for the calculation of the partial extrinsic term (3.11) is a crucial part of the multichannel regression defined in section 3.2.

3.3.1   Theoretical considerations

As mentioned in section 1.3, we face two problems: First of all, we deal with a high-dimensional system (of typically $K = 28$ channels in applications), and secondly, signals recorded by electrodes located spatially close together show strong inter-correlations. Without any automatic reduction to a smaller set of channels, which rejects inter-correlated channels, numeric problems will necessarily arise.

This numerical behavior is even aggravated, as statistics, like for example the covariance function, are not known in practice and therefore have to be estimated from the data. This step unfortunately generates an additional estimation error. Thus, limiting the extrinsic channel set to a small number of *significant* channels helps to improve the numerical stability of the algorithm as well.

The question is now how to dynamically[9] select a small subset of channels in an efficient way assuring that

- important channels with significant contributions are selected so that as little information as possible is lost

- channels with high cross-correlation but little "extrinsic information" are rejected.

An obvious approach would be to put the focus of this selection on a "natural" parameter: the spatial position of the electrodes. One could, for example, select a certain number of spatially nearest electrodes assuring that all of the information in this specific region is well captured. The problem of this method is that information about spatial positions of the electrodes is required.[10]

If these positions are not known, one could calculate ordinary correlation coefficients and select a subset of channels with the highest correlation coefficients. However, this method is not applicable in practice, as it only selects

---

[8]Note that the notation of the intrinsic coefficients $a_{s;k,k}$ is coherent with this convention, as it describes the influence of channel k on itself.

[9]As stated in 3.2, $\mathbb{L}_k$ is determined for each $\widehat{x}_k$.

[10]Another disadvantage is the constant subset selection over time. We are going to discuss the implementation of temporal modifications of the subset $\mathbb{L}_k$ in chapter 4.

channels with high correlation. This might lead, more than ever, to potential numeric problems – what we initially wanted to avoid.

Therefore, we propose an iterative channel selection algorithm which we present in the next subsection.

3.3.2 Channel selection algorithm

A possible iterative procedure selecting an appropriate $\mathbb{L}_k$ for each $\widehat{x}_k$ is represented in pseudo code in algorithm 3.1.

Algorithm 3.1 Channel selection

```
for each regressand x_k[n], k=1..K
    extrinsic channel set: L = {}
    extension pool: P = {1,..K}\{k}
    loop
        calculate BIC with channel set L
        for each i in P
            calculate BIC(i) with channel set L_i = {L, i}
        end for
        i_opt = arg min BIC(i)
        if BIC(i_opt) < BIC
            extend extrinsic channel set: L = {L, i_opt}
            reduce extension pool: P = P \ i_opt
            continue loop
        else
            exit loop
        end if
    end loop
end for
```

Its main idea is to iteratively add channels bottom-wise-up until the *Bayesian information criterion (BIC),* a measure of goodness of the fit in an estimated statistical model, is satisfied:

$$\min\left\{\ln(S_{\text{err}}) + \frac{M\,\ln T}{T}\right\}, \tag{3.13}$$

where S_{err} is the residual sum of squares, M the total number of parameters[11] and T the number of samples.

BIC is an extension of the original *Akaike information criterion (AIC):*[12]

$$\min\left\{\ln(S_{\text{err}}) + \frac{2M}{T}\right\}. \tag{3.14}$$

---

[11]The total number of parameters is the sum of the intrinsic lags and all extrinsic lags: $M = s_S + ch \cdot q_Q$, where ch is the number of selected (extrinsic) channels.

[12]This famous criterion, used in numerous publications, was presented in 1974 by Akaike in [Aka74].

As the AIC tends to overfit, Schwarz adopted it using Bayesian arguments and introduced the BIC in [Sch78].[13] This is why (3.13) is also referred to as *Schwarz criterion (SC)*.

When comparing (3.13) and (3.14), we see that the BIC penalizes free parameters more than the AIC, leading to lower-dimensional models. Due to this property, we use the BIC in the channel selection algorithm.[14]

In detail, the algorithm performs the following steps (compare algorithm 3.1):

1. For a given intrinsic channel x_k, it starts with an empty extrinsic channel set $\mathbb{L}$ and a full extension pool $\mathbb{P}$ containing all possible extrinsic channels.

2. Using the current extrinsic channel set, it calculates a cost function used for the Bayesian information criterion (BIC).

3. Now the search for the best additional channel starts:

   - For each additional channel i belonging to the extension pool $\mathbb{P}$, an extended regression (using $\mathbb{L} \cup \{i\}$ as extrinsic channel set) delivers a cost function;
   - the best channel i_{opt} (this means: the one belonging to the smallest cost function) is preliminarily chosen.

4. If the optimal cost function is smaller than the one from the non-extended regression performed in step 2, the associated optimal channel i_{opt} is taken:

   - the extended set $\mathbb{L} \cup \{i_{opt}\}$ becomes the new extrinsic channel set $\mathbb{L}$;
   - the channel i_{opt} is removed from the extension pool $\mathbb{P}$;
   - the algorithm continues at point 2.

5. otherwise

   - the algorithm is left, returning a (locally) optimal extrinsic channel set $\mathbb{L}$.

If the algorithm is finally left, this means that by adding any channel (even the optimal among the remaining ones) the fit is impaired: The (local) minimum of the cost function is therefore found, as demanded by the BIC criterion.

For a better understanding, figure 3.1 illustrates an example of a possible temporal and spatial distribution of regressors $x_l[n-q]$ (gray squares) summed up in the regressand $\widehat{x}_k[n]$ estimating $x_k[n]$ (black square):

- Intrinsic channel $k = 2$

- Corresponding extrinsic channel set $\mathbb{L}_2 = \{1, 3, 5\}$

---

[13]Mathematically spoken: The BIC is a consistent estimator of the true model order, the AIC not. For details on necessary assumptions and the proof see [HD88].

[14]Note that the An algorithm, which we will mention later in 3.3.3, suggests using BIC in its core procedure as well.

- Intrinsic lag set $\mathbb{S} = \{2, 3, 4, 5\}$

- Extrinsic lag set $\mathbb{Q} = \{1, 2, 3, 4, 5\}$

Figure 3.1: ***Temporal and spatial distribution of regressors.*** *The current sample n (to be estimated) is symbolized in black, selected regressors in gray.*

Hereby, channels (represented by lines in figure 3.1) are selected by the channel selection algorithm described above; intrinsic and extrinsic temporal lags are given.

3.3.3 Remarks on the algorithm

Of course, as this algorithm does not try all possible variants in an exhaustive way[15], it can only detect local minima.

1. Its bottom-up approach is similar to the one of the *An algorithm* presented in [AG89], but does not include a later dynamical removal of already selected channels: Even if this led to an overall improvement, a channel is preserved, once it has been added due to the optimum criterion. This design could lead to the constellation that the algorithm chooses a *local minimum*.

2. Furthermore, as this procedure is a pure channel selection algorithm, it does not affect temporal lags by definition. It neither optimizes the intrinsic/extrinsic lags by increasing or decreasing the lag order of the regression

---

[15]A little thought experiment: In order to choose, for *one* given intrinsic channel x_k, *all possible extrinsic channel subsets* (including the empty one) from a total set of $K = 28$ channels, one would have to try

$$\sum_{i=0}^{K-1} \binom{K-1}{i} = 2^{K-1} = 2^{27} \approx 1.34 \cdot 10^8.$$

model nor allows partial lag selection per channel. If a channel is selected, all associated lags are automatically taken; if it is rejected, none of its associated lags is used in the regression. Once again, this limitation could lead to the detection of a *suboptimal local minimum.*

Room for further improvement of this algorithm is therefore given.

3.4   Dependency measure EIPR

In this section we present a novel dependency measure, the *extrinsic-to-intrinsic-power ratio (EIPR)*, aiming at the identification of mutual dependencies of multivariate signals. EIPR can be applied to EEG/ECoG data for indicating synchronization and coupling effects of brain regions during epileptic seizures.

Several methods based on autoregressive modeling have been proposed: In subsection 2.1.2 we presented techniques which analyze cross-correlations and cross-spectra of multichannel autoregressive models fitted to brain signal data.

3.4.1   Variance terms

In contrast to these approaches, we perform a *direct analysis* of the linear regression terms[16] associated to the respective channels.

Using the estimated model coefficients $a_{\cdot;k,l}$ we first express variances of the intrinsic and extrinsic regression terms:

- The variance of the intrinsic regression term $\dot{x}_k[n]$ can be written as[17]

$$
\begin{aligned}
\sigma_{\dot{x}_k}^2 &= \mathbb{E}\left\{\left(\dot{x}_k[n]\right)^2\right\} \\
&= \mathbb{E}\left\{\left(\sum_s a_{s;k,k} x_k[n-s]\right)^2\right\} \\
&= \mathbb{E}\left\{\sum_s \sum_{s'} a_{s';k,k} x_k[n-s'] a_{s;k,k} x_k[n-s]\right\} \\
&= \sum_s \sum_{s'} a_{s';k,k} a_{s;k,k} \mathbb{E}\left\{x_k[n-s'] x_k[n-s]\right\} \\
&= \sum_s \sum_{s'} a_{s;k,k} r_{x_k}[s-s'] a_{s';k,k}
\end{aligned}
\tag{3.15}
$$

because of

$$
\begin{aligned}
\mathbb{E}\left\{x_k[n-s'] x_k[n-s]\right\} &= \mathbb{E}\left\{x_k[(n-s')] x_k[(n-s')-(s-s')]\right\} \\
&= r_{x_k}[s-s'].
\end{aligned}
$$

---

[16]See (3.10) and (3.12) on page 23 in section 3.2.

[17]Our signals $\mathbf{x}$ are real-valued, therefore we do not use any absolute values in the definition of the variance, but directly calculate it as $\sigma_{\mathbf{x}}^2 \triangleq \mathbb{E}\left\{\mathbf{x}^2\right\}$.

- Analogically, the variance of the partial extrinsic regression terms $\vec{x}_{k,l}[n]$ can be expressed as

$$
\begin{aligned}
\sigma^2_{\vec{x}_{k,l}} &= \mathbb{E}\left\{ \left(\vec{x}_{k,l}[n] \right)^2 \right\} \\
&= \mathbb{E}\left\{ \left(\sum_q a_{q;k,l} x_l[n-q] \right)^2 \right\} \\
&= \sum_q \sum_{q'} a_{q;k,l} r_{x_l}[q-q'] a_{q';k,l}.
\end{aligned}
\tag{3.16}
$$

- Similarly, the variance of the (total) extrinsic regression term $\vec{x}_k$ is given by

$$
\begin{aligned}
\sigma^2_{\vec{x}_k} &= \mathbb{E}\left\{ \left(\vec{x}_k[n] \right)^2 \right\} \\
&= \mathbb{E}\left\{ \left(\sum_{l \in \mathbb{L}_k} \vec{x}_{k,l} \right)^2 \right\} \\
&= \sum_{l \in \mathbb{L}_k} \sum_{l' \in \mathbb{L}_k} \mathbb{E}\left\{ \left(\sum_q a_{q;k,l} x_l[n-q] \right) \left(\sum_{q'} a_{q';k,l'} x_{l'}[n-q'] \right) \right\} \\
&= \sum_{l \in \mathbb{L}_k} \sum_{l' \in \mathbb{L}_k} \sum_q \sum_{q'} a_{q;k,l} a_{q';k,l'} r_{x_l x_{l'}}[q-q'].
\end{aligned}
\tag{3.17}
$$

After these theoretical considerations, we want to add three recapitulatory remarks for the sake of clarity:

1. If the model coefficients and the autocovariance function of the channel are known, so are the desired variance terms.
   This is the case, because the coefficients are estimated by the regression model, and the autocovariance function is easily estimated by the empiric autocovariance function from the original signal data.

2. The variance terms are time-independent, leading to time independent dependency measures in the next subsection.
   In fact, this is a logical consequence of hypothesis 2 (stationarity) implying time-invariance of coefficients and the covariance function. However, for reasons of completeness, we want to indicate it here to make sure that the reader is well aware of this property.[18]

3. Note that, a priori, the total extrinsic variance $\sigma^2_{\vec{x}_k}$ is *not* the sum of the corresponding partial extrinsic variances $\sigma^2_{\vec{x}_{k,l}}$:

$$
\sigma^2_{\vec{x}_k} \neq \sum_{l \in \mathbb{L}_k} \sigma^2_{\vec{x}_{k,l}}.
$$

---

[18]This time-invariance will change in chapter 4.

The inegality above only turns into an egality if all spatial correlations are zero.

3.4.2   Dependency measures

Based on the variance terms (3.15) and (3.16) defined in the last subsection, we introduce *extrinsic-to-intrinsic-power ratio (EIPR)* which quantifies coupling or synchronization effects of signal pairs (x_k, x_l):

$$\eta_{k,l} \triangleq \frac{\sigma^2_{\vec{x}_{k,l}}}{\sigma^2_{\dot{x}_k}} \; . \tag{3.18}$$

Being the ratio of variances of the partial extrinsic regression term $\vec{x}_{k,l}$ and the intrinsic regression term $\dot{x}_k$, EIPR takes large values for large partial extrinsic regression variance and small intrinsic regression variance. This is the case when channel x_l contributes significant information to the explanation of channel x_k: Exactly here we want to measure a dependency.

Note that EIPR – in contrast to DTF (2.6) or PDC (2.9) presented in subsection 2.1.2 – is not normalized to the interval $[0, 1]$. It only (trivially) respects the lower bound: $\eta_{k,l} \geq 0$.

Following the logic above, we introduce a second, related measure: the *total extrinsic-to-intrinsic-power ratio (TEIPR)*. As the reader can guess, it is based on the variance terms (3.15) and (3.17) and is obviously defined as

$$\eta_k \triangleq \frac{\sigma^2_{\vec{x}_k}}{\sigma^2_{\dot{x}_k}} \; . \tag{3.19}$$

TEIPR is the ratio of variances of the (total) extrinsic regression term $\vec{x}_k$ and the intrinsic regression term $\dot{x}_k$ and therefore a measure for the total synchronization of one channel with neighboring brain regions. Possible applications of this measure could therefore be the temporal allocation of epileptic seizures or spatial determination of epileptic foci.

It is important to note that TEIPR η_k is *not necessarily* the sum of the corresponding EIPRs $\eta_{k,l}$

$$\eta_k \neq \sum_l \eta_{k,l} \, ,$$

unless all spatial correlations are zero.[19]

---

[19]Only in this case – as stated in subsection 3.4.1 – the total extrinsic variance $\sigma^2_{\vec{x}_k}$ is the sum of the corresponding partial extrinsic variances $\sigma^2_{\vec{x}_{k,l}}$ allowing

$$\sum_{l \in \mathbb{L}_k} \eta_{k,l} = \sum_l \frac{\sigma^2_{\vec{x}_{k,l}}}{\sigma^2_{\dot{x}_k}} = \frac{\sum_l \sigma^2_{\vec{x}_{k,l}}}{\sigma^2_{\dot{x}_k}} = (\text{OK!}) = \frac{\sigma^2_{\vec{x}_k}}{\sigma^2_{\dot{x}_k}} = \eta_k.$$

3.5 Link to the classical AR-model

When considering our regression model 3.8 with lag sets $\mathbb{S} = \{1...s_S\}$ and $Q = \{1...q_Q\}$, we solve in fact a classical multivariate AR-system of order $p = \max(s_S, q_Q)$:

$$\mathbf{x}[n] = \sum_{i=1}^{p} \mathbf{A}_i \mathbf{x}[n-i] + \epsilon[n],$$

where $\epsilon[n]$ is zero-mean white noise with covariance matrix $\mathbf{\Sigma}_\epsilon$.

Hereby, coefficients of orders not contained in the respective lag set are set to zero. If, for instance, $s_S = 4$ and $q_Q = 4$, all extrinsic coefficients $a_{4;k,l} = 0$, whereas the intrinsic ones $a_{4;k,k}$ (on the main diagonal of $\mathbf{A}_4$) are estimated.

Furthermore, dynamic channel selection is compatible with this model as well. As discussed in section 3.3, if a channel is selected or rejected, this is done for all lags. Coefficients of not selected channels are therefore simply set to zero in all coefficient matrices $\mathbf{A}_i$, $i = 1...p$.

For instance, the estimated coefficient matrix series

$$\widehat{\mathbf{A}}_i = \begin{pmatrix} \widehat{a}_{i;1,1} & 0 & \widehat{a}_{i;1,3} & \cdots \\ \widehat{a}_{i;2,1} & \widehat{a}_{1;2,2} & 0 & \cdots \\ 0 & 0 & \widehat{a}_{i;3,3} & \cdots \\ \vdots & \vdots & \vdots & \ddots \end{pmatrix}$$

would reflect the following case:

- x_1 is explained by itself and x_3

- x_2 is explained by x_1 and itself

- x_3 is only explained by itself.

Note that the diagonal never contains zeros, as the intrinsic regression term (3.10) must be part of the autoregressive explanation of each channel x_k.

Chapter 4

Implementation

As already mentioned in the introduction to chapter 3, the theoretical model based on the hypotheses of zero-mean and stationary data cannot be applied to ECoG data directly.

This is why in this chapter we are going to present modified versions of the initial method which are adapted to a realistic description of neuro-biological signal properties. However, the main idea presented in chapter 3 is still valid and therefore stays the same.

On the following pages, we are – step by step – going to refine our modeling approach in order to get closer to the real nature of ECoG signals: First, we consider our raw signals to be short-time stationary and present an implementation of the original method adapted to this new context. In a second step, we then completely abandon any hypothesis of time-invariance and use a self-adaptive algorithm for correctly estimating instationary signals.

Here we focus on the presentation of the method; results obtained are presented in chapter 5.

4.1 MMSE regression

For this first implementation step[1], we follow a very natural approach by asking ourselves a question, which we have – intentionally – completely ignored up to now: How can all derived statistics be completely time-independent if we know that seizures start, end and propagate during the recorded time?

This objection is, of course, true: The (second-order) statistics of ECoG signals do not only vary, but they have to – otherwise we would not be able to detect any seizures. Therefore, a model exclusively based on the method described in chapter 3 would not have any explanatory power at all.

In order to arrive at a meaningful model assuring that we can see what we want to see, we absolutely have to improve our modeling approach by segmenting our recorded ECoG signal.

---

[1]Its idea is described in [HK07].

4.1.1   Windowing

As we want to detect low-frequency changes of the seizure status[2], the approach chosen is the following: We segment our ECoG data by demanding stationarity within overlapping (raw signal) blocks of a certain length. The technical implementation of this idea is termed *windowing.* Figure 4.1 illustrates this concept with the help of the exemplary window design parameters *time of window* $T_{win} = 6$s and *time of overlap* $T_{ol} = 4$s.
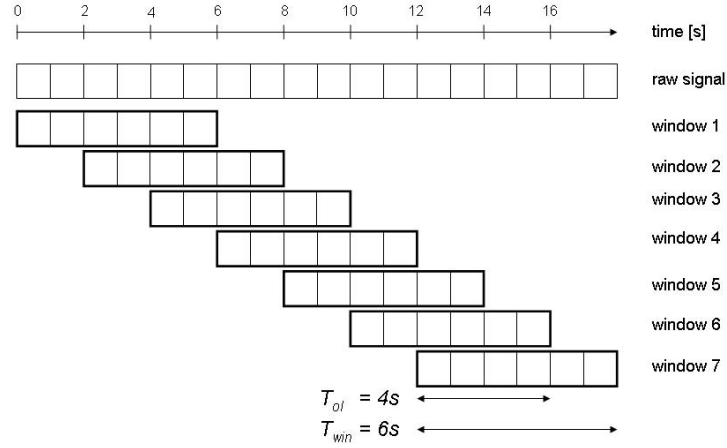
Figure 4.1: ***Exemplary signal segmentation with overlapping windows.*** *The raw signal is transformed into windows lasting for 6s with an overlap of 2s.*

This leads to the following two hypotheses 1' and 2' which we are going to use from now on:

Hypothesis 1': Within a window, the signal $\mathbf{x}[n]$ is zero-mean: $\mathbb{E}\mathbf{x}[n] = \mathbf{0}$.

Hypothesis 2': The signal $\mathbf{x}[n]$ is *short-time stationary*: Within each window it especially fulfills time-invariance of the covariance matrix $\mathbf{R}_{\mathbf{x},p}$.

We want to add two annotations on technical details for the sake of clarity:

1. When speaking about signals $\mathbf{x}[n]$ (or channels $x_k[n]$ respectively), the sample index n is now, of course, limited to each window and does *not* run through the whole recording time.
   Let us, for example, consider a window of length $T_{win} = 6$s at a sampling frequency of $f_s = 128$Hz. Then each window consists of $N_{win} = 6$s $\cdot$ 128Hz $= 768$ samples, and the sample index is limited to $n \in \{1, ..., 768\}$ in every single window.

---

[2]We do not want to detect high-frequency signal components, but track "slow" changes like seizure propagation.

2. Hypothesis 1' is probably not respected a priori, but this does not cause any problems: Within each window, the regression algorithm simply processes transformed signals $\tilde{\mathbf{x}}[n]$ obtained by

$$\tilde{\mathbf{x}}[n] = \mathbf{x}[n] - \bar{\mathbf{x}},$$

where $\bar{\mathbf{x}}$ is the mean of the signal $\mathbf{x}[n]$ in this window.[3]

These adaptions have convenient consequences:

- The method of chapter 3 itself can be applied to the ECoG signals in each window under the assumption that they respect hypotheses 1' and 2': There, our regression model (3.8) from section 3.2 is valid, can use the channel selection algorithm from section 3.3 and delivers time-invariant coefficients $a_{k,l}$, variance terms $\sigma^2_{\tilde{x}_k}, \sigma^2_{\tilde{x}_{k,l}}$ and finally EIPRs $\eta_{k,l}$.

- As the dependency measures are constant within a window, but differ from one to another, we observe changes of the seizure status from one window to another. We therefore have a *temporary resolution* with an associated frequency of

$$f = \frac{1}{T_{win} - T_{ol}} \,.$$

Now that we have elaborated a real-world solution, the only aspect which still remains unclarified is the estimation of the model coefficients $a_{.;k,l}$. We will explain our approach – which we have in fact never even indicated before – in the following subsection: *minimum mean-square-estimation (MMSE)*.

4.1.2 Wiener-Hopf-equation

Before describing the estimation of our model coefficients $a_{.;k,l}$ by means of MMSE, let us insert a short theoretical subsection for deducing the normal equation solving the minimal MSE-problem: the *Wiener-Hopf-equation*.

Minimal mean-sqare-estimation (MMSE) is a method based on Bayseian philosophy: In contrast to the classical approach, which considers the parameter of interest to be deterministic but unknown, the MMSE, being a Bayseian approach, assumes the parameter of interest to be a random variable. Its particular realization must be estimated with the help of second-order-statistics which are assumed to be known.

For the following, we limit ourselves to real-valued data; for a more detailed discussion the reader is invited to consult [Kay93] and [Mar87], which contain – apart from the formulation for the general complex case – a more detailed view on this topic.

---

[3]When speaking about signals $\mathbf{x}[n]$ respecting hypothesis 1', we will from now on implicitly assume that they have been transformed: For simplicity reasons, we will sloppily write $\mathbf{x}[n]$ instead of $\tilde{\mathbf{x}}[n]$.

Let $x[n] \in \mathbb{R}^{1 \times T}$ be a stationary, zero-mean signal (consisting of one component). Using an autoregressive model of order p, the estimation $\hat{x}[n]$ is based on past values $x[i], i < n$.

The stacked vector of past values shall be denoted by

$$\mathbf{x}[n^-] = (x[n-1], ..., x[n-p])^T$$

and the vector of coefficients

$$\mathbf{a} = (a_1, ..., a_p)^T.$$

The estimation error at sampling time n is therefore given by

$$e[n] = x[n] - \mathbf{a}^T \mathbf{x}[n^-]. \tag{4.1}$$

The Wiener approach for resolution of the prediction problem consists of minimizing the estimation of the square of the prediction error (4.1):[4]

$$\mathbb{E}\left\{e[n]^2\right\} \rightarrow \min \tag{4.2}$$

By developing (4.2) we obtain

$$
\begin{aligned}
\mathbb{E}\left\{e[n]^2\right\} &= \mathbb{E}\left\{\left(x[n] - \mathbf{a}^T \mathbf{x}[n^-]\right)\left(x[n] - \mathbf{a}^T \mathbf{x}[n^-]\right)\right\} \\
&= \begin{cases} \mathbb{E}\left\{x[n]x[n]\right\} \\ +\mathbf{a}^T \mathbb{E}\left\{\mathbf{x}[n^-]x[n]\right\} + \mathbb{E}\left\{x[n]\mathbf{x}[n^-]\right\}^T \mathbf{a} \\ +\mathbf{a}^T \mathbb{E}\left\{\mathbf{x}[n^-]\mathbf{x}[n^-]^T\right\} \mathbf{a} \end{cases} \\
&= \sigma_x^2 - \mathbf{a}^T \mathbf{r}_{x,p} - \mathbf{r}_{x,p}^T \mathbf{a} + \mathbf{a}^T \mathbf{R}_{x,p} \mathbf{a}, \tag{4.3}
\end{aligned}
$$

where $\mathbf{R}_{x,p}$ denotes the *autocovariance matrix*[5] (from lag 0 to $p-1$) and $\mathbf{r}_{x,p}$ the *autocovariance vector* (3.6), both presented in section 3.1.

Note that both $\mathbf{R}_{x,p}$ and $\mathbf{r}_{x,p}$ are a priori known and - due to the hypothesis of stationarity - independent of n. Our specific means in (4.3), although containing the finite set n^-, are therefore time-independent and can be replaced by the known, time-invariant second-order statistics $\mathbf{R}_{x,p}$ and $\mathbf{r}_{x,p}$.

Rearranging (4.3) and completing the square yields

$$
\begin{aligned}
\mathbb{E}\left\{e[n]^2\right\} &= \mathbf{a}^T \mathbf{R}_{x,p} \mathbf{a} - \mathbf{a}^T \mathbf{r}_{x,p} - \mathbf{r}_{x,p}^T \mathbf{a} + \sigma_x^2 \\
&= \begin{cases} \left(\mathbf{a}^T \mathbf{R}_{x,p} - \mathbf{r}_{x,p}^T\right) \mathbf{R}_{x,p}^{-1} \left(\mathbf{R}_{x,p}\mathbf{a} - \mathbf{r}_{x,p}\right) & \text{dep. of } a \\ -\mathbf{r}_{x,p}^T \mathbf{R}_{x,p}^{-1} \mathbf{r}_{x,p} + \sigma_x^2 & \text{indep. of } a. \end{cases} \tag{4.4}
\end{aligned}
$$

---

[4]As stated before, we are only considering the case of real-valued signals here and therefore write $\mathbb{E}\{e[n]^2\}$ instead of $\mathbb{E}\left\{|e[n]|^2\right\}$.

[5]Here, $\mathbf{R}_{x,p}$ is the univariate covariance matrix (3.5).

Therefore, minimizing the MSE is equivalent[6] to minimizing the part depending on $\mathbf{a}$ in (4.4):

$$\min MSE \Longleftrightarrow \mathbf{R}_{x,p}\mathbf{a} - \mathbf{r}_{x,p} = 0. \qquad (4.5)$$

The equation (4.5) is called *Wiener-Hopf-equation* and delivers, by simple inversion, the optimal parameter vector $\mathbf{a}$ (in the sense of MMSE):

$$\mathbf{a} = \mathbf{R}_{x,p}^{-1}\mathbf{r}_{x,p}. \qquad (4.6)$$

The optimal estimation error is a simple consequence of (4.4): As its second part, independent of a and therefore constant, cannot be minimized, the optimal estimation error is given by:

$$\mathbb{E}\left\{e[n]^2\right\} = -\mathbf{r}_{x,p}^T \mathbf{R}_{x,p}^{-1}\mathbf{r}_{x,p} + \sigma_x^2.$$

4.1.3 Link to OLS

We also want to mention that the Wiener approach, departing from Bayesian theory, delivers the same form of normal equation as the classical ordinary least-squares (OLS) approach to AR-model identification: the *Yule-Walker-equation*.[7]

As we have

$$\mathbf{R}_{\mathbf{x},p}\mathbf{a} = \mathbf{r}_{x,p}$$

$$\begin{pmatrix} r_x[0] & r_x[1] & \cdots & r_x[p] \\ r_x[1] & r_x[0] & & r_x[p-1] \\ \vdots & & \ddots & \vdots \\ r_x[p] & r_x[p-1] & \cdots & r_x[0] \end{pmatrix} \begin{pmatrix} a_1 \\ a_2 \\ \vdots \\ a_p \end{pmatrix} = \begin{pmatrix} r_x[1] \\ r_x[2] \\ \vdots \\ r_x[p] \end{pmatrix}, \quad (4.7)$$

the Wiener-Hopf-equation is formally identical with the Yule-Walker-equations.[8]

In fact, as we do *not* know the second-order-statistics in our case, we will have to estimate them. We are going to discuss the resulting problems in subsection 4.1.5.

Equation (4.7) then becomes

$$\widehat{\mathbf{R}}_{\mathbf{x},p}\widehat{\mathbf{a}} = \widehat{\mathbf{r}}_{x,p}$$

$$\begin{pmatrix} \widehat{r}_x[0] & \widehat{r}_x[1] & \cdots & \widehat{r}_x[p] \\ \widehat{r}_x[1] & \widehat{r}_x[0] & & \widehat{r}_x[p-1] \\ \vdots & & \ddots & \vdots \\ \widehat{r}_x[p] & \widehat{r}_x[p-1] & \cdots & \widehat{r}_x[0] \end{pmatrix} \begin{pmatrix} \widehat{a}_1 \\ \widehat{a}_2 \\ \vdots \\ \widehat{a}_p \end{pmatrix} = \begin{pmatrix} \widehat{r}_x[1] \\ \widehat{r}_x[2] \\ \vdots \\ \widehat{r}_x[p] \end{pmatrix} \qquad (4.8)$$

and is now identical with the Yule-Walker-equation using Yule-Walker-estimates.

---

[6] $\mathbf{R}_{x,p}$ is non-singular.

[7] For its deduction see for example [Mar87] or [BD91].

[8] Compare section 2.3 in [Vai08] as well.

4.1.4   Coefficient estimation

After the reader has now been introduced into the concept of windowing and the deduction of the Wiener equation, we finally want to describe how the model coefficients $a_{.;k,l}$ are estimated.

Given our regression model (3.8) from section 3.2, we want to find optimal model coefficients $a_{.;k,l}$ for all channels $k \in \{1...K\}$.We therefore subsequently solve K Wiener-Hopf-equations: for each (intrinsic) channel x_k we calculate

$$\mathbf{a}_k = \mathbf{R}_{\mathbf{x}_k,p}^{-1}\mathbf{r}_{\mathbf{x}_k,p}. \tag{4.9}$$

We hereby use stacked vectors $\mathbf{a}_k$ and $\mathbf{x}_k$:

Stacked signal sample vector $\mathbf{x}_k$ contains all relevant samples of the intrinsic channel as well as the ones of extrinsic channels:

$$\mathbf{x}_k[n] \triangleq (x_k[n-1], ..., x_k[n-s_S], \vec{\mathbf{x}}_k[n-1], ..., \vec{\mathbf{x}}_k[n-q_Q])^T$$

with the partial stacked signal sample vector $\vec{\mathbf{x}}_k[n]$ containing samples at time n of all extrinsic channels listed in the extrinsic channel set $\mathbb{L}_k = \{l_1, ..., l_L\}$:[9]

$$\vec{\mathbf{x}}_k[n] \triangleq (x_{l_1}[n], ..., x_{l_L}[n]).$$

Stacked parameter vector $\mathbf{a}_k$ contains all regression parameters associated to the samples stacked above:

$$\mathbf{a}_k \triangleq \left(a_{1;k,k}, ..., a_{s_S;k,k}, \vec{\mathbf{a}}_{1;k}, ..., \vec{\mathbf{a}}_{q_Q;k}\right)^T$$

with

$$\vec{\mathbf{a}}_{q;k} \triangleq \left(a_{q;k,l_1}, ..., a_{q;k,l_L}\right).$$

Furthermore, in conformity with the last subsection 4.1.2, $\mathbf{R}_{\mathbf{x}_k,p}$ denotes the covariance matrix and $\mathbf{r}_{\mathbf{x}_k,p}$ the covariance vector.

This notation might seem unnecessarily complicated, but is fully justified, because it has a huge advantage: Despite our variable selection of channels and potentially different intrinsic and extrinsic lag sets, the regressand can be written easily now – as it is the case with a "standard" AR model – as

$$\widehat{x}_k[n] = \mathbf{a}_k^T \mathbf{x}_k[n]. \tag{4.10}$$

Once more, the time for an illustrative example has come, which the reader might wish to see for the sake of clarity: let our intrinsic channel be the first:

---

[9]As all properties of this channel set depend on the channel k (it changes from channel to channel!), we would have to write $\mathbb{L}_k = \{l_{k,1}...l_{k,L_k}\}$ in order to express this fact correctly. However, we prefer a sloppier notation for better readability and ask the reader to keep in mind what we mean.

$k = 1$, the intrinsic lag set $\mathbb{S} = \{s_1, s_2\} : S = 2$, the extrinsic lag set $\mathbb{Q} = \{q_1, q_2, q_3\} : Q = 3$ and the extrinsic channel set $\mathbb{L}_1 = \{l_1, l_2\} = \{2, 3\}$.[10]
We therefore solve the first (of our K) Wiener-Hopf-equation, delivering the coefficients for the first channel: Our stacked signal sample vector $\mathbf{x}_1[n]$ is

$$
\begin{aligned}
\mathbf{x}_1[n] \quad = \quad & (x_1[n - s_1], x_1[n - s_2], \\
& \underbrace{x_2[n - q_1], x_3[n - q_1]}_{\vec{\mathbf{x}}_1[n - q_1]}, \underbrace{x_2[n - q_2], x_3[n - q_2]}_{\vec{\mathbf{x}}_1[n - q_2]}, \underbrace{x_2[n - q_3], x_3[n - q_3]}_{\vec{\mathbf{x}}_1[n - q_3]})^T,
\end{aligned}
$$

and the estimated coefficients are calculated as

$$
\mathbf{a}_1 \quad = \quad \mathbf{R}_{\mathbf{x}_1,p}^{-1}\mathbf{r}_{\mathbf{x}_1,p}
$$

$$
\begin{pmatrix}
a_{s_1;1,1} \\
a_{s_2;1,1} \\
a_{q_1;1,2} \\
a_{q_1;1,3} \\
a_{q_2;1,2} \\
a_{q_2;1,3} \\
a_{q_3;1,2} \\
a_{q_3;1,3}
\end{pmatrix}
=
\begin{pmatrix}
\mathbb{E}\left\{x_1[n - s_1]^2\right\} & \cdots & \\
& & \\
& \vdots \quad\quad \ddots \quad\quad \vdots & \\
& & \\
& \cdots \quad \mathbb{E}\left\{x_3[n - q_3]^2\right\}
\end{pmatrix}^{-1}
\begin{pmatrix}
\mathbb{E}\left\{x_1[n - s_1]x_1[n]\right\} \\
\mathbb{E}\left\{x_1[n - s_2]x_1[n]\right\} \\
\mathbb{E}\left\{x_2[n - q_1]x_1[n]\right\} \\
\mathbb{E}\left\{x_3[n - q_1]x_1[n]\right\} \\
\mathbb{E}\left\{x_2[n - q_2]x_1[n]\right\} \\
\mathbb{E}\left\{x_3[n - q_2]x_1[n]\right\} \\
\mathbb{E}\left\{x_2[n - q_3]x_1[n]\right\} \\
\mathbb{E}\left\{x_3[n - q_3]x_1[n]\right\}
\end{pmatrix}
$$

Again, we have the Yule-Walker equation (4.7).

4.1.5   Estimation of the covariance matrix

We want to finalize the presentation of this first approach with the remark that the temporal and spatial second order statistics which are needed by the Wiener-Hopf-equations are in fact *not* known. We therefore have to estimate the covariance matrix from the raw signals, which are *considered* to be short-time-stationary by hypothesis 2'. This assures that we are allowed − within one window − to compute a time-invariant empiric covariance matrix

$$
\widehat{\mathbf{R}}_{\mathbf{x},p} =
\begin{pmatrix}
\widehat{\mathbf{R}}_{\mathbf{xx}}[0] & \widehat{\mathbf{R}}_{\mathbf{xx}}[-1] & \cdots & \widehat{\mathbf{R}}_{\mathbf{xx}}[-p + 1] \\
\widehat{\mathbf{R}}_{\mathbf{xx}}[1] & \widehat{\mathbf{R}}_{\mathbf{xx}}[0] & & \widehat{\mathbf{R}}_{\mathbf{xx}}[-p + 2] \\
\vdots & & \ddots & \vdots \\
\widehat{\mathbf{R}}_{\mathbf{xx}}[p - 1] & \widehat{\mathbf{R}}_{\mathbf{xx}}[p - 2] & \cdots & \widehat{\mathbf{R}}_{\mathbf{xx}}[0]
\end{pmatrix},
$$

which figures as an estimator for the covariance matrix $\mathbf{R}_{\mathbf{x},p}$.

In order to estimate the needed covariance functions $\mathbf{R}_{\mathbf{xx}}[s]$, [Mar87] suggests using the following biased estimators $\widehat{\mathbf{R}}_{\mathbf{xx}}[s]$ which guarantee the positive semi-

---

[10]We denote intrinsic and extrinsic lags by a completly symbolic notation, although the lag sets were restricted to a more specific form in chapter 3. This should assure that the reader really understands which coefficient is placed on which position.

definity of $\widehat{\mathbf{R}}_{\mathbf{x},p}$:

$$\widehat{\mathbf{R}}_{\mathbf{xx}}[s] = \frac{1}{N} \sum_{n=1}^{N-s} x[n+s]x[n]^T,$$

where $N = T_{win} \cdot f_s$ is the length of a window in samples.

This delivers an estimated parameter vector $\widehat{\mathbf{a}}_k$ which we use in fact:

$$\widehat{\mathbf{a}}_k = \widehat{\mathbf{R}}_{\mathbf{x}_k,p}^{-1} \widehat{\mathbf{r}}_{\mathbf{x}_k,p}.$$

Herby, the window length is important for the quality of the estimation of the second-order-statistics: On the one hand, too short windows do not provide sufficient samples to estimate the covariance matrix properly. On the other hand, the longer the window, the more the hypothesis of short-time-stationarity is violated.[11] In both cases, the model estimation error itself is impaired by an estimation error of the empiric covariance matrix.

If the reader is interested in (asympotical) statistical properties of the estimator for the covariance matrix,[12] he is invited to consult [BD91] or [HD88].

This difficulty directly leads us to the next section 4.2, where we are going to present a more elaborated coefficient estimation technique.

4.2   RLS regression

In section 4.1 we presented a first approach to the estimation of the model coefficients $a_{k,l}$, based on windowing and MMSE.

However, this method is not very exact, imposing the simplifying but questionable hypothesis of short-time-stationarity: Whenever a seizure starts or ends or propagates − what we want to detect − in the middle of a window, this hypothesis is, by definition, violated. Unfortunately, as we use sliding windows, this situation cannot be avoided − we tacitly accept it.

We implicitly assume that at least in all other cases, the hypothesis of short-time-stationarity is respected.

On the following pages, we are going to discard this implicit assumption of [HK07] and go one step further: We are going to use a method which is exact in mathematical terms being able to cope with instationary signals better: *recursive-least-squares estimation (RLS)*.

4.2.1   Deduction of RLS algorithm

We start this section with the presentation of the *exponentially-weighted recursive-least-squares* algorithm. We hereby follow the derivation presented in [Hay02],

---

[11]As we have already stated in the introduction to this section, this happens at the latest when a seizure starts/ends/propagates.

[12]E.g. under which conditions $\widehat{\mathbf{R}}_{\mathbf{x},p}$ is an asymptotically unbiased or even a consistent estimator for $\mathbf{R}_{\mathbf{x},p}$.

but do so without detailed steps in order to make the lecture easier for the reader and provide him with a better overview.

If the reader is interested in a detailed deduction and a deeper understanding of the construction of the RLS algorithm, he might consult [Hay02].

For simplicity reasons, we limit ourselves to a one-dimensional description of the algorithm; in subsection 4.2.2 we are going to give the multivariate extension which we need for our estimation purposes.

4.2.1.1 Preliminaries and theoretical considerations

The basic idea of a recursive implementation of the method of least squares is that

- the computation is started with *prescribed initial conditions*

- from sample to sample, the information contained in a new one is used to *update the old estimates*.

For each sample, we now obtain estimated parameters – they are not time-independent any more. The algorithm can therefore adapt itself to the data and better follow instationarities than an implementation using OLS.

As in 4.1.2, let us consider a zero-mean signal $x[n]$, $n = 1...N$ (consisting of one component), but *not* necessarily stationary now. By fitting it to an AR-model of order p, the estimate $\widehat{x}[n]$ is obtained from past samples $x[k]$, $k < n$.

We denote our *input data vector* at time n (containing the last p samples) by

$$\mathbf{x}[n^-] \triangleq (x[n-1], x[n-2], ..., x[n-p])^T$$

and the corresponding *coefficient vector* at time n by

$$\mathbf{a}[n] \triangleq (w_1[n], w_2[n], ..., w_p[n])^T.$$

As the algorithm runs through the data samples $n = p+1...N$, the cost function $\mathcal{E}[n]$, which is to be minimized, takes a variable length of observable data.[13] This cost function $\mathcal{E}[n]$ makes use of a *weighting factor* $\beta[n, i]$:

$$\mathcal{E}[n] \triangleq \sum_{i=p+1}^{n} \beta[n, i] \, e[i]^2, \tag{4.11}$$

where $e[i]$ is the difference between the desired response $x[i]$ and the estimated output $\widehat{x}[i]$:

$$\begin{aligned} e[i] &\triangleq x[i] - \widehat{x}[i] \\ &= x[i] - \mathbf{a}^T[n]\mathbf{x}[i^-]. \end{aligned} \tag{4.12}$$

---

[13]We therefore explicitly indicate the corresponding sample index: $\mathcal{E}[n]$.

The weighting factor $\beta[n, i] \in (0, 1]$ is introduced so that data in the distant past are "forgotten". This ensures that the algorithm can adapt itself better to statistical variations in case of an instationary signal.

Note that the coefficient vector $\mathbf{a}[n]$ remains fixed during the time period for which the cost function $\mathcal{E}[n]$ is defined.[14]

A special form of this weighting factor is the commonly used *exponential weighting factor* (or *forgetting factor*) defined by

$$\beta[n, i] \triangleq \lambda^{n-i},$$

where λ is a positive constant close but smaller than unity:

- When $\lambda = 1$, all past data samples stay in memory, and we have ordinary least squares. As this case corresponds to *infinite memory*, we can only use this parameter setting with a stationary signal.

- When $\lambda < 1$, distant past data are – as mentioned above – "forgotten": the farther in the past, the more these data samples are extenuated. This setting is therefore intended for instationary signals.
  A past sample is usually considered to be negligible ("forgotten") if its attenuation factor falls below e^{-1}. We therefore get the number M of non-negligible samples by

$$\lambda^M < e^{-1} \iff M > \frac{-1}{\ln \lambda}.$$

At a given sampling frequency f_s these samples correspond to a memory time constant of

$$\tau_\lambda = \frac{M}{f_s}.$$

Table 4.1 on page 42 shows typical values of the forgetting factor λ and corresponding memory time constants at an exemplary signal sampling frequency of $f_s = 128 Hz$.

forgetting factor λ	M non-negligible samples	memory time constant τ_λ
0.900	10	0.08s
0.950	20	0.16s
0.990	100	0.80s
0.995	200	1.60s
0.999	1000	7.80s

Table 4.1: *Memory time constants for typical forgetting factors*

For the sake of clarity we want to give a short example now:

---

[14]We therefore write $\mathbf{a}^T[n]$ instead of $\mathbf{a}^T[i]$ in (4.12).

Let $x[n]$ be an instationary signal which is modeled by an autoregressive (time-dependent) model of order $p = 2$ and $\lambda \lneqq 1$. At any moment n, we therefore have

$$
\begin{aligned}
\mathbf{a}[n] &= (a_1[n], a_2[n])^T \\
\mathbf{x}[n^-] &= (x[n-1], x[n-2])^T .
\end{aligned}
$$

Let the algorithm have reached sample $n = 10$. Then the cost function $\mathcal{E}[10]$ to be minimized yields

$$
\begin{aligned}
\mathcal{E}[10] &= \sum_{i=3}^{10} \lambda^{10-i} \left(x[i] - \mathbf{a}[10]^T \mathbf{x}[i^-] \right)^2 \\
&= \lambda^9 \left(x[3] - \mathbf{a}[10]^T \mathbf{x}[3^-] \right)^2 \\
&\quad + \lambda^8 \left(x[4] - \mathbf{a}[10]^T \mathbf{x}[4^-] \right)^2 \\
&\quad \vdots \\
&\quad + \lambda^0 \left(x[10] - \mathbf{a}[10]^T \mathbf{x}[10^-] \right)^2 .
\end{aligned}
$$

As already stated, the number of summands of the cost function (and therefore the number of data samples evaluated) grows when the algorithm steps forward and n increases. Note that, however $\mathbf{a}[n]$ and $\mathbf{x}[n^-]$ do *not* grow: They contain two elements (as we assume a model of order 2) at any moment n.[15]

As a result of this minimization[16], the algorithm delivers a coefficient vector estimate $\widehat{\mathbf{a}}[10]$ – and steps forward to sample n = 11, where the procedure described above starts again delivering $\widehat{\mathbf{a}}[11]$.

Now that the reader has already got a vague idea of the RLS algorithm, we want to continue with our theoretical considerations needed for the derivation of the recursive algorithm.

For regularization reasons, the cost function $\mathcal{E}[n]$ is expanded as the sum of two components: the sum of weighted error squares as in (4.11) and an additional *regularizing term*:

$$
\mathcal{E}[n] \triangleq \sum_{i=p+1}^{n} \lambda^{n-i} \left| x[i] - \mathbf{w}^T[n]\mathbf{x}[i] \right|^2 + \delta\lambda^p \left\| \mathbf{w}[p] \right\| . \tag{4.13}
$$

In this regularizing term, δ is a positive real number termed the *regularization parameter*. This term is included in $\mathcal{E}[n]$ to stabilize the solution by smoothing it.

The effect of including the regularizing term in (4.13) is equivalent to a reformulation of the *time-average covariance matrix* $\mathbf{\Phi}_{x,p}[n]$ of the input vector

---

[15]In our case of $n = 10$ we have:
$\mathbf{a}[10] = (a_1[10], a_2[10])^T$ and $\mathbf{x}[10^-] = (x[9], x[8])^T$ ... $\mathbf{x}[3^-] = (x[2], x[1])^T$.
[16]On the next few pages, we are going to see how this is done exactly.

x:

$$
\begin{aligned}
\mathbf{\Phi}_{x,p}[n] \quad &\triangleq \quad \sum_{i=p+1}^{n} \lambda^{n-i} \mathbf{R}_{\mathbf{x}[i^-],p} + \delta\lambda\mathbf{I}_{p\times p} \\
&= \quad \sum_{i=p+1}^{n} \lambda^{n-i}\mathbf{x}[i^-]\mathbf{x}[i^-]^T + \delta\lambda\mathbf{I}_{p\times p}\,, \qquad (4.14)
\end{aligned}
$$

where $\mathbf{I}_{p\times p}$ is the p-by-p identity matrix. A covariance matrix modified in such a way is said to be *diagonally loaded* and has the advantage of being non-singular and therefore invertible at all stages of computation.

Analogically, but without the use of a regularization term, the *time-average covariance vector* $\mathbf{z}_{x,p}[n]$ is defined:

$$
\begin{aligned}
\mathbf{z}_{x,p}[n] \quad &\triangleq \quad \sum_{i=p+1}^{n} \lambda^{n-i}\mathbf{r}_{x,p} \\
&= \quad \sum_{i=p+1}^{n} \lambda^{n-i}\mathbf{x}[i^-]x[i]. \qquad (4.15)
\end{aligned}
$$

The normal equation of the recursive-least-squares problem now takes the usual form

$$
\mathbf{\Phi}_{x,p}[n]\,\widehat{\mathbf{a}}[n] = \mathbf{z}_{x,p}[n]. \qquad (4.16)
$$

4.2.1.2   Recursive algorithm deduction

By isolating the n-th summand in the sum of (4.14), we easily find a recursive representation of $\mathbf{\Phi}_{x,p}[n]$:

$$
\begin{aligned}
\mathbf{\Phi}_{x,p}[n] \quad &= \quad \lambda\underbrace{\left(\sum_{i=p+1}^{n-1} \lambda^{n-i-1}\mathbf{x}[i^-]\mathbf{x}[i^-]^T + \delta\lambda\mathbf{I}_{M\times M}\right)}_{\mathbf{\Phi}_{x,p}[n-1]} + \mathbf{x}[n^-]\mathbf{x}[n^-]^T \\
&= \quad \lambda\mathbf{\Phi}_{x,p}[n-1] + \mathbf{x}[n^-]\mathbf{x}[n^-]^T.
\end{aligned}
$$

$\mathbf{\Phi}_{x,p}[n]$ is therefore computed by adding a "correcting term" to its temporal antecessor.

Similarly, we find a recursive expression for $\mathbf{z}_{x,p}[n]$:

$$
\mathbf{z}_{x,p}[n] = \lambda\mathbf{z}_{x,p}[n-1] + \mathbf{x}[n^-]x[n].
$$

In order to compute the least-squares-estimate $\widehat{\mathbf{a}}[n]$, we have to compute the inverse covariance matrix $\mathbf{\Phi}_{x,p}^{-1}[n]$. For convenience reasons, we set

$$
\mathbf{P}_{x,p}[n] \triangleq \mathbf{\Phi}_{x,p}^{-1}[n].
$$

By using the *Matrix inversion lemma*[17], we obtain a recursive representation for $\mathbf{P}_{x,p}[n]$ as well − the *Riccati equation* for the RLS algorithm:

$$\mathbf{P}_{x,p}[n] = \lambda^{-1}\mathbf{P}_{x,p}[n-1] - \lambda^{-1}\mathbf{k}[n]\mathbf{x}^T[n^-]\mathbf{P}_{x,p}[n-1], \qquad (4.17)$$

where $\mathbf{k}[n]$ is the gain vector:

$$\mathbf{k}[n] = \frac{\mathbf{P}_{x,p}[n-1]\mathbf{x}[n^-]}{\lambda + \mathbf{x}[n^-]^T\mathbf{P}_{x,p}[n-1]\mathbf{x}[n^-]} \,. \qquad (4.18)$$

Let us quickly derive a property of the gain vector which we will need afterward:

By multiplying (4.18) by its right-hand-side denominator, rearranging the result and then using (4.17), we obtain

$$
\begin{aligned}
\mathbf{k}[n] &= \lambda^{-1}\mathbf{P}_{x,p}[n-1]\mathbf{x}[n^-] - \lambda^{-1}\mathbf{k}[n]\mathbf{x}[n^-]^T\mathbf{P}_{x,p}[n-1]\mathbf{x}[n^-] \\
&= \underbrace{\left(\lambda^{-1}\mathbf{P}_{x,p}[n-1] - \lambda^{-1}\mathbf{k}[n]\mathbf{x}[n^-]^T\mathbf{P}_{x,p}[n-1]\right)}_{\mathbf{P}_{x,p}[n]} \mathbf{x}[n^-] \\
&= \mathbf{P}_{x,p}[n]\mathbf{x}[n^-].
\end{aligned}
\qquad (4.19)
$$

This result can be used as the definition of the gain vector $\mathbf{k}[n]$: It is the input data vector $\mathbf{x}[n^-]$ transformed by the inverse of the time-average covariance matrix $\mathbf{\Phi}_{x,p}[n]$.

Now that we have found a recursive representation of the inverse time-average covariance matrix and the gain vector, we want to develop a recursive computation algorithm for the coefficient vector estimate $\widehat{\mathbf{a}}[n]$.

By using the recursive expression of $\mathbf{z}_{x,p}[n]$ (4.15) we get

$$
\begin{aligned}
\widehat{\mathbf{a}}[n] &= \mathbf{P}_{x,p}[n]\,\mathbf{z}_{x,p}[n] \\
&= \lambda\mathbf{P}_{x,p}[n]\,\mathbf{z}_{x,p}[n-1] + \mathbf{P}_{x,p}[n]\mathbf{x}[n^-]x[n].
\end{aligned}
$$

Inserting the recursive representation of $\mathbf{P}_{x,p}[n]$ (4.14) yields

$$
\begin{aligned}
\widehat{\mathbf{a}}[n] &= \mathbf{P}_{x,p}[n-1]\mathbf{z}_{x,p}[n-1] - \mathbf{k}[n]\mathbf{x}[n^-]^T\mathbf{P}_{x,p}[n-1]\mathbf{z}_{x,p}[n-1] \\
&\quad + \mathbf{P}_{x,p}[n]\mathbf{x}[n^-]x[n] \\
&= \widehat{\mathbf{a}}[n-1] - \mathbf{k}[n]\mathbf{x}[n^-]^T\widehat{\mathbf{a}}[n-1] + \mathbf{P}_{x,p}[n]\mathbf{x}[n^-]x[n].
\end{aligned}
$$

Finally, by exploiting the relation (4.19) which we established before, we obtain the desired recursive equation for the update of the coefficient vector estimate $\widehat{\mathbf{a}}[n]$:

$$
\begin{aligned}
\widehat{\mathbf{a}}[n] &= \widehat{\mathbf{a}}[n-1] + \mathbf{k}[n]\left(\mathbf{x}[n] - \mathbf{x}[n^-]^T\widehat{\mathbf{a}}[n-1]\right) \\
&= \widehat{\mathbf{a}}[n-1] + \mathbf{k}[n]\xi[n],
\end{aligned}
\qquad (4.20)
$$

---

[17]See [Hay02] for the lemma (which is also sometimes referred to as *Woodbury's identity*) and details of this step.

where the term between the brackets is the *a-priori-estimation error* $\xi[n]$:

$$\xi[n] \triangleq x[n] - \widehat{\mathbf{a}}[n-1]^T \mathbf{x}[n^-]. \qquad (4.21)$$

Note the following important difference:

A-priori-estimation error or *one-step-prediction error* is given in (4.21). It represents the estimation error we make by estimating the current sample $x[n]$ based on the *old* least-squares coefficient estimate $\widehat{\mathbf{a}}[n-1]$ that was made one sample before.

A-posteriori-estimation error or *residual error* is, in general, different from the a-priori-estimation error and is given in (4.12). Here, we measure the error by estimating the current sample $x[n]$ by using *current* least-square estimate $\widehat{\mathbf{a}}[n]$.

Figure 4.2 illustrates the difference between the two errors showing the estimated samples in red and the given data points in black.
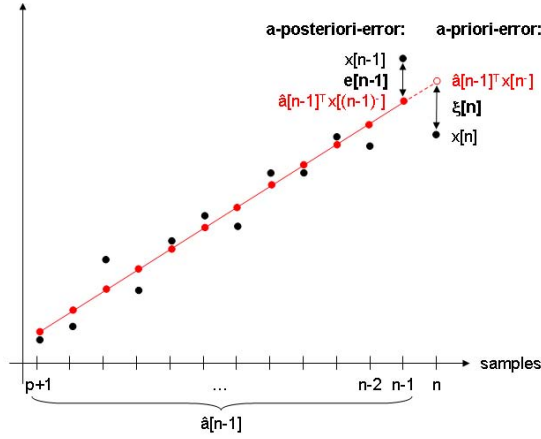
Figure 4.2: *A-priori- and a-posteriori-estimation errors. The residual error is given for sample $n-1$, the one-step-prediction error for sample n (using the estimate from sample $n-1$).*

It is important to note, however, that the optimum criterion leading to the RLS algorithm minimizes the cost function $\mathcal{E}[n]$ (4.13), which is based on the a-posteriori-estimation error $e[n]$ and *not* on the a-priori-estimation error $\xi[n]$.

4.2.1.3   Algorithm summary

Equations (4.17), (4.18), and finally (4.20) with (4.21) all together form the univariate RLS algorithm.

Algorithm 4.1 summarizes the calculation steps which we deduced before and shows the necessary initializations at the beginning of the algorithm. Note

that for numeric reasons[18], the gain vector is computed via the intermediate quantity $\pi[n]$.

Algorithm 4.1 Univariate RLS

---

i n i t i a l i z a t i o n :

$$\begin{aligned} \widehat{\mathbf{a}}[p] &= \mathbf{0} \\ \mathbf{P}_{x,p}[p] &= \delta^{-1}\mathbf{I}_{p\times p} \quad \begin{cases} \delta \text{ small} & \text{for high SNR} \\ \delta \text{ large} & \text{for low SNR} \end{cases} \end{aligned}$$

f o r   n=(p+1):N

$$\begin{aligned} \pi[n] &= \mathbf{P}_{x,p}[n-1]\mathbf{x}[n^-] \\ \mathbf{k}[n] &= \frac{\pi[n]}{\lambda + \mathbf{x}[n^-]^T\pi[n]} \\ \xi[n] &= x[n] - \widehat{\mathbf{a}}[n-1]^T\mathbf{x}[n^-] \\ \widehat{\mathbf{a}}[n] &= \widehat{\mathbf{a}}[n-1] + \mathbf{k}[n]\xi[n] \\ \mathbf{P}_{x,p}[n] &= \lambda^{-1}\mathbf{P}_{x,p}[n-1] - \lambda^{-1}\mathbf{k}[n]\mathbf{x}[n]^T\mathbf{P}_{x,p}[n-1] \end{aligned}$$

e n d   f o r

For the selection of the regularization parameter δ and the resulting convergence behavior see [Hay02]. In the following, we will simply set this parameter to unity.

4.2.2   Multivariate extension

The univariate RLS algorithm from subsection 4.2.1 takes a one-component input signal x[n]. As we have several input channels (selected by our channel algorithm), we cannot use this algorithm directly.

We therefore have a look at a multivariate extension proposed by [MSAW01] which does in fact nothing else than we did in subsection 4.1.5 for estimating the model coefficients $a_{\cdot;k,l}$ by a MMSE regression: stacking the channels and coefficients.

4.2.2.1   Preliminaries and theoretical considerations

Let $\mathbf{x}[n] = (x_1[n], ..., x_K[n]) \in \mathbb{R}^{N\times K}$ be a K-dimensional zero-mean signal. It is modeled by a time-dependent multivariate AR-model of order p

$$\mathbf{x}[n] = \sum_{i=1}^{p} \mathbf{A}_i[n]\mathbf{x}[n-i] + \epsilon[n],$$

where $\epsilon[n]$ is zero-mean white noise with covariance matrix $\boldsymbol{\Sigma}_\epsilon$.

---

[18]Once again, the interested reader is invited to consult [Hay02] for further details.

- We therefore have p coefficient *matrices* $\mathbf{A}_i[n] \in \mathbb{R}^{K \times K}$ which shall be stacked together in one single matrix:

$$\mathbf{A}[n] \triangleq (\mathbf{A}_1[n], ..., \mathbf{A}_p[n]) \in R^{K \times Kp}.$$

- Similarly, we build a stacked observation vector $\mathbf{X}[n^-]$ consisting of p signal samples at all lags $i = 1, ..., p$:

$$\mathbf{X}[n^-] \triangleq (\mathbf{x}[n-1], ..., \mathbf{x}[n-p]) \in R^{1 \times Kp}.$$

The normal equation for a multivariate least-squares problem is given[19] by

$$\widehat{\mathbf{A}} = \mathbf{R}_{\mathbf{x},p}^{-1} \mathbf{r}_{\mathbf{x},p} \tag{4.22}$$

with $\mathbf{R}_{\mathbf{x},p}^{-1}$ being the *multivariate covariance matrix* (3.4) and $\mathbf{r}_{\mathbf{x},p}$ the *multivariate covariance vector* (3.7) defined in section 3.1.

As we use stacked lines in our notation, we have to transpose equation (4.22). This leads to the normal equation of our multivariate recursive least-squares problem:

$$\widehat{\mathbf{A}}[n] = \mathbf{z}_{\mathbf{x},p}[n]^T \mathbf{P}_{\mathbf{x},p}[n], \tag{4.23}$$

where – analogically to the normal equation for the univariate case (4.16) – $\mathbf{P}_{\mathbf{x},p}[n]$ is the *inverse time-average multivariate covariance matrix* and $z_{x,p}[n]$ the *time-average multivariate covariance vector*.[20]

For a mathematically more detailed view on multiple least-squares estimation, the reader is referred to [Lüt93] or [BD91].

4.2.2.2   Algorithm summary

Given this notation, [MSAW01] proposes a multivariate extension to the univariate RLS algorithm. It strictly follows the univariate one and is summarized in algorithm 4.2.

The computation order, however, differs from the univariate case:

- First, the inverse time-average covariance matrix $\mathbf{P}_{x,p}$ is calculated directly using formula (4.17): Without using the pre-calculated gain vector, expression (4.18) is directly evaluated in (4.17).

- The gain vector $\mathbf{K}[n]$ is computed afterward using relation (4.19).

Again, we simply set the regularization parameter to unity, as it is proposed in [MSAW01].

Note that in this multivariate case we denote all entities by capital letters, as they all are matrices or stacked vectors. For a better understanding we list the dimensions and the meaning of each matricial entity which appears in algorithm 4.2 in table 4.2.

---

[19]This generalization was first published in [TB81].
[20]Compare the univariate definitions (4.14) and (4.15).

Algorithm 4.2 Multivariate RLS

---

i n i t i a l i z a t i o n :

$$\widehat{\mathbf{A}}[p] = \mathbf{0}$$

$$\mathbf{P}_{x,p}[p] = \delta^{-1}\mathbf{I}_{Kp \times Kp} \quad \begin{cases} \delta \text{ small} & \text{for high SNR} \\ \delta \text{ large} & \text{for low SNR} \end{cases}$$

f o r n=(p+1):N

$$\mathbf{H}[n] = \lambda^{-1}\mathbf{P}_{x,p}[n-1]$$

$$\mathbf{P}_{x,p}[n] = \mathbf{H}[n]\left(\mathbf{I}_{Kp \times Kp} - \frac{\mathbf{X}[n^-]^T\mathbf{X}[n^-]\mathbf{H}[n]}{\mathbf{X}[n^-]\mathbf{H}[n]\mathbf{X}[n^-]^T + 1}\right)$$

$$\mathbf{K}[n] = \mathbf{X}[n^-]\mathbf{P}_{x,p}[n]$$

$$\mathbf{\Xi}[n] = \mathbf{x}[n] - \mathbf{X}[n^-]\widehat{\mathbf{A}}[n-1]^T$$

$$\widehat{\mathbf{A}}[n] = \mathbf{A}[n-1] + \mathbf{\Xi}[n]^T\mathbf{K}[n]$$

e n d f o r

Matricial entity	Dimensions	Meaning
$\mathbf{H}[n]$	$Kp \times Kp$	-
$\mathbf{P}_{p,x}[n]$	$Kp \times Kp$	inverse time-average covariance matrix
$\mathbf{K}[n]$	$1 \times Kp$	gain vector
$\mathbf{\Xi}[n]$	$1 \times K$	a-priori-estimation error
$\widehat{\mathbf{A}}[n]$	$K \times Kp$	coefficient matrix estimate

Table 4.2: *Matricial entities in the multivariate RLS algorithm*

If the reader wishes a visualization of the typical behavior of the multivariate RLS algorithm, he is invited to jump to section 5.4, where we present regression results of test signals.

4.2.3   Coefficient estimation

Now that the reader is familiar with the RLS algorithm, we want to return to the initial aim: estimating our model coefficient $a_{.;k,l}[n]$ by means of recursive least-squares.

Despite the improvements from subsection 4.2.2, we still have a little problem: The multivariate RLS algorithm estimates the coefficients for all channels (thus $a_{.;1,l}[n], ..., a_{.;K,l}[n]$) at the same time. Using this method directly would mean that the same extrinsic channel set is used for all (intrinsic) channels. Of course, we do not want to accept this behavior and therefore proceed in the following way:

1. For each (intrinsic) channel x_k, we use − within a window − the multi-

variate RLS algorithm with an extrinsic channel set $\mathbb{L}_k$, which is constant within this window. $\mathbb{L}_k$ is determined by an adapted channel selection algorithm, which we are going to describe in the next subsection 4.2.4.[21]

2. When considering the result of the RLS algorithm (the coefficient estimate matrix $\widehat{\mathbf{A}}[n]$) we realize that we calculated too much: In fact, we can only use the line corresponding to our intrinsic channel, and we have to discard the rest.

A logic work-around saving computation time therefore is to slightly adapt the multivariate RLS algorithm and to calculate – instead of the whole matrix $\widehat{\mathbf{A}}[n]$ – *only the line* (corresponding to the current intrinsic channel) which we really need.[22]

In table 4.3 we show the new dimensions of the entities calculated in the adapted algorithm: As indicated in bold, only $\boldsymbol{\Xi}[n]$ and $\widehat{\mathbf{A}}[n]$ are slimmed. Note that the algorithm 4.2 itself is hereby not affected.

Matricial entity	Dimensions	Meaning
$\mathbf{H}[n]$	$Kp \times Kp$	-
$\mathbf{P}_{p,x}[n]$	$Kp \times Kp$	inverse time-average covariance matrix
$\mathbf{K}[n]$	$1 \times Kp$	gain vector
$\boldsymbol{\Xi}[n]$	$\mathbf{1 \times 1}$	**scalar** a-priori-estimation error
$\widehat{\mathbf{A}}[n]$	$\mathbf{1 \times Kp}$	coefficient **vector** estimate

Table 4.3: *Matricial entities in the adapted multivariate RLS algorithm*

3. We finally have to copy the estimated coefficients (corresponding to the intrinsic channel) onto the right place of the final coefficient estimation matrix $\widehat{\mathbf{A}}[n]$, which contains – for all intrinsic channels – the coefficients of all extrinsic channels and lags.

We prefer giving a practical example to describing this process theoretically, as an example quickly makes clear what happens in this step:

Let us assume we used the RLS algorithm for estimating the coefficients for the intrinsic channel $k = 1$: $\widehat{a}_{.;1,l}[n]$. We use an AR-model of order $p = 2$, and the channel selection algorithm chooses 2 extrinsic channels to be included in the regression: $x_2[n]$, $x_4[n]$. Our adapted RLS algorithm therefore takes three input channels and delivers the line vector $\widehat{\mathbf{B}}[n]$[23]

$$\widehat{\mathbf{B}}[n] \quad = \quad (\underbrace{\widehat{b}_{1;1,1}, \widehat{b}_{1;1,2}, \widehat{b}_{1;1,3}}_{\text{lag 1}} \mid \underbrace{\widehat{b}_{2;1,1}, \widehat{b}_{2;1,2}, \widehat{b}_{2;1,3}}_{\text{lag 2}})[n].$$

---

[21]There we also explain the use of windowing: The reader might wonder why we use it despite the application of the adaptive RLS algorithm.

[22]For simulations shown in section 5.5, this optimization brings computation time savings of about 2%.

[23]We exceptionally call it $\widehat{\mathbf{B}}[n]$ here, so that we can better distinguish in the following.

where the indices in the vector refer to the (sorted) channels used in the algorithm: the intrinsic channel x_1 has index 1, the first extrinsic channel x_2 has index 2, but the second extrinsic channel x_4 has channel 3 (*not* 4). We therefore clearly see that we have to copy these coefficients onto the right places by translating the indices of the subset used in the RLS algorithm to the ones of the initial reference system $1...K$.

Figure 4.3[24] illustrates this positioning for $K = 5$: As the intrinsic channel is x_1, only the first line of the final coefficient matrix $\widehat{\mathbf{A}}[n]$ is affected by this operation − whereas the second line will be filled in the next loop, when x_2 is the intrinsic channel.
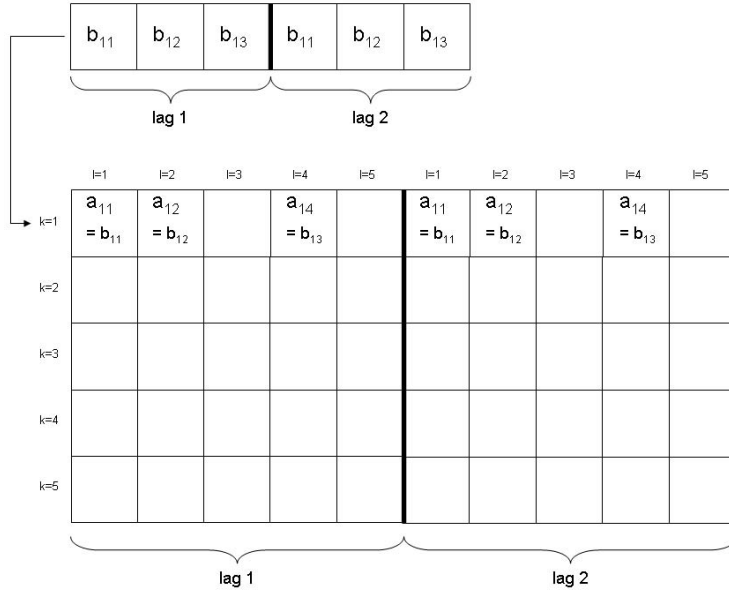
Figure 4.3: ***RLS coefficients positioning.*** *Estimated coefficients $\widehat{b}_{\cdot;1,l}[n]$ of the intrinsic channel $k = 1$ are copied onto correct positions in the final estimation matrix $\widehat{\mathbf{A}}[n]$.*

Note that this iterative approach is equivalent to a simultaneous solution, as described in subsection 4.2.2 in equation (4.23) of the normal equation

$$\widehat{\mathbf{A}}[n] = \mathbf{z}_{\mathbf{x},p}[n]^T \widetilde{\mathbf{P}}_{\mathbf{x},p}[n]$$

within a window.[25] Hereby, $\widetilde{\mathbf{P}}_{x,p}[n]$ is the inverse time-average covariance matrix masked in an appropriate way: By setting zeros on the respective places, we could simply "switch off" not-selected channels.

---

[24]For simplicity reasons, we omit the sampling index and the estimator hats in the figure as well.

[25]In section 3.5, we showed that this is the case for the time-invariant model.

However, it is not efficient in terms of computing time to use this method, because we would

1. first have to determine the optimal channel set for each channel (which delivers the estimated coefficients as well) within a window

2. then mask the matrix $\mathbf{P}_{\mathbf{x},p}[n]$ obtaining $\widetilde{\mathbf{P}}_{\mathbf{x},p}[n]$

3. and finally run the classic multivariate RLS algorithm with $\widetilde{\mathbf{P}}_{\mathbf{x},p}[n]$ in this window (although the coefficients are already known; they only have to be copied to the right places, as described above).

Nevertheless, it shows that we *do identify* a classic multivariate AR-model.

We finally want to indicate that the approach shown above uses the same temporal lags for both the intrinsic and the extrinsic channels. This means that we restrict our model from chapter 3 to the case $\mathbb{S} = \mathbb{Q}$.

4.2.4   Adaption of the channel selection algorithm

As already stated before, the extrinsic channel set $\mathbb{L}_k$ is determined within a window – as it is the case with the MMSE regression from section 4.1 – for each (intrinsic) channel x_k.

The RLS algorithm itself would redundantize the use of overlapping windows[26], but the channel selection algorithm needs them: It determines the extrinsic channel set by minimizing a cost function which uses data from a certain time interval (a window). Therefore, the result of this optimization is the same in this whole interval. We obtain a constant extrinsic channel set within a window.[27]

As the RLS algorithm automatically delivers the one-step-prediction error, there is no need to use the AIC criterion in the selection process any more: Its goal is to artificially correct the mistake made by taking the residual error as basis for the cost function.
Therefore, we adapt the initial algorithm 3.1 as follows:

- We use RLS regression in the algorithm instead of MMSE.

- For each intrinsic channel x_k we directly take the *variance of the one-step-prediction-error* as the cost function which is to be minimized by the optimal extrinsic channel set $\mathbb{L}_k$.

Algorithm 4.3 presents the channel selection algorithm for RLS with the modification mentioned above. Of course, all advantages and weak points of the initial channel selection algorithm 3.1, which we discussed in section 3.3, do not change and all positive and negative consequences occur here as well.[28]

---

[26]For the windowing technique see subsection 4.1.1.

[27]Furthermore, the RLS algorithm needs – while stepping through the samples of a window – a constant set of channels implying a constant number of estimates. Otherwise it would not be able to perform the update of new estimates with the help of old ones with every sample.

[28]As we discussed this topic in detail in section 3.3, we do not address this issue here.

Algorithm 4.3 Channel selection with RLS algorithm

```
for  each  regressand  x_k[n],  k=1..K
      extrinsic  channel  set:  L = {}
      extension  pool:  P = {1,..K}\{k}
      loop
            calculate  V = Var(a-priori-error)  with  channel  set  L
            for  each  i  in  P
                  calculate  V(i)  with  channel  set  L_i = {L, i}
            end  for
            i_opt = arg  min  V(i)
            if  V(i_opt) < V
                  extend  extrinsic  channel  set:  L = {L, i_opt}
                  reduce  extension  pool:  P = P \ i_opt
                  continue  loop
            else
                  exit  loop
            end  if
      end  loop
end  for
```

4.2.5 Coefficient stream assembly

As mentioned in the subsection before, we still use windowing in order to be able to apply the channel selection algorithm.[29]

However, as the RLS algorithm delivers a stream of coefficient matrices $\mathbf{A}[n]$ within each window, the temporal resolution has changed: Its resolution is not window-to-window, but sample-to-sample. We would therefore wish to profit from this increased temporal resolution and create one continuous coefficient stream out of the N_{win} different ones.

Herby, we have to face two difficulties:

Overlapping windows First of all, the windows overlap each other – a wanted consequence of how we designed our windowing method.[30]
Therefore we have to find an appropriate way of reconstructing one data stream: the inverse operation of windowing.

Abrupt statistical changes Furthermore, the used channel set abruptly changes from window to window, and so does the behavior of the coefficient estimates and the derived EIPR-measure. However, if we want to find a physiologically meaningful description of the epileptic seizure status, we need a "smooth" measure which does *not* depend on arbitrary window overlaps.

---

[29]In the following, we therefore use the notation defined in subsection 4.1.1 when speaking about windows.
[30]See figure 4.1 in subsection 4.1.1.

Therefore we also have to be careful to assemble the different data streams in a "smooth" way.

A possible solution satisfying these two constraints is inspired by the *overlap-add-method* described in [Dob01] and [Smi99]:

1. We multiply each window with a *window function*. This window function is designed to fade in the coefficients at the beginning of the current window as smoothly as possible and to fade them out at the end of the window in the same way.
   A possible way to assure the smoothness of the data (continuity of the data *and* continuity of all derivatives) is the use of the *raised cosine window function*

$$f[n] = \begin{cases} 0 & n \in [1,\, L_z] \\ \frac{1}{2}\left(1 - \cos\left[\frac{n-(L_r+1)}{L_r-1}\pi\right]\right) & n \in [L_z+1,\, L_z+L_r] \\ 1 & n \in [L_z+L_r+1,\, L_{win}-L_r] \\ 1 - \frac{1}{2}\left(1-\cos\left[\frac{n-(L_w-L_r+1)}{L_r-1}\pi\right]\right) & n \in [L_{win}-L_r+1,\, L_{win}], \end{cases}$$

   where L_{win} is the length of the window in samples, L_r is the length of the roll-on/roll-off-phase and L_z is the length of zero-padding.
   Zero-padding at the beginning of each window is important due to the initial transient effect of the RLS algorithm: The first coefficient estimates of each window, $A[i]$ with i small, have to be discarded – which is assured by zero-padding.
   Figure 4.4 on page 54 shows an example of the raised cosine window function for $L_z = 100$, $L_r = 200$, $L_{win} = 1000$.
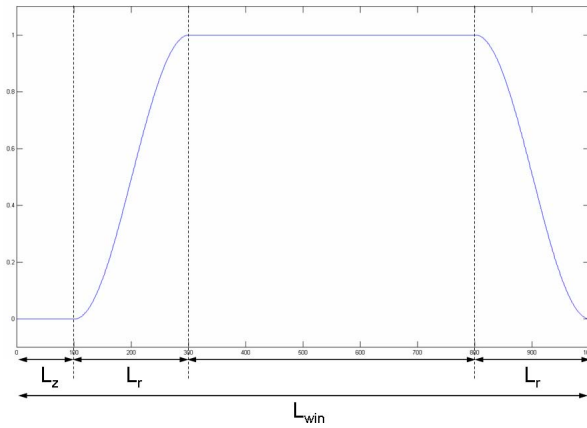
Figure 4.4: *Raised-cosine window function.* *The current window is faded in and out in a smooth way; the initial samples are ignored due to zero-padding.*

2. Then we sum up (overlapping) windows and normalize the result. A crucial point hereby is that the overlapping windows themselves must be designed in such a way that the result of the window functions added up is constant: Whenever one window is faded in, another one has to be faded out. Otherwise we would weight some parts of a window more than others and prioritize them. Of course, the beginning and the end of the final continuous coefficient stream have to be discarded, as the described method causes a transient effect at the beginning and the end.
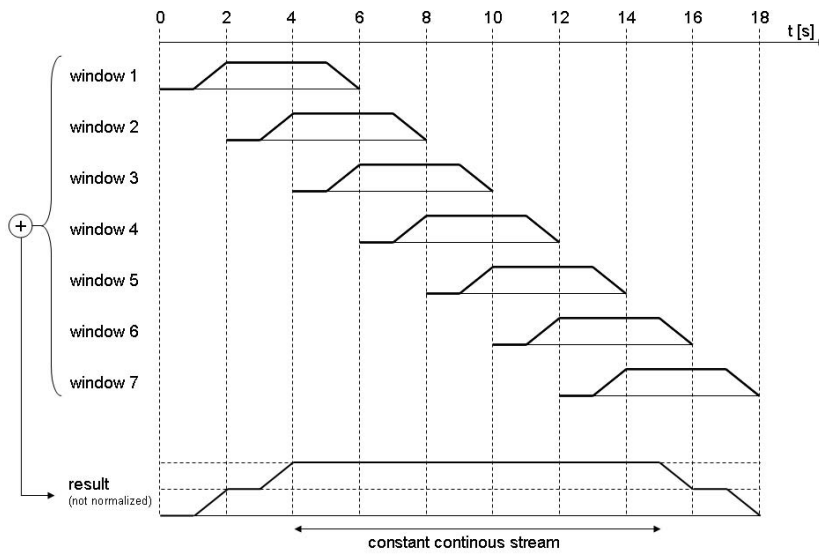
Figure 4.5: *Assembly of the continuous coefficient stream. Due to the design of the window functions, the overlapping windows can be re-assembled to a continuous stream. Note the transient effect at the beginning and the end of the stream.*

The above figure 4.5 illustrates the case of all coefficients in all windows constantly set to unity – we therefore see the pure addition of the window function in different windows.[31] Parameters are exemplarily set for illustration purposes: design parameters $T_{win} = 6$s, $T_{ol} = 4$s and window function design parameters $L_{win} = T_{win} \cdot f_s = 6$s $\cdot$ 128Hz $= 768$ and $L_z = L_r = 1$s $\cdot$ 128Hz $= 128$.

The raised cosine is hereby displayed as a combination of straight lines for simplicity reasons; furthermore the resulting stream is not normalized[32] for a better understanding. Note the mentioned transient effect.

---

[31] As we multiply the window function with coefficients set to 1, we obtain the window function itself in each window.

[32] In the illustrated case, we would obviously have to divide the resulting stream by 2.

4.2.6 Stream dependency measures

Now that we have described how we obtain *one continuous* stream of coefficients $\widehat{a}_{.;k,l}[n]$, we have to ask ourselves how to calculate time-dependent variance terms $\sigma^2_{\dot{x}_k}[n]$ and $\sigma^2_{\vec{x}_{k,l}}[n]$ out of them.

Let us first assume we know how to do it: Once we have got them, we can easily compute the EIPR measures $\eta_{k,l}[n]$ as described in section 3.4. We simply use equation (3.18) for calculating the EIPR – with the difference that we do not do so for each window, but *for each sample.* We obtain an (obviously time-dependent) *stream of EIPR-measures*:

$$\eta_{k,l}[n] = \frac{\sigma^2_{\vec{x}_{k,l}}[n]}{\sigma^2_{\dot{x}_k}[n]}\ . \tag{4.24}$$

We will see in section 5.5 that this stream is indeed physiologically meaningful, changing its properties in a "smooth" way.

Let us go back to the initial problem of calculating time dependent variances of the partial estimation contribution terms and mention two aspects:

- Unfortunately, the method developed in subsection 3.4.1 cannot be applied here: If we wanted to use it, we would have to take the whole coefficient stream as input – which does not make any sense at all, as we would not have any temporal resolution any more.

- Of course we could (more or less arbitrarily) choose windows and calculate our variance terms within them. But by following this approach, we would lose our increased temporal resolution whose elaboration has cost us so much effort.

Therefore, we must ask ourselves: How can we calculate variances for each single sample in a meaningful way without losing too much accuracy?
The approach proposed by us is simple and inspired by the weighted recursive least squares:

1. First of all, we have to calculate intrinsic ($\dot{x}_k[n]$) and extrinsic estimation contributions ($\vec{x}_{k,l}[n]$) out of the (estimated) coefficients $\hat{a}_{.;k,l}[n]$ for each sample n: According to model equations 3.10 and 3.12, we compute a stream of contributions[33]

$$\begin{aligned}
\dot{x}_k[n] &= \sum_{s=1}^{p}\widehat{a}_{s;k,k}[n]x_k[n-s] \\
\vec{x}_{k,l}[n] &= \sum_{l\in\mathbb{L}_k}\sum_{s=1}^{p}\widehat{a}_{s;k,l}[n]x_l[n-s].
\end{aligned} \tag{4.25}$$

---

[33]Note that in the case of RLS regression an estimated model coefficient $\widehat{a}_{s;k,l}[n]$ is determined by four factors: lag s, sample index n and the two channels k,l.

2. Then we calculate *weighted variances* of the partial estimation contribution terms (4.25), which point out the present sample and extenuate the influence of samples in the past. This follows the idea of the weighted RLS algorithm: the farther in the past, the more these samples are "forgotten". We denote the weighted variances by the same symbols as the time-independent ones (3.15) and (3.16), but add the sample index.
They are calculated within windows of length l (samples), which we typically set to $l = 256$ samples.[34]
The *time-dependent intrinsic variance* is therefore given by

$$\sigma_{\dot{x}_k}^2[n] \quad \triangleq \quad \frac{1}{\sum_{i=n-l+1}^{n} \lambda^{n-i}} \sum_{i=n-l+1}^{n} \left(\dot{x}_k[i] - \overline{\dot{x}_k[n]} \right)^2 \lambda^{n-i} \quad (4.26)$$

and analogically the *time-dependent partial extrinsic variance* as

$$\sigma_{\vec{x}_{k,l}}^2[n] \triangleq \frac{1}{\sum_{i=n-l+1}^{n} \lambda^{n-i}} \sum_{i=n-l+1}^{n} \left(\vec{x}_{k,l}[i] - \overline{\vec{x}_{k,l}[n]} \right)^2 \lambda^{n-i}, \qquad (4.27)$$

with l being the length of the sliding window.
In both cases, λ is the forgetting factor used in the RLS algorithm and $\overline{\dot{x}_k[n]}$ respectively $\overline{\vec{x}_{k,l}[n]}$ the weighted mean of partial estimation contributions at sample n:

$$\overline{\dot{x}_k[n]} \quad \triangleq \quad \frac{1}{\sum_{i=n-l+1}^{n} \lambda^{n-i}} \sum_{i=n-l+1}^{n} \dot{x}_k[i] \lambda^{n-i}$$

$$\overline{\vec{x}_{k,l}[n]} \quad \triangleq \quad \frac{1}{\sum_{i=n-l+1}^{n} \lambda^{n-i}} \sum_{i=n-l+1}^{n} \vec{x}_{k,l}[i] \lambda^{n-i}. \qquad (4.28)$$

Note that means (4.28) *do* depend on the current sample n, as they are calculated within the window (of length l) determined by the sample index n. However, they are constant in the sums in expressions (4.26) and (4.27) (for each n).

At the very end we want to state that the time-dependent total extrinsic variance $\sigma_{\vec{x}_k}^2[n]$, which is needed for the computation of a time-dependent TEIPR[35], would not be that easy to calculate:

As we showed in section 3.4, the total extrinsic variance (3.17) is *not* the sum of the corresponding partial extrinsic variances (3.16). Of course, this is the case with the time-dependent extrinsic variance as well − therefore we are not allowed to calculate it from time dependent partial extrinsic variance terms (4.27) we know.

However, as we do not need TEIPR in this work, we do not further investigate this topic.

---

[34] As table 4.1 indicates, a typical value of the weighting factor $\lambda = 0.995$ implies a forgetting time of $\tau_\lambda = 2$s, corresponding to 250 samples.
[35] TEIPR is defined in (3.19).

Chapter 5

Results

In this chapter we are finally going to present results obtained by the application of the two methods mentioned in chapter 4, which are based on MMSE and RLS regresssion.

We start with a short description of the data basis and then present results of the initial method proposed by [HK07]. Afterward we question the hypothesis of short-term stationarity and check the ECoG recordings for (short-term) stationarity. Finally, after the illustration of a typical behavior of the RLS algorithm thanks to test signals, we are going to present results of our advanced regression method based on RLS.

5.1 Data basis

The ECoG recordings analyzed in this chapter come from a patient suffering from temporal lobe epilepsy. 28-channel ECoG signals were recorded at a sampling frequency of 256Hz with reference to an electrode outside the seizure focus. After removal of line interference by an appropriate notch filter at 50Hz, they were downsampled to 128Hz.

In this chapter, we evaluate ECoG data recorded on 17/10/2002 from 12:45:36 to 12:47:36 – seizure onset was 15 seconds after the start of recording time at 12:45:51.

Figure 5.1 indicates the electrode positions together with the channel numbers which we use in our calculations.[1]
According to the clinicians' visual inspection of the raw ECoG signals, the temporal and spatial evolution of the seizure was as follows:

1. Seizure onset at 12:45:51 on the right hemisphere at electrodes D6, D7 (channels 26, 27).

2. Propagation to electrodes D4, D5 (channels 24, 25) and C1-C6 (channels 15-20).

---

[1]We showed a surgeon's draft of this electrode configuration in figure 1.5 in section 1.2.
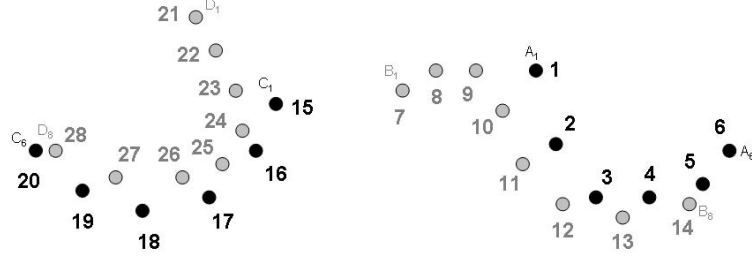
Figure 5.1: *Channel numbers of implanted ECoG electrodes.*
Channel number used in calculations is given next to the respective elec-
trode. Roman letters indicate the clinical identification of the electrodes.

3. At 12:46:04 propagation to the left hemisphere to electrodes B4, B5 (chan-
   nels 10, 11).

4. At 12:47:00 end of the seizure on the left hemisphere at electrodes B4, B5
   (channels 10, 11).

We are going to use these diagnostic findings as a reference description for a
comparison with our results throughout the following section.

5.2   MMSE results

We start our seizure propagation analysis with the initial method proposed by
[HK07], based on MMSE in windows where the signal is assumed to be short-
time stationary.

5.2.1   Choice of model order

As mentioned in section 3.3, the channel selection algorithm does not optimize
the temporal lag order, but one constant model order has to be chosen manually.
Therefore we have to find the appropriate extrinsic and intrinsic lag sets $\mathbb{S}$ and
$\mathbb{Q}$. For simplicity reasons, we set $\mathbb{S} = \mathbb{Q} = [1..p]$.

   In order to find the optimal p, we subsequently perform the channel selection
with increasing lags sets from $\mathbb{S} = \mathbb{Q} = [1..1]$ up to $\mathbb{S} = \mathbb{Q} = [1..10]$. Per channel
and window, we determine the optimal lag order: As described in algorithm 3.1,
the channel selection algorithm adds channels until the information criterion is
minimized (for given lag sets). We therefore obtain such a minimum in each
step of our iterative lag set enlargement, and we choose the lag order which is
associated to the minimum of these minima.

   For comparison reasons, we also used AIC as an information criterion in the
channel selection algorithm.

   Figure 5.2 shows the distribution of optimal temporal lags for both AIC and
BIC. We obtain the same order of magnitude, but AIC indicates – as expected
– slightly higher lag orders than BIC.
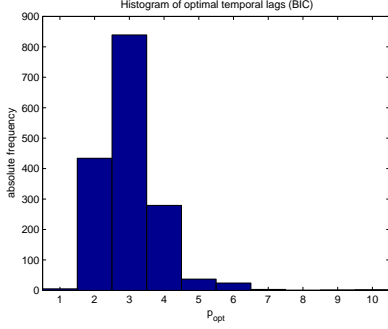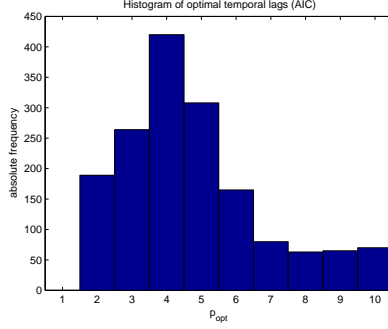
Figure 5.2 (a)   Figure 5.2 (b)

Figure 5.2: ***Distribution of optimal temporal lags (MMSE).*** *His-togram of optimal temporal lags for BIC in figure 5.2 (a), for AIC in figure 5.2 (b).*

The results of these simulations are in accordance with the ones shown in literature: By application of the AIC criterion, [KKB04] chooses $p = 4$ for multivariate autoregressive modeling of EEG data, [KDTB01] takes $p = 5$ and [KMK+03] (at a higher sampling frequency of $f_s = 200$Hz) $p = \{6, ...8\}$.

Anyway, as [FBK85] indicates, the results of autoregressive modeling of EEG/ECoG data are rather insensitive to the exact model order: As the minimum of the information criterion is broad and flat, we have a certain range of acceptable values. Therefore we choose $p = 4$ for our calculations, resulting in the temporal lag sets $\mathbb{S} = \mathbb{Q} = [1..4]$. According to the indications of BIC in figure 5.2 (a), we might slightly overestimate the model, but we prefer to do so rather than underestimate it.[2]

5.2.2   Model verification

Now that we have determined a realistic lag order, we want to examine results of the MMSE regression. Parameters used in the computation are shown in table 5.1: Temporal lag sets were determined in the last subsection 5.2.1, window parameters are manually chosen with respect to sufficient estimation quality of the empiric covariance matrix.[3]

In the following, we are going to examine results in an exemplary way: We study channel 1 (which is outside the seizure focus throughout the recording time) and channel 11 (affected from 12:46:04 on) on the left hemisphere and channel 16 (affected before 12:46:04) on the right hemisphere.[4]

---

[2]For a detailed discussion on the mathematical consequences of under- and overfitting compare [BD91].

[3]Compare the discussion in subsection 4.1.5 on this topic.

[4]For the exact positions of the electrodes see figure 5.1.

	Parameter	Value
MMSE regression	Extrinsic temporal lag set	$\mathbb{Q} = [1..4]$
	Intrinsic temporal lag set	$\mathbb{S} = [1..4]$
Window design	Window length	$T_{win} = 6$s
	Time of window overlap	$T_{ol} = 4$s

Table 5.1: *Parameters used in MMSE regression*

5.2.2.1   Plot of residual errors

We consider plots of residual errors in window 20, which lies right in the middle of the time of epileptic activity and contains recordings from seconds 38 to 44 (which is 23 to 29 seconds after seizure onset).

Figure 5.3 shows three exemplary channels in this 6s-lasting window: on top channel 1, in the middle channel 11 and at the bottom channel 16. Channel 1 is almost not affected by epileptic activity at this time, whereas channel 11 (being in the seizure focus during these 6s) represents typical spikes indicating strong epileptic activity. Channel 16 shows rhythmic activity.

The respective original signal is displayed in blue and the residual errors in red in all three plots of figure 5.3.
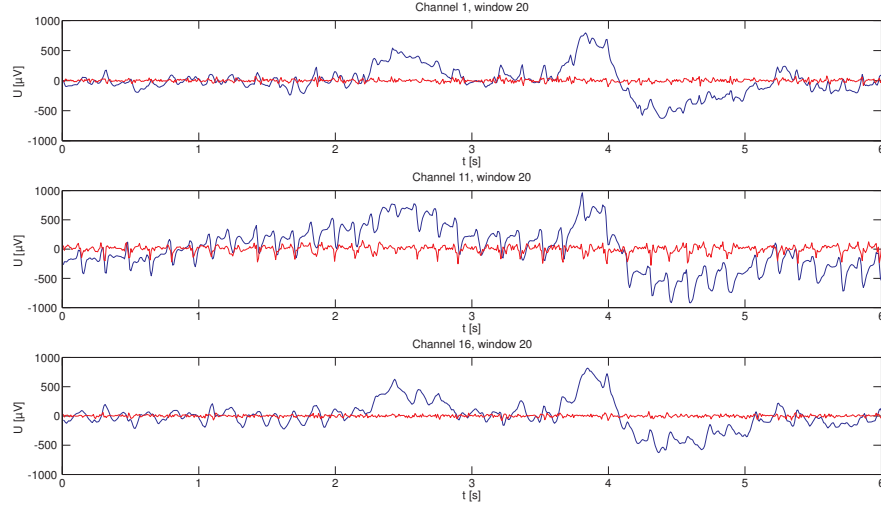
Figure 5.3: *Residual errors (MMSE). Residuals of channels 1, 11 and 16 (in red) in exemplary 6s-window 20.*

As channels 1 and 16 are almost not affected by epileptic activity in this window, the respective residual error is smaller than the one of channel 11 which is in the seizure focus at that time.

5.2.2.2   Extrinsic channel set

Before studying the regression quality of our model, it might be interesting to have a quick look at the number of extrinsic channels chosen by the channel selection algorithm.

Figure 5.4 displays the evolution of the extrinsic channel set from one window to another of channels 1, 11 and 16 for the whole recording period of 120s.
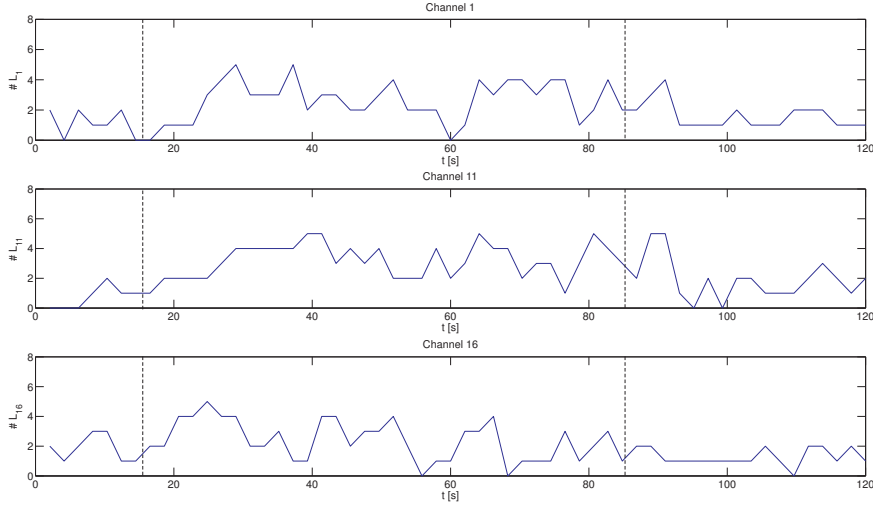
Figure 5.4: *Evolution of the extrinsic channel set* $\mathbb{L}_k$ *(MMSE). Window-wise evolution for channels 1, 11 and 16 during the full 120 seconds. Begin and end of seizure indicated by dashed lines.*

In the time of epileptic activity this number goes up to 5, whereas it is reduced down to 0 in interictal periods. As table A.3 in annex A illustrates, the algorithm selects approximately 2 extrinsic channels per intrinsic channel on average.

If we ran the channel selection algorithm with the same parameters but with AIC as information criterion instead of BIC, the average size of the extrinsic channel set would be four to five times larger, as table A.3 indicates.

Therefore, BIC does not only indicate a smaller lag order (as shown in subsection 5.2.1), but also selects fewer channels. This leads to a low-dimensional regression model justifying our preference for BIC.

5.2.2.3   Regression fit

The well-known *coefficient of correlation* R^2 is a measure of goodness of fit of a regression model.[5]

As we are interested in the coefficient of correlation explaining the model fit

---

[5] If needed, the reader finds more details in [Hac05] or in any other book on econometrics.

for each channel k, we define R_k^2 channel-wise (for each window):

$$R_k^2 \triangleq 1 - \frac{SS_{err_k}}{SS_{tot_k}} \,. \tag{5.1}$$

Hereby, SS_{err_k} is the *residual sum of squares* of channel k and SS_{tot_k} the *total sum of squares* of channel k. They are given by

$$
\begin{aligned}
SS_{err_k} &\triangleq \sum_{n=1}^{L_{win}} \left(x_k[n] - \widehat{x}_k[n]\right)^2 \\
SS_{tot_k} &\triangleq \sum_{n=1}^{L_{win}} \left(x_k[n] - \overline{x}_k\right)^2
\end{aligned}
$$

with $\overline{x}_k$ being the mean of channel k and n the lag index within the given window.

Figure 5.5 shows the temporal evolution of R_k^2 (5.1) for the three exemplary channels (arranged as before).
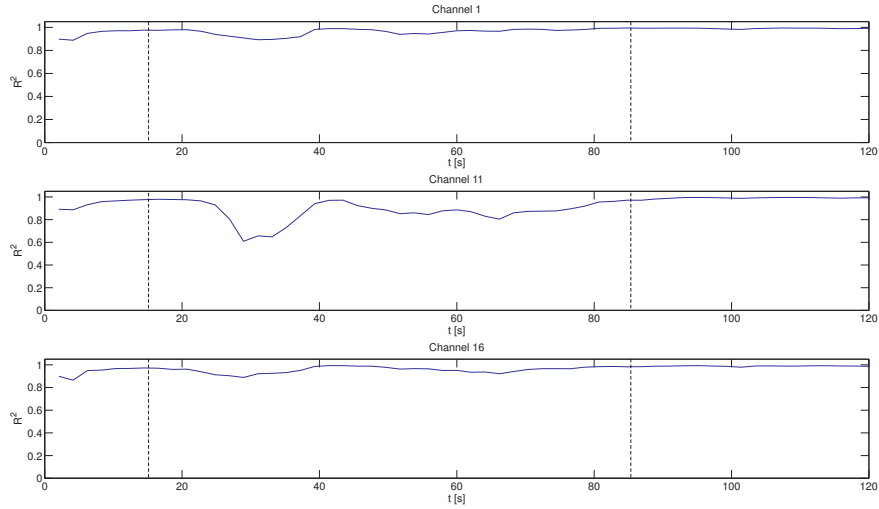
Figure 5.5: ***Evolution of*** R_k^2 ***(MMSE).*** *Window-wise evolution for channels 1, 11 and 16 during the full 120 seconds. Begin and end of seizure indicated by dashed lines.*

Explanatory power of the model is clearly given, but in times of epileptic activity the arising instationarity apparently reduces the estimation quality (as it is the case for channel 11).

Table A.1 in annex A shows the average coefficient of correlation for all 28 channels.

5.2.2.4 Autocorrelation of residual errors

Finally, we also want to analyze whether the model is well specified meaning that the residual terms are not autocorrelated.

Figure 5.6 illustrates the temporal evolution of the Durbin-Watson statistic for the three exemplary channels: as before, channel 1 is placed on top, channel 11 in the middle and channel 16 at the bottom.
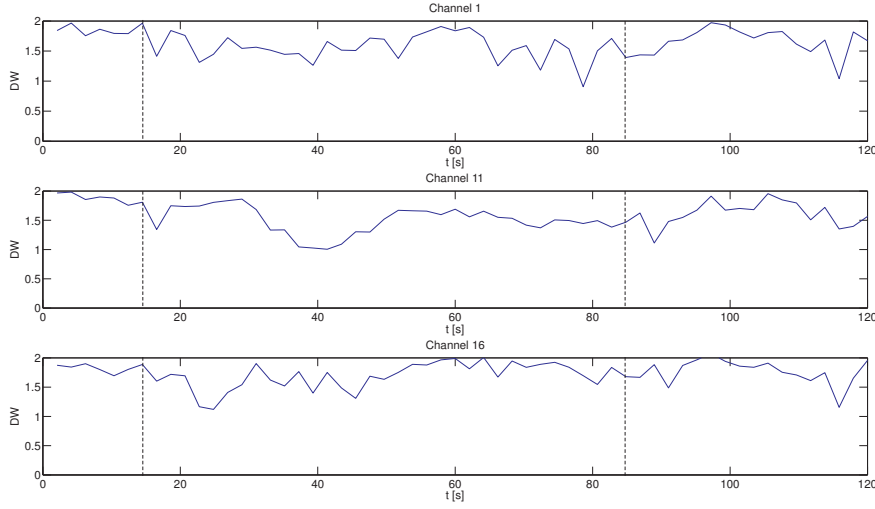
Figure 5.6: *Evolution of the Durbin-Watson-statistic (MMSE).* *Window-wise evolution for channels 1, 11 and 16 during the full 120 seconds. Begin and end of seizure indicated by dashed lines.*

The residual terms of all channels are autocorrelated of order 1, as the DW statistic constantly stays below the value of 2. The situation for the other channels is similar, as table B.2 in annex A indicates: It shows the average values of the Durbin-Watson statistic for all 28 channels, which are all significantly below 2.

In order to check for autocorrelation of higher order, we apply the *Box-Ljung test* to the residuals of the three channels 1, 11 and 16 in window 20, which we plotted in figure 5.3. Calculations were performed with the free statistical software package *R*, rejection or acceptance of the null hypothesis is done by interpretation of the *p-value*.

Table 5.2 on page 66 summarizes the results of the Box-Ljung test:[6] The residuals of all considered channels are autocorrelated up to lag order 4.[7]

Therefore, instead of going further into the results of this modeling approach, we would rather have a look at our hypothesis of short-term stationarity.

---

[6] See [JB76] for statistical details of the Box-Ljung test.
[7] The similar *Box-Pierce test* (described in [BP70]) delivers exactly the same results.

Channel 1 (window 20)				
Lag order	$\mathcal{H}_0$	**p-value**	**Interpretation**	**Result**
2	independence	$2.7 \cdot 10^{-6}$	$\mathcal{H}_0$ rejected	autocorrelation
3	independence	$1.1 \cdot 10^{-8}$	$\mathcal{H}_0$ rejected	autocorrelation
4	independence	$1.3 \cdot 10^{-12}$	$\mathcal{H}_0$ rejected	autocorrelation

Channel 11 (window 20)				
Lag order	$\mathcal{H}_0$	**p-value**	**Interpretation**	**Result**
2	independence	$< 2.7 \cdot 10^{-6}$	$\mathcal{H}_0$ rejected	autocorrelation
3	independence	$< 2.2 \cdot 10^{-6}$	$\mathcal{H}_0$ rejected	autocorrelation
4	independence	$< 2.2 \cdot 10^{-6}$	$\mathcal{H}_0$ rejected	autocorrelation

Channel 16 (window 20)				
Lag order	$\mathcal{H}_0$	**p-value**	**Interpretation**	**Result**
2	independence	$2.7 \cdot 10^{-5}$	$\mathcal{H}_0$ rejected	autocorrelation
3	independence	$7.3 \cdot 10^{-11}$	$\mathcal{H}_0$ rejected	autocorrelation
4	independence	$6.2 \cdot 10^{-15}$	$\mathcal{H}_0$ rejected	autocorrelation

Table 5.2: *Box-Ljung test on higher-order residual autocorrelation (MMSE)*

5.3   Signal instationarity

Due to the results shown in section 5.2 the question arises: Do we really have short-time-stationarity of the raw ECoG signals outside seizure periods? And even if so, can we accept that this property is violated, more than ever, during a seizure?

Therefore we want to see whether our hypothesis of short-time-stationarity is sufficiently realistic.

5.3.1   Periodogram of the transfer function

In order to get a first impression on the "degree of stationarity", we have a look at the *periodogram of the transfer function*. As described in section 2.1, we fit an AR model to the signal, calculate the transfer function and then plot frequency over time.

The fitting of the AR model is automatically done by a Matlab software package called *ARFIT*.[8] The transfer function is then calculated by fast-Fourier-transformation (FFT) window-wise (window design parameters: $T_{win} = 2$s and $T_{ol} = 1$s) and is plotted – frequency over time[9] – in false color representation:

---
[8]This package is described in detail in [SN01]; the theoretical background for the optimized algorithm developed by the authors themselves is explained in [NS01].

[9]The periodogram shows the frequency band up to 64Hz (half of the sampling frequency).

Red indicates strong contribution at this frequency, dark blue low importance.

Figure 5.7 shows the periodogram of the transfer function of channel 11 of our raw ECoG recordings: recording time 17/10/2002 12:45:36 - 12:47:36, seizure onset 15 seconds after the start.
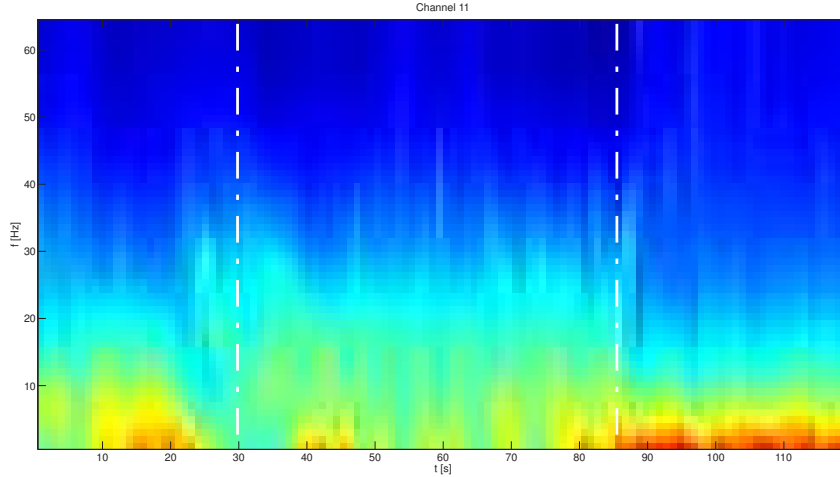
Figure 5.7: *Periodogram of channel 11 of ECoG recording. Begin and end of epileptic activity on channel 11 indicated by dash-dotted lines: agitated structural changes in ictal period.*

We observe ribbons of frequency areas; however, they are not continuous over time, but abruptly changed or interrupted. These structural breaks (of the red ribbon in the low-frequency band, for example) occur so often that we cannot divide the signal into a small number of segments each representing a constant regime. Furthermore, the first structural breaks occur before seizure onset: They appear within the first 15 seconds.

5.3.2 Statistical tests

Although the periodogram of the transfer function has already given us a first indication that the hypothesis of short-time-stationarity might be violated during seizures as well as interictally, we want to consult a number of statistical tests. We are not going to address the mathematical background of the tests in detail, but only describe their aim: For the statistical background, we are going to refer the reader to the respective papers.

We apply the following two tests to our preprocessed ECoG data:

Dickey-Fuller test is named after the statisticians Dickey and Fuller who developed this test in the 1970s. It tests whether a unit root is present in an autoregressive model of order 1:

$$x[n] = \rho x[n-1] + \epsilon[n],$$

where $\epsilon[n]$ is normally distributed white noise: $\epsilon[n] \sim \mathrm{NID}(0, \sigma^2)$.

If this was the case, we would have $|\rho| = 1$, and the model would be instationary.[10] Therefore, the null hypothesis of the Dickey-Fuller-test is instationarity: $\mathcal{H}_0 : |\rho| = 1$.

Apart from this version of the AR-model, the Dickey-Fuller-test can also check for stationarity of an AR-model with drift

$$x[n] = \mu + \rho x[n-1] + \epsilon[n]$$

and of an AR-model with drift and trend

$$x[n] = \mu + \beta n + \rho x[n-1] + \epsilon[n].$$

These three versions of the basic Dickey-Fuller test are explained in detail in [DF79].

Note that an extension for higher-order autoregressive models exists, which is termed *Augmented Dickey-Fuller test (ADF)*. It is described in [SD84].

KPSS test is named after the statisticians Kwiatkowski, Phillips, Schmidt and Shin. As the Dickey-Fuller test fails to reject the null hypothesis of instationarity in certain cases, they developed an alternative test in the early 1990s. Although it also tests for a unit root in time series, its null hypothesis is inverse to the one of the Dickey-Fuller test. It assumes that the time series can be decomposed into the sum of a deterministic trend ξn, a random walk $r[n]$ and a stationary error $\epsilon[n]$:

$$x[n] = \xi n + r[n] + \epsilon[n].$$

The random walk is

$$r[n] = r[n-1] + u[n]$$

with $u[n] \sim \mathrm{NID}(0, \sigma^2)$. Therefore, the null hypothesis of stationarity is simply: $\mathcal{H}_0 : \sigma^2 = 0$, $\xi = 0$.

For a detailed elaboration of the test see [KPSS92].

The following tables 5.3 and 5.4 show the results of the statistical tests mentioned above applied to 6s-lasting windows.

As in section 5.2, we exemplarily chose channels 1 and 11 on the left hemisphere and channel 16 on the right.[11] Calculations were done with the free statistical software package R: Apart from the standard Dickey-Fuller test and the KPSS test we also performed an Augmented Dickey-Fuller test with lag order 9.[12] Rejection or acceptance of the null hypothesis is done by interpretation of the *p-value*.

---

[10]Of course, it would be "even more" instationary if $|\rho| > 1$.

[11]For their location see figure 5.1.

[12]R suggests an optimal lag order: $p = (L_{win} - 1)^{1/3}$. As we have $L_{win} = T_{win} \cdot f_s = $ 6s $\cdot$ 128Hz $= 768$, R chooses $p = 9$.

Table 5.3 summarizes the results of window 20, which lies right in the middle of the time of epileptic activity:[13] All three channels 1, 11 and 16 are concordantly considered to be instationary. This is not surprising, because changes of the epileptic seizure status cause instationarity, which we discussed at the beginning of section 4.1.

Channel 1 (window 20)				
Test	$\mathcal{H}_0$	**p-value**	**Interpretation**	**Result**
DF	instationarity	0.5064	$\mathcal{H}_0$ not rejected	instationarity
ADF	instationarity	0.3157	$\mathcal{H}_0$ not rejected	instationarity
KPSS	stationarity	< 0.01	$\mathcal{H}_0$ rejected	instationarity

Channel 11 (window 20)				
Test	$\mathcal{H}_0$	**p-value**	**Interpretation**	**Result**
DF	instationarity	0.0900	$\mathcal{H}_0$ not rejected	instationarity
ADF	instationarity	0.3460	$\mathcal{H}_0$ not rejected	instationarity
KPSS	stationarity	< 0.01	$\mathcal{H}_0$ rejected	instationarity

Channel 16 (window 20)				
Test	$\mathcal{H}_0$	**p-value**	**Interpretation**	**Result**
DF	instationarity	0.5696	$\mathcal{H}_0$ not rejected	instationarity
ADF	instationarity	0.3009	$\mathcal{H}_0$ not rejected	instationarity
KPSS	stationarity	< 0.01	$\mathcal{H}_0$ rejected	instationarity

Table 5.3: *Stastical tests on stationarity – ictal ECoG recordings*

For comparison reasons, we also want to have a look at preictal signal recordings and consider window 5.[14]

The results of the different tests in table 5.4 on page 70 are alarming: Although we examine preictal recordings (we could hope that at least they would be stationary), only channel 11 is concordantly considered to be stationary, whereas the Dickey-Fuller and KPSS test do not agree on the stationarity of channels 1 and 16.

5.3.3 Conclusion

The results of these examinations are appallingly clear and lead to one single conclusion: Our hypothesis of short-time-stationarity 2' from section 4.1 is simply *not valid*. As we do deal with instationary signals, we unfortunately cannot use MMSE, but have to apply another, more appropriate method.

---

[13]It contains recordings from seconds 38 to 44 (which is 23 to 29 seconds after seizure onset).

[14]It contains recordings from seconds 8 to 14 (this is 7 to 1 seconds before seizure onset).

Channel 1 (window 5)				
Test	$\mathcal{H}_0$	**p-value**	**Interpretation**	**Result**
DF	instationarity	< 0.01	$\mathcal{H}_0$ rejected	stationarity
ADF	instationarity	< 0.01	$\mathcal{H}_0$ rejected	stationarity
KPSS	stationarity	0.0204	$\mathcal{H}_0$ rejected	instationarity

Channel 11 (window 5)				
Test	$\mathcal{H}_0$	**p-value**	**Interpretation**	**Result**
DF	instationarity	< 0.01	$\mathcal{H}_0$ rejected	stationarity
ADF	instationarity	< 0.01	$\mathcal{H}_0$ rejected	stationarity
KPSS	stationarity	> 0.10	$\mathcal{H}_0$ not rejected	stationarity

Channel 16 (window 5)				
Test	$\mathcal{H}_0$	**p-value**	**Interpretation**	**Result**
DF	instationarity	< 0.01	$\mathcal{H}_0$ rejected	stationarity
ADF	instationarity	< 0.01	$\mathcal{H}_0$ rejected	stationarity
KPSS	stationarity	< 0.01	$\mathcal{H}_0$ rejected	instationarity

Table 5.4: *Statistical test on stationarity – preictal ECoG recordings*

5.4   RLS with test signals

In section 4.2 we presented such an appropriate method: *exponential recursive least-squares estimation*. Before applying it to our ECoG data, we want to have a look at the typical behavior of this adaptive algorithm.

First of all, we create an artificial test signal $\mathbf{x}[n]$ lasting for 120s consisting of two channels. This is done with the help of the Matlab package ARFIT.[15] For comparison reasons, we suppose a hypothetical sampling frequency of $f_s = 128$Hz – therefore we have $\mathbf{x}[n] \in \mathbb{R}^{15360 \times 2}$.

We use two bivariate autoregressive models (5.2) and (5.3) of order 2 for the construction of this test signal $\mathbf{x}[n]$:

$$\mathbf{x}[n] \quad = \quad \begin{cases} \dot{\mathbf{x}}[n] & n \in [1, ..., 7680] \\ \ddot{\mathbf{x}}[n] & n \in [7681, ...15360] \end{cases}.$$

- The first bivariate AR model is defined as

$$\dot{\mathbf{x}}[n] \triangleq \dot{\mathbf{w}} + \dot{\mathbf{A}}_1 \dot{\mathbf{x}}[n-1] + \dot{\mathbf{A}}_2 \dot{\mathbf{x}}[n-2] + \dot{\epsilon}[n] \tag{5.2}$$

---

[15]We presented it in subsection 5.3.1. ARFIT can be used for both simulating an autoregressive process and for fitting a signal to an AR model.

with coefficients

$$\dot{\mathbf{w}} \triangleq \begin{pmatrix} 0.25 \\ 1 \end{pmatrix} \quad \dot{\mathbf{A}}_1 \triangleq \begin{pmatrix} 0.4 & 1.2 \\ 0.3 & 0.7 \end{pmatrix} \quad \dot{\mathbf{A}}_2 \triangleq \begin{pmatrix} 0.35 & -0.3 \\ -0.4 & -0.5 \end{pmatrix}$$

and $\dot{\epsilon}[n]$ being normally distributed, zero-mean white noise with its covariance matrix

$$\dot{\mathbf{\Sigma}}_{\dot{\epsilon}} \quad \triangleq \quad \begin{pmatrix} 1 & 0.5 \\ 0.5 & 1.5 \end{pmatrix}.$$

- In order to cause an instationarity, the second AR model is of the same order
$$\ddot{\mathbf{x}}[n] \triangleq \ddot{\mathbf{w}} + \ddot{\mathbf{A}}_1\ddot{\mathbf{x}}[n-1] + \ddot{\mathbf{A}}_2\ddot{\mathbf{x}}[n-2] + \ddot{\epsilon}[n], \qquad (5.3)$$
but the matricial coefficients differ:

$$\ddot{\mathbf{w}} \triangleq \dot{\mathbf{w}} \qquad \ddot{\mathbf{A}}_1 \triangleq \begin{pmatrix} -0.1 & 0.3 \\ 0.5 & 0.9 \end{pmatrix} \qquad \ddot{\mathbf{A}}_2 \triangleq \begin{pmatrix} -0.35 & 0.7 \\ -0.4 & -0.5 \end{pmatrix}.$$

Again, $\ddot{\epsilon}[n]$ is normally distributed white noise with its covariance matrix $\ddot{\mathbf{\Sigma}}_{\ddot{\epsilon}} \triangleq \dot{\mathbf{\Sigma}}_{\dot{\epsilon}}$.

In the next step, we use the exponential RLS algorithm (with $p = 3$ for control reasons) for fitting this instationary signal.[16] By setting the forgetting factor $\lambda < 1$, the RLS algorithm can adapt itself to the signal leading to a smaller one-step prediction error. However, at the moment when the instationarity occurs, the one-step prediction error explodes, because the RLS algorithm naturally needs some time for re-adjusting itself to the new regime.

When choosing a value of $\lambda < 1$, we encounter two opposite tendencies:

- Smaller values of λ lead to a better adaptability of the algorithm, because samples far in the past (belonging to another regime) are "forgotten" faster.

- On the other hand, the smaller the number of samples in memory, the poorer the estimation quality of the second-order statistics used.

Therefore, the final estimation quality is a trade-off between adaptability and use of information contained in the signal. When plotting the variance of the one-step prediction error over λ, the resulting graph is a parabola, attaining a certain minimum which depends on data properties.

Figure 5.8 on page 72 illustrates this behavior for the test signal $\mathbf{x}[n]$ defined above: The minimum of the one-step prediction error − and therefore the "optimal" estimation quality − is obtained for $\lambda \approx 0.995$.
After these preliminaries, we finally want to show some results of the RLS algorithm. For illustration purposes, we performed the estimation of our test

---

[16]Hereby, the channel selection algorithm is disabled − we force the algorithm to use all (two) channels.
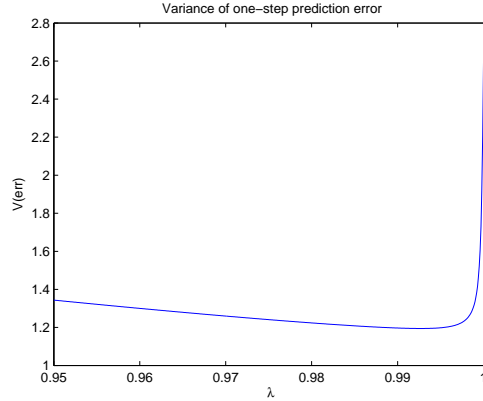
Figure 5.8: *Forgetting factor λ vs. variance of one-step prediction error. Minimum for $\lambda \approx 0.995$.*

signal $\mathbf{x}[n]$ with two characteristic values of the forgetting factor: $\lambda = 1$ and $\lambda = 0.995$.

Figures 5.9 and 5.10 below show the coefficient paths for the estimation of channel 1. In each picture, the first row shows the extrinsic coefficients $a_{i;1,2}$ ($a_{1;1,2}$ in the first column, $a_{2;1,2}$ in the middle, $a_{3;1,2}$ in the right column) and the second depicts the intrinsic coefficients $a_{i;1,1}$ (lags as before).

- Figure 5.9 illustrates the case of $\lambda = 1$, where the RLS algorithm performs in fact a simple OLS estimation.
  The coefficient paths shown reflect this property: In the first regime, the algorithm delivers a good approximation – the estimated coefficients of lags 1 and 2 converge to the imposed values. Furthermore, as we defined an AR model of order 2, $a_{3;i,j} = 0$, the respective estimated coefficients approach the value of zero correctly.
  However, after the appearance of instationarity, the algorithm cannot adapt itself to the new statistics. Coefficient paths only change slowly into the right direction, as more and more samples of the new regime are loaded into memory and the statistics of this new regime gain more and more influence.[17]

- Figure 5.10 illustrates the case of $\lambda = 0.995$, which is close to the optimal forgetting factor shown in figure 5.8 above.
  The algorithm now progressively adapts itself to the test signal $\mathbf{x}[n]$: In the first regime, all estimated coefficients oscillate around the imposed values. Then, the algorithm immediately reacts to the instationarity, and the estimated coefficients converge – with different speed and quality – to their new values, where they oscillate again.

---

[17] Note that although we used two successive AR models of order two for the construction of the test signal $\mathbf{x}[n]$, the coefficients $a_{3;i,j}$ do not even slowly approach zero after instationarity.
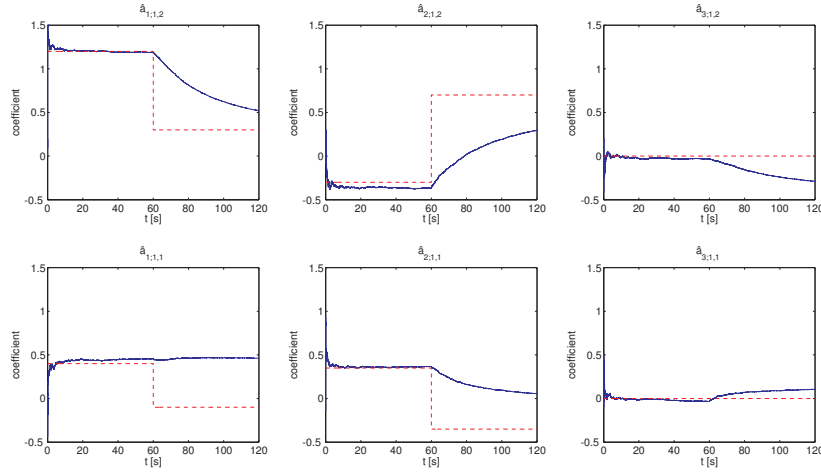
Figure 5.9: *Test signal coefficient paths for* $\lambda = 1$. *Only slow adaptation of the estimated coefficients after appearance of instationarity.*
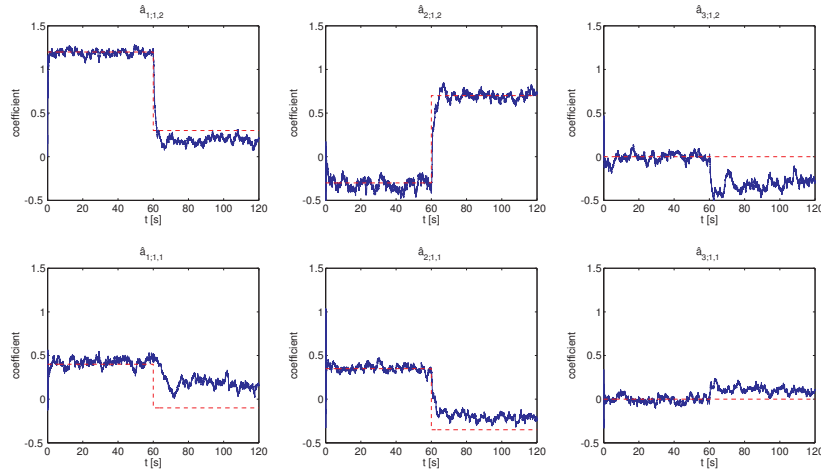
Figure 5.10: *Test signal coefficient paths for* $\lambda = 0.995$. *Immediate convergence of the estimated coefficients to new regime after appearance of instationarity.*

We also want to compare the one-step-prediction errors resulting from the estimations performed above. As figure 5.11 on page 74 illustrates, the one-step prediction error explodes in both cases at the moment of instationarity. However, it immediately returns to its average value in case of $\lambda = 0.995$ (in the left graph), whereas it does so only slowly in the case of $\lambda = 1$ (in the right graph).
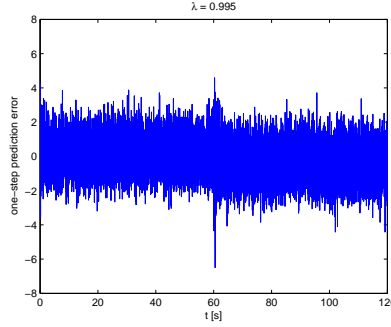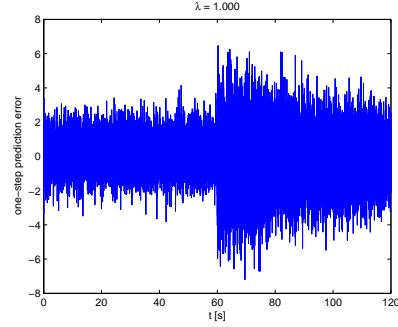
Figure 5.11 (a)　　　　　　　　　　　*Figure 5.11 (b)*

Figure 5.11: *One-step estimation errors of test signal. After instationarity, immediate return to the average value of the one-step prediction error for $\lambda = 0.995$ in figure 5.11 (a); compared to a slow return in case of $\lambda = 1$.*

5.5　RLS results

After this short introduction into the typical behavior of the RLS algorithm, we want to examine our advanced RLS-based regression method and present results of a potential epileptic seizure propagation analysis.

Throughout this section we are going to use a forgetting factor of $\lambda = 0.995$, as optimal values of λ found by simulation are in this order of magnitude. This value was obtained by minimizing the variance of the one-step estimation error: We showed similar results for test signals in figure 5.8.

5.5.1　Choice of model order

First of all, we have to determine a reasonable lag order for the RLS algorithm.

In order to find a sufficiently optimal p, we proceed as if we had the MMSE regression in section 5.2: We subsequently perform the channel selection with increasing lag order from $p = 1$ to $p = 10$. Per channel and window we determine the optimal p: As described in algorithm 4.3, the channel selection algorithm adds channels until – this is the only difference to section 5.2 – the one-step prediction error is minimized. Nevertheless, the result is the same as in section 5.2: We obtain such a minimum in each step of our iterative lag order enlargement, and we choose the lag order which is associated to the minimum of these minima.

Figure 5.12 shows the distribution of optimal temporal lags: Similarly to the simulation using MMSE regression with BIC as information criterion,[18] lags 3 and 4 are chosen most frequently.

---

[18]Compare figure 5.2 on page 61.
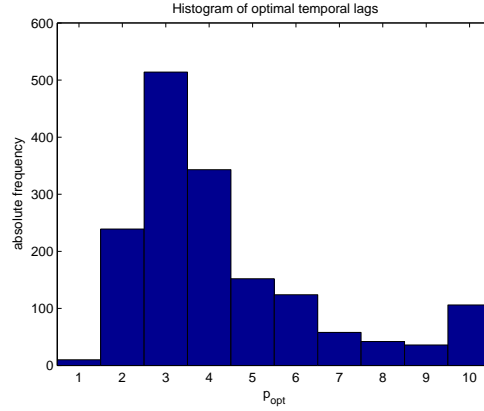
Figure 5.12: *Distribution of optimal temporal lags (RLS).*

We therefore set – in perfect accordance with the model based on MMSE regression – the lag order to $p = 4$ for the following computations.[19]

5.5.2 Model verification

Now that we have determined a realistic lag order, we want to examine results of the RLS regression. Parameters used in the computation are shown in table 5.5: The lag order was determined in subsection 5.5.1, window parameters are chosen accordingly to the ones for MMSE in table 5.1,[20] and parameters for the design of the window function (used in coefficient stream assembly) are chosen manually.[21]

	Parameter	Value
RLS algorithm	Forgetting factor	$\lambda = 0.995$
	Lag order	$p = 4$
Window design	Window length	$T_{win} = 6\text{s}$
	Time of window overlap	$T_{ol} = 4\text{s}$
Window	Time of roll-on/off	$T_r = 1.5\text{s}$
function design	Time of zero-padding	$T_z = 0.5\text{s}$

Table 5.5: *Parameters used in RLS regression*

As in section 5.2, we consider channels 1 (which is outside the seizure focus throughout the recording time) and 11 (affected from 12:46:04 on) on the left hemisphere and 16 (affected before 12:46:04) on the right hemisphere.[22]

---

[19]Again, we might risk overestimating the model, but we prefer to do so rather than underestimate it.

[20]We use windows for the channel set selection: compare algorithm 4.3 in subsection 4.2.4.

[21]Consult figure 4.5 on page 55 for an illustration of the coefficient stream assembly.

[22]Again, for the exact positions of the electrodes see figure 5.1.

5.5.2.1   Plot of residual errors

First of all we consider plots of residual errors during a 6s-lasting period corresponding to the time covered by window 20.[23] This allows comparison with the residual errors obtained by MMSE (in figure 5.3).

Figure 5.13 shows the original signal in blue and the residual error in red. Following the convention of section 5.2, we put channel 1 on top, channel 11 in the middle and channel 16 at the bottom.
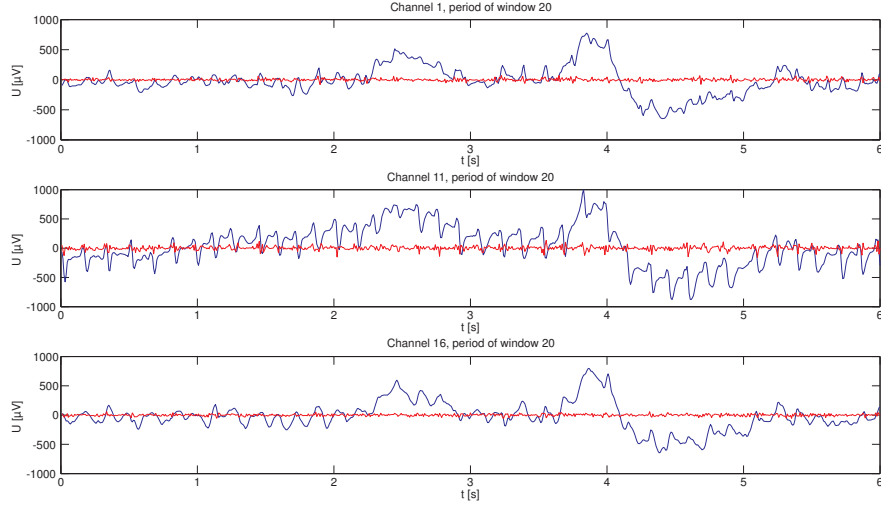
Figure 5.13: *Residual errors during 6s-period (RLS)*. *Residual errors of channels 1, 11 and 16 in the exemplary 6s-lasting window 20.*

Again, as channels 1 and 16 are almost not affected by epileptic activity during these six seconds, the respective residual error is smaller than the one of channel 11 (being in the seizure focus). However, thanks to the adaptive capacity of the RLS algorithm, this difference is less evident than in the case of MMSE regression in figure 5.3.

As our method based on RLS delivers a stream of coefficients, we are able to plot the stream of residual errors of the three exemplary channels over the whole recording period. Figure 5.14 on page 77 demonstrates that the residual errors stay small throughout all different regimes in these 120 seconds.

5.5.2.2   Extrinsic channel set

As in section 5.2, we study the evolution of the extrinsic channel sets of our three exemplary channels before examining the regression quality of our model.

Figure 5.15 plots the number of selected (extrinsic) channels from one window to another.[24]

---

[23]In order to remind the reader: It contains recordings from seconds 38 to 44 (23 to 29 seconds after seizure onset).

[24]We *do* use windows for determining the channel set; compare subsection 4.2.4.
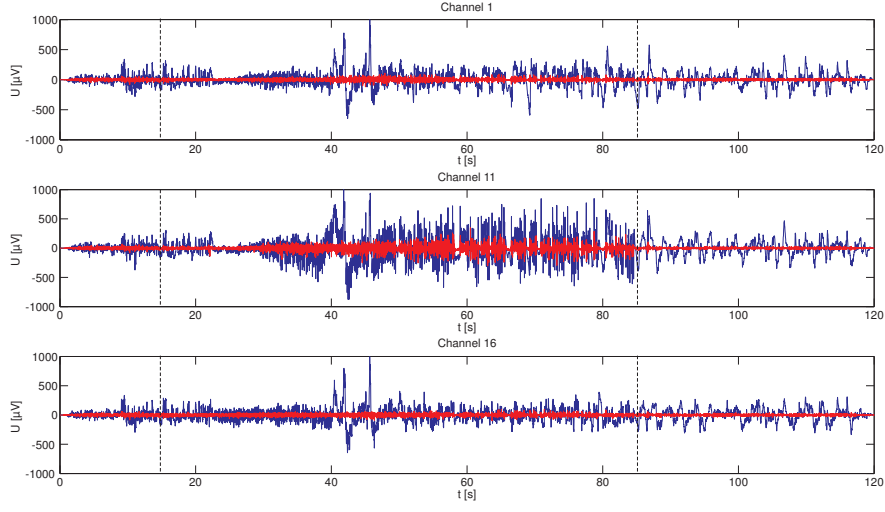
Figure 5.14: *Residual errors of full recording time (RLS).* *Residual errors of channels 1, 11 and 16 (in red) stay small throughout the full 120 seconds. Begin and end of seizure indicated by dashed lines.*
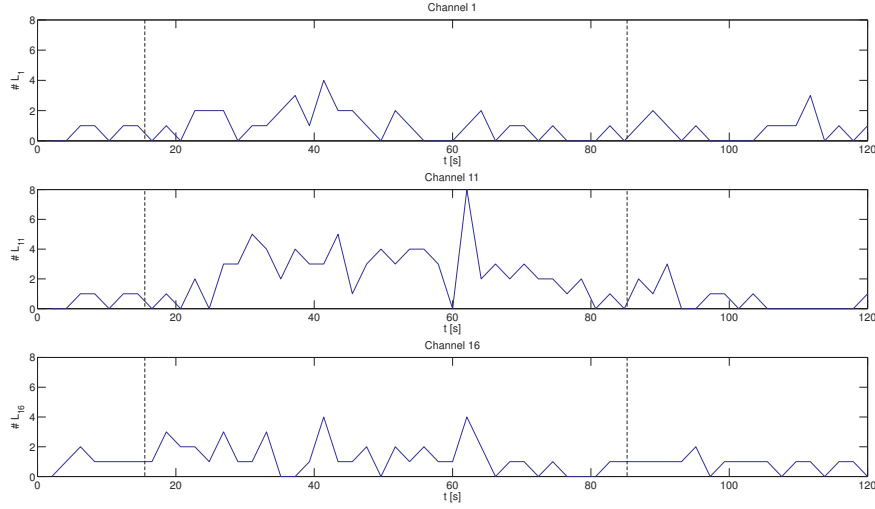
Figure 5.15: *Evolution of extrinsic channel set $\mathbb{L}_k$ (RLS).* *Sample-wise evolution for channels 1, 11 and 16 during 120s: increased values in times of epileptic activity. Begin and end of seizure indicated by dashed lines.*

These results are in accordance with the ones obtained by the channel selection algorithm based on MMSE using BIC as information criterion (shown in figure 5.4). Although on average fewer channels are selected now, we speak about the same order of magnitude.

We obtain a "clearer" picture now, as the evolution of selected channels is more distinct: In interictal periods, the algorithm chooses hardly any extrinsic

channels – the respective intrinsic channel is only explained by its own past. In ictal windows, however, a large number of extrinsic channels is selected leading to an enhanced extrinsic explanation of the signal.

Consider, for instance, $\mathbb{L}_{11}$ from seconds 30 to 70 in figure 5.15 above: We have intensified ictal channel selection.[25]

Table B.6 in annex B details the average (temporal) values of the extrinsic channel set for all 28 channels.

5.5.2.3   Regression fit

For evaluating the RLS regression we consider two different coefficients of correlation, both defined channel-wise for the whole data stream:

In-sample coefficient of correlation is defined similarly to (5.1) in section 5.2:

$$R_k^2[n] \quad \triangleq \quad 1 - \frac{SS_{err_k}[n]}{SS_{tot_k}[n]}, \qquad\qquad (5.4)$$

where the residual sum of squares and the total sum of squares of channel k are both calculated within exponentially weighted windows.[26]

Out-of-sample coefficient of correlation is a better measure of the regression quality proposed in [DH05]. It is – in strict analogy to (5.4) – given by

$$\widetilde{R}_k^2[n] \quad \triangleq \quad 1 - \frac{\widetilde{SS}_{err_k}[n]}{SS_{tot_k}[n]}, \qquad\qquad (5.5)$$

but uses the *sum of squares of the one-step-prediction error* of channel k (which we intuitively denote by $\widetilde{SS}_{err_k}$) instead of the residual sum of squares of channel k SS_{err_k}.
Again, nominator and denominator are calculated within exponentially weighted windows.

Figure 5.16 shows the temporal evolution of R_k^2 (in-sample) in red and of $\widetilde{R}_k^2$ (out-of-sample) in blue for the three exemplary channels (arranged as usual).

We see that the model has excellent explanatory power. Even in times of epileptic activity, the rising instationarity degrades the estimation quality only little – and especially to a lesser extent than in the case of the MMSE regression (in figure 5.5).

Note that (by definition) the in-sample coefficient takes higher values in instationary regimes than the out-of-sample version.

Table B.1 in annex B details the average values of the in-sample and out-of-sample coefficient of correlation for all 28 channels.

---

[25]Compare section 5.1: The seizure focus moves to channel 11 at 12:46:04, which is 28 seconds after the recording start.

[26]Compare the exponentially-weighted-windows-based computation of the variance terms in subsection 4.2.6.
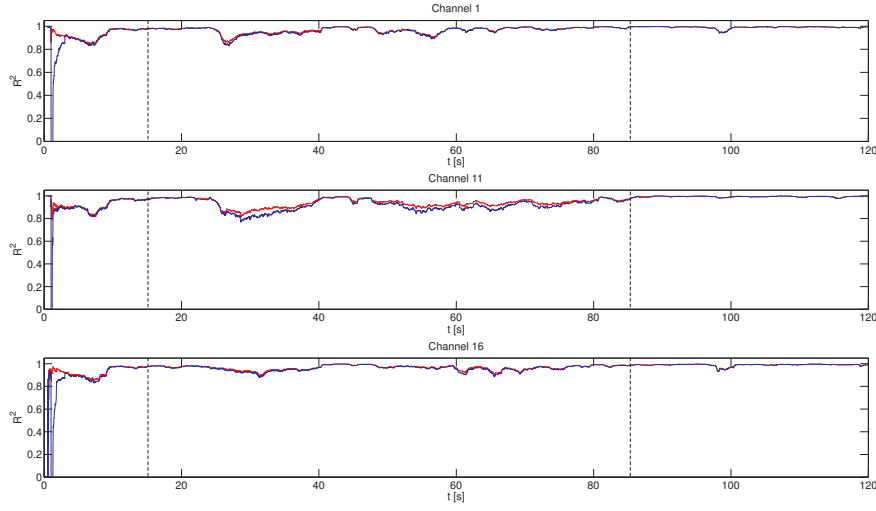
Figure 5.16: *Evolution of R_k^2 and $\widetilde{R}_k^2$ (RLS)*. Sample-wise evolution of in-sample-R^2 (red) and out-of-sample-R^2 (blue) for channels 1, 11 and 16 during 120s: Tolerable quality fall-off in times of epileptic activity. Begin and end of seizure indicated by dashed lines.

5.5.2.4 Autocorrelation of residual errors

After these promising results, we finally want to see whether the use of RLS instead of MMSE in our regression method could correct the problem we were facing in section 5.2: high autocorrelation of the residual terms.
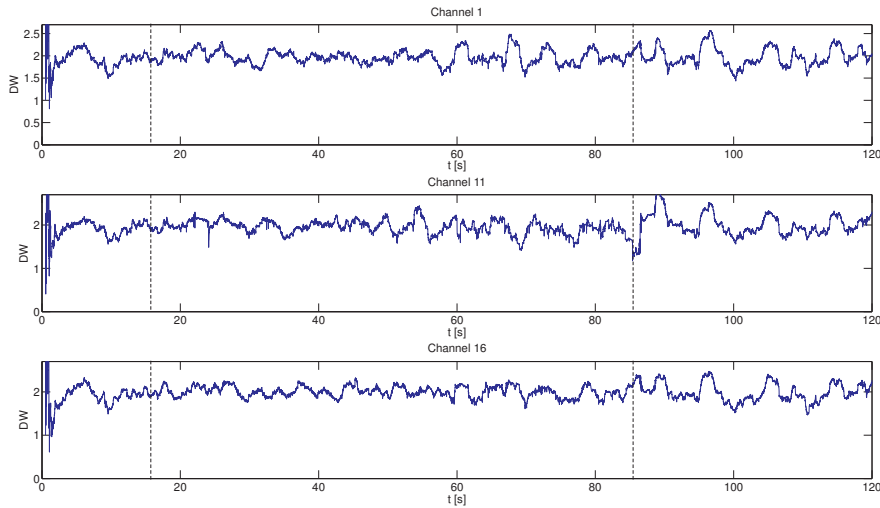
Figure 5.17: *Evolution of Durbin-Watson statistic (RLS)*. Sample-wise evolution for channels 1, 11 and 16 during 120s: no autocorrelation even in times of epileptic activity. Begin and end of seizure indicated by dashed lines.

Figure 5.17 above shows the evolution of the Durbin-Watson statistic for the three channels 1, 11 and 16 (plots on usual positions).

Thanks to the use of the adaptive RLS algorithm, the statistic of all three channels now oscillates around the value of 2, indicating no or only weak residual autocorrelation of order 1. In other words: our model is sufficiently well specified.

As we did in section 5.2, we exemplarily examine the residuals on higher-order autocorrelation. In order to be able to compare the results to the ones from section 5.2 (given in table 5.2), we only consider the recording time covered by window 20. Residuals of the RLS regression in this 6s-window are plotted in figure 5.13.

Table 5.6 summarizes the results of the Box-Ljung test applied to the residuals in this time interval. As usual, computations are done with the free statistical software package R, and the obtained p-values are interpreted.

Channel 1 (time corresponding to window 20)				
Lag order	$\mathcal{H}_0$	p-value	Interpretation	Result
2	independence	0.2503	$\mathcal{H}_0$ accepted	no autocorrelation
3	independence	0.4255	$\mathcal{H}_0$ accepted	no autocorrelation
4	independence	0.3052	$\mathcal{H}_0$ accepted	no autocorrelation

Channel 11 (time corresponding to window 20)				
Lag order	$\mathcal{H}_0$	p-value	Interpretation	Result
2	independence	0.3469	$\mathcal{H}_0$ accepted	no autocorrelation
3	independence	0.4337	$\mathcal{H}_0$ accepted	no autocorrelation
4	independence	< 0.01	$\mathcal{H}_0$ rejected	autocorrelation

Channel 16 (time corresponding to window 20)				
Lag order	$\mathcal{H}_0$	p-value	Interpretation	Result
2	independence	0.9118	$\mathcal{H}_0$ accepted	no autocorrelation
3	independence	0.9370	$\mathcal{H}_0$ accepted	no autocorrelation
4	independence	0.6695	$\mathcal{H}_0$ accepted	no autocorrelation

Table 5.6: *Box-Ljung test on higher-order residual autocorrelation (RLS)*

As we see, the Box-Ljung test confirms − as the Durbin-Watson statistic did before in figure 5.17 − the amelioration of our model.[27]

---

[27] However, if we apply the Box-Ljung test to the whole 120s-lasting stream of residuals (of channels 1, 11 and 16), it rejects the hypothesis of independence for the lag orders shown in table 5.6.

5.5.3 Interpretation of results

In this subsection we study results obtained by our model which we checked for correctness in the last subsection: We consider the influence of epileptic activity (increased synchronization effects) on the evolution of the coefficient paths, the one-step prediction error and the partial estimation contributions.

Afterward we finally show the temporal evolution of our synchronization measure EIPR.

We limit ourselves – for the sake of clarity and shortness – to the consideration of channel 11, which shows epileptic activity from seconds 30 to 85.

5.5.3.1 Coefficient paths

As already done in section 5.4 in the case of test signals, we now consider the evolution of the coefficient paths derived from ECoG recordings.

Figure 5.18 shows the assembled stream of coefficients paths of our AR(4) regression model (with different channel sets in each window): In the first row, one finds all extrinsic coefficients from lag 1 (on the left) up to lag 4 (on the right) – and in the second the intrinsic coefficients in the same order (from lag 1 on the left to lag 4 on the right).[28]
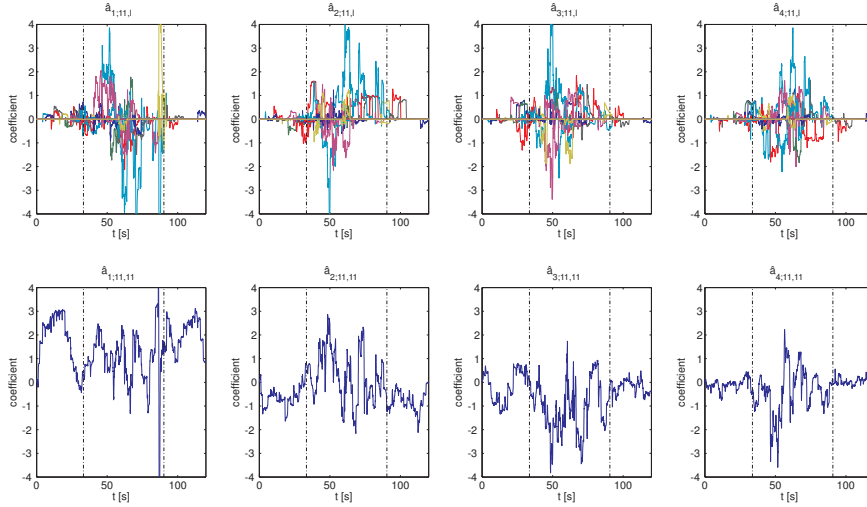
Figure 5.18: *Coefficient paths of channel 11. Enforced extrinsic contributions as well as higher intrinsic lag order in ictal periods. Begin and end of epileptic activity on channel 11 indicated by dash-dotted lines.*

We clearly see the influence of the increased instationarity in the ictal period from seconds 30 to 85:

- The extrinsic contributions (of all lags) are enforced during this period: more channels are selected, and the coefficients of the respective channels

---

[28]The coefficient stream was assembled as described in subsection 4.2.5 and then – for obtaining a smoother picture – processed by a moving average filter of 32 samples (0.25s).

show larger values than pre- and postictally. Before and after the seizure, they range around zero – the channel is therefore mainly described by its own past.

• When considering the higher-order intrinsic coefficients (particularly the one of lag 4) in the second line of figure 5.18, they take values significantly different from zero during these 55 seconds, whereas they oscillate around zero pre- and postictally.

Note that the peak at second 80, appearing in the path of the intrinsic coefficient of lag 1 as well as in the paths of two extrinsic coefficients of lag 1, is a numerical artefact.[29]

5.5.3.2   One-step prediction errors

The one-step prediction error of channel 11 is perfectly compatible with the observations made. As figure 5.19 illustrates, the error (in red) balloons during the 55s-lasting ictal period.
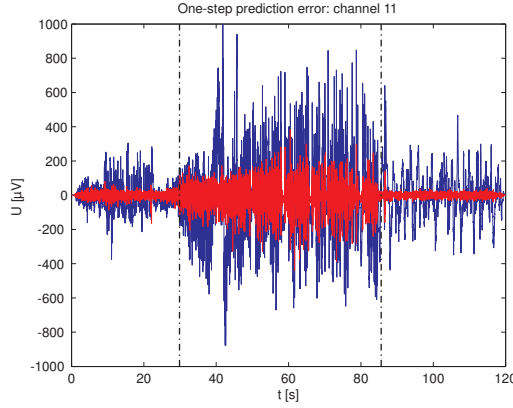
Figure 5.19: *One-step prediction error of channel 11. Larger values in ictal periods. Begin and end of epileptic activity on channel 11 indicated by dash-dotted lines.*

5.5.3.3   Partial estimation contributions

When wanting to interpret the influence of synchronization effects on the model behavior, the coefficient paths can be a first indication. However, it is more meaningful to consider the partial estimation contributions.

In our model equation 3.8, we defined the regressed signal as the of sum of two contributions: an intrinsic and an extrinsic contribution, and the latter being the sum of all partial extrinsic contributions

$$\widehat{x}_k[n] \triangleq \dot{x}_k[n] + \sum_{l \in \mathbb{L}_k} \vec{x}_{k,l}[n]. \tag{5.6}$$

---

[29]This could result, for instance, from the eye motion of the patient.

Comparing the values of the intrinsic and extrinsic contributions in 5.6 allows us to directly see the importance of the respective term to explain the original signal.

The conclusions drawn from the coefficient paths are confirmed by figure 5.20 on page 83 showing the different partial estimation contributions:

The intrinsic contribution $\dot{x}_{11}$ is given in light blue in the background, the different extrinsic partial estimation contributions $\vec{x}_{11,l}$ in the foreground. In pre- and postictal periods the channel is only explained by its intrinsic contributions, whereas in seconds 30 to 85 the extrinsic contributions get explanatory power.
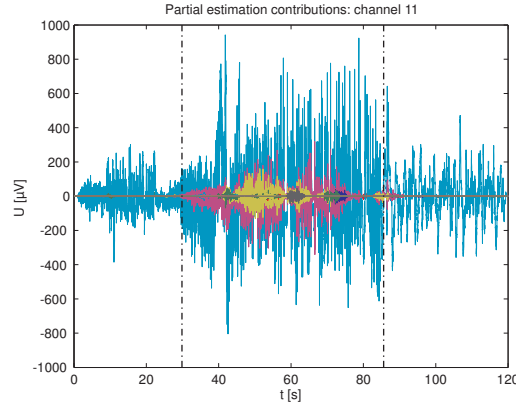
Figure 5.20: **Partial estimation contributions of channel 11.** *Enforced extrinsic contributions in ictal periods. Begin and end of epileptic activity on channel 11 indicated by dash-dotted lines.*

5.5.3.4   EIPR analysis

We want to conclude this subsection with a view on the (time-dependent) EIPR, the extrinsic-to-intrinsic power ratio defined in equation 4.24 in subsection 4.2.6.
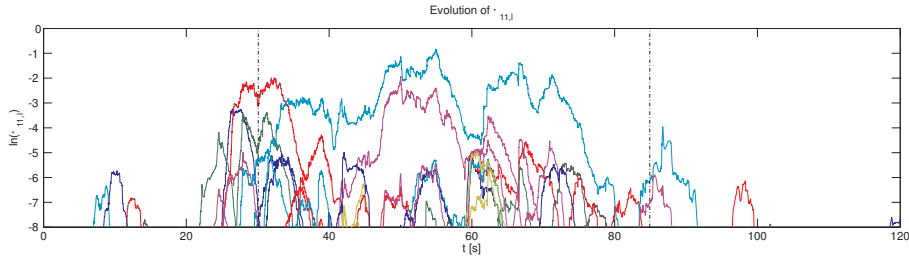
Figure 5.21: **Evolution of EIPR** $\eta_{11,l}$ **(RLS).** *Continuous evolution of EIPR, with small values pre- and postictally and large ones in ictal periods. Begin and end of epileptic activity on channel 11 indicated by dash-dotted lines.*

Figure 5.21 on page 83 shows the evolution of all $\eta_{11,l}$ measuring the synchronization effects between channel 11 and all channels l, $l \in [1..10, 12..28]$. In order to obtain a well arranged picture, we consider the logarithm of EIPR, and values below -8 are truncated.

We observe an important property which confirm the usefulness of the definition of this measure: Each $\eta_{11,l}$ takes small values pre- and postictally, whereas we observe large values of certain channel pairs during the ictal period (seconds 30 to 85). This behavior is in perfect accordance with model results examined before and reveals the physiologically appropriate character of EIPR.

Therefore, we approach our final goal of epileptic seizure propagation analysis: Plotting the temporal evolution of the $\eta_{k,l}$ of all channel pairs (k, l) in a spatio-temporal map[30] and masking them below a common (manually set) threshold allows us to track the propagation of the seizure focus.

5.5.4   Introduction of dead time

Before we plot this spatio-temporal map, we have to resolve one last problem: the manual determination of the common threshold. When artefacts appear in the raw ECoG signal, we obtain values of EIPR in the same order of magnitude as in ictal periods. It is therefore difficult to set a threshold which allows to correctly "mask" the EIPR evolution: being high enough to truncate it pre- and postictally, but low enough to display the EIPR in times of epileptic activity in our intended spatio-temporal map.

As figure 5.20 illustrates, the extrinsic estimation contributions rise in the ictal period, but are still small in comparison to the intrinsic contribution. We therefore penalize the intrinsic channel by introducing a dead time d: our intrinsic lag order now ranges in $[d + 1..p]$.[31]

This assures that the past of its own (intrinsic) channel becomes less and the one of the extrinsic channels more important for the explanation of the signal. Consequently, we obtain an evolution of EIPR, which is better shaped, allowing to set an appropriate threshold.

A dead time of $d = 2$ turned out to be appropriate for showing the desired effect, as systematic examinations showed.

5.5.4.1   Choice of model order

Realizing this dead time in the case of MMSE regression would be easy, as we would simply have to set the lag sets accordingly. In the case of RLS, however, this is not possible, as the design of the initial RLS algorithm does not allow a dead time.

---

[30] It would show the electrode positions on the cortex; we will present a possible map in subsection 5.5.4.3.

[31] This would correspond to the lag sets $\mathbb{S} = [d + 1..p]$ and $\mathbb{Q} = [1..p]$ in the case of MMSE regression.

Instead of modifying the RLS algorithm, we simply decide to manipulate the raw data stream: We create the desired dead time by shifting the raw data of the intrinsic channel 2 samples forward in comparison to the position of the extrinsic channels. Then we can apply our RLS algorithm to this new data stream and correct the position of the estimated sample afterward.

The inconvenience of this method is that we obtain different lag orders: If the lag order of the intrinsic channel is given by p, we only have $p - d$ for the extrinsic channels.

It is obvious that the optimal lag order changes, if we modify the model by omitting the last two samples of the intrinsic channel. As figure 5.22 indicates, we take $p = 6$ as lag order. This means that in fact we use − as described above − lag order 4 for extrinsic channels and lag order 6 for the intrinsic ones.
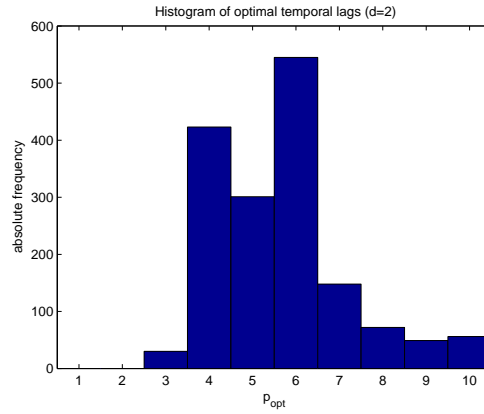
Figure 5.22: *Distribution of optimal temporal lags (RLS with dead time).* *Lags 1 and 2 are blocked due to the introduction of the dead time (d=2).*

Note that − surprisingly − this result is in good accordance with the optimal lag order for RLS without dead time, indicated by figure 5.12.

5.5.4.2 Residual autocorrelation

We do not give a detailed evaluation of this model, but refer the reader to tables B.4, B.5 and B.6 in annex B.

Instead, we only want to show the evolution of the Durbin-Watson statistic of the three exemplary channels 1, 11 and 16: As figure 5.23 on page 86 illustrates, the introduction of a dead time unfortunately causes strong autocorrelation of the residual errors.

This behavior is not surprising, but a logical consequence of the introduction of dead time: Information contained in the omitted samples is not taken into consideration, but "remains" in the error terms.
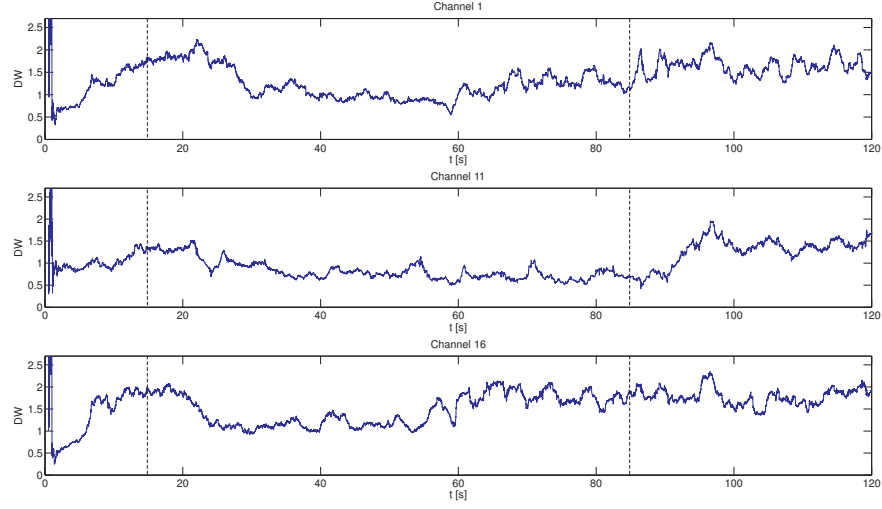
Figure 5.23: *Evolution of the Durbin-Watson-statistic (RLS with dead time).* *Sample-wise evolution for channels 1, 11 and 16 reveals residual autocorrelation. Begin and end of seizure indicated by dashed lines.*

The following theoretical reflections formalize this fact:

Let us assume we had a (for simplicity reasons) stationary AR(p) process[32]

$$\mathbf{x}[n] = \sum_{k=1}^{p} \mathbf{A}_k \mathbf{x}[n-k] + \epsilon[n],$$

with $\epsilon[n]$ being zero-mean white noise with covariance matrix $\boldsymbol{\Sigma}_\epsilon$.

We estimate this process by an AR(p)-model with dead time d:

$$\widehat{\mathbf{x}}[n] = \sum_{k'=d+1}^{p} \mathbf{B}_k \mathbf{x}[n-k].$$

In the following we show − by transforming into the frequency domain − that the residual error $\widehat{\mathbf{x}}[n] - \mathbf{x}[n]$ cannot be white for $d > 0$:

The signal itself is

$$\begin{aligned} \mathbf{X}(f) &= \sum_{k=1}^{p} \mathbf{A}_k \mathbf{X}(f) e^{-2\pi i f k} + \epsilon(f) \\ &= \frac{\epsilon(f)}{\mathbf{1} - \sum_{k=1}^{p} \mathbf{A}_k e^{-2\pi i f k}} \, . \end{aligned} \qquad (5.7)$$

---

[32]In our instationary case, the principle is the same.

Therefore the estimated signal is given by

$$
\begin{aligned}
\widehat{\mathbf{X}}(f) &= \sum_{k'=d+1}^{p} B_{k'} X(f) e^{-2\pi i f k'} \\
&= \sum_{k'=d+1}^{p} B_{k'} \frac{\epsilon(f)}{1 - \sum_{k=1}^{p} \mathbf{A}_k e^{-2\pi i f k}} e^{-2\pi i f k'}.
\end{aligned}
\tag{5.8}
$$

Expressions (5.7) and (5.8) deliver the residual error

$$
\begin{aligned}
\mathbf{X}(f) - \widehat{\mathbf{X}}(f) &= \frac{\epsilon(f)}{1 - \sum_{k=1}^{p} \mathbf{A}_k e^{-2\pi i f k}} \left(1 - \sum_{k'=d+1}^{p} \mathbf{B}_{k'} e^{-2\pi i f k'} \right) \\
&= \underbrace{\epsilon(f)}_{\text{const}} \frac{1 - \sum_{k'=d+1}^{p} \mathbf{B}_{k'} e^{-2\pi i f k'}}{1 - \sum_{k=1}^{p} \mathbf{A}_k e^{-2\pi i f k}}.
\end{aligned}
\tag{5.9}
$$

Expression (5.9) can only be constant if the second factor is constant. This is the case if the sums in nominator and denominator are identical.[33] Therefore, for $d > 0$, the residual error cannot be white, as its frequency-domain-expression (5.9) is not constant.

However, further investigation is needed in order to understand the consequences of the introduction of dead time better.

5.5.4.3   Seizure propagation

Let us ignore the residual autocorrelation for a moment and consider the evolution of EIPR: For comparison reasons, figure 5.24 shows the logarithm of all $\eta_{11,l}$ again.
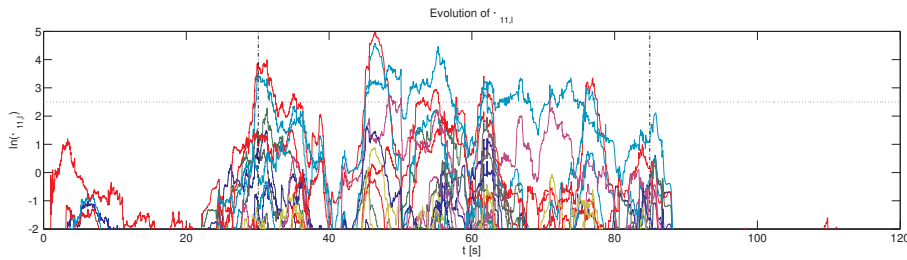
Figure 5.24: *Evolution of EIPR $\eta_{11,l}$ (RLS with dead time). Analog results to regression without dead time, but better indication of epileptic activity: EIPR attenuated pre- and postictally. Begin and end of epileptic activity on channel 11 indicated by dash-dotted lines.*

We observe a picture which is in accordance with the EIPR evolution obtained by RLS without dead time in figure 5.21: large values in times of epileptic

---

[33]The error $\epsilon(f)$ is constant in the frequency domain, as it is assumed to be white.

activity, small ones pre- and postictally. Furthermore, due to the penalization of the intrinsic channels, more extrinsic channels were selected, and the EIRP ranges in a higher order of magnitude.

It is now easy to manually determine a common threshold which correctly masks the EIPRs of all channels for the desired spatio-temporal representation. Figure 5.24 indicates this threshold of 2.0 by a dotted line.

Figure 5.25 finally shows the desired spatio-temporal map of the EIPR evolution of all channels, allowing to track the seizure propagation. For the sake of brevity, we limit ourselves to the period of 12:45:45 to 12:47:05 and choose a temporal resolution of one second.

The representation in figure 5.25 has to be read as follows:

- Synchronization effects between a pair of channels (k, l), which are measured by $\eta_{k,l}$, are represented by a flash. Hereby, the flash points from channel l to channel k.

- The thickness of the arrow is an indicator for the magnitude of EIPR, and values below the manually set threshold of 2.5 are not displayed.

- Clusters of flashes can be interpreted as the focus of the epileptic seizure at this moment. Hereby, the involved flashes point to or from the center of the focus.[34]

---

[34]The physiological signification of the directed EIRP measure has to be investigated further on.
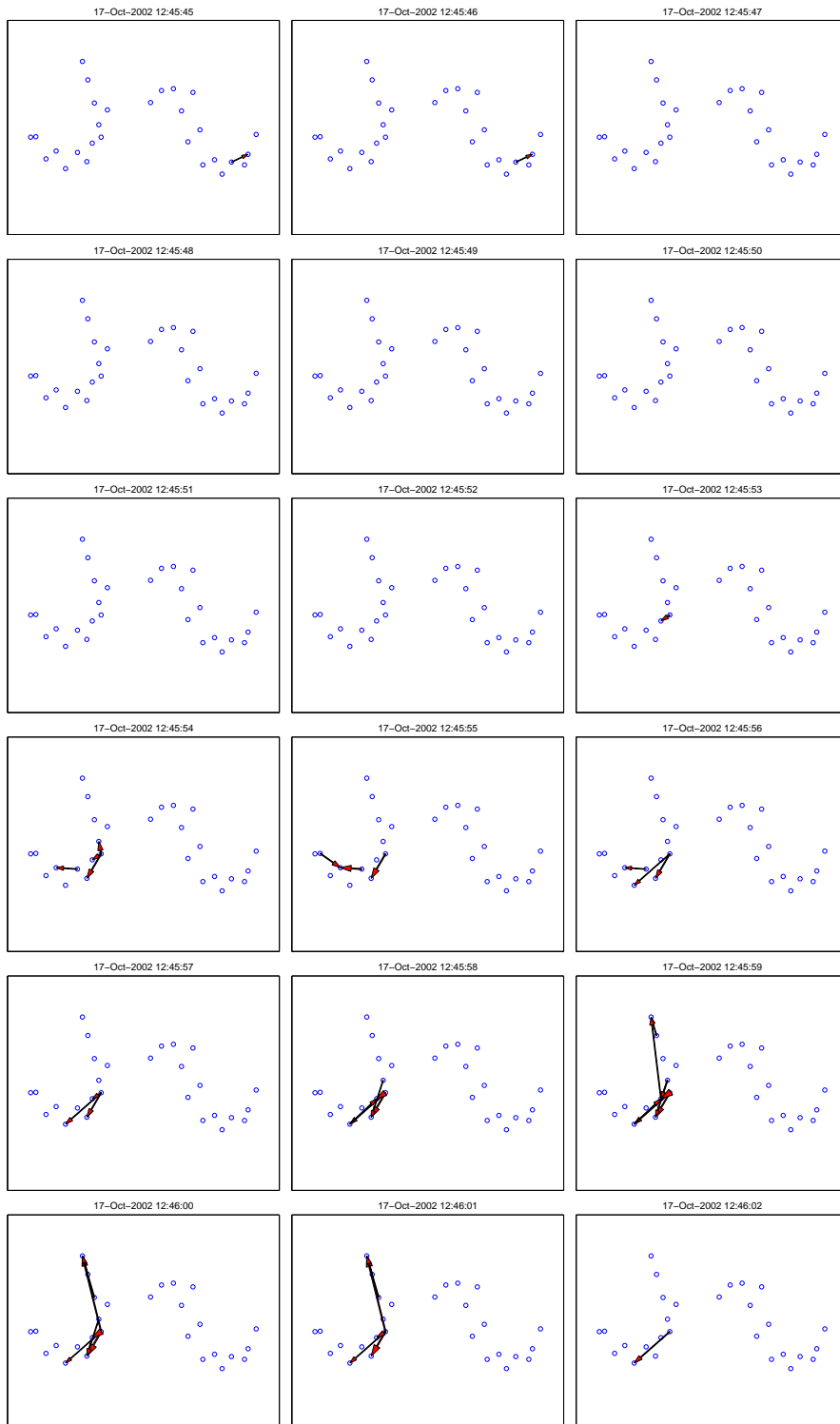
Figure 5.25 (a): 12:45:45 - 12:46:02
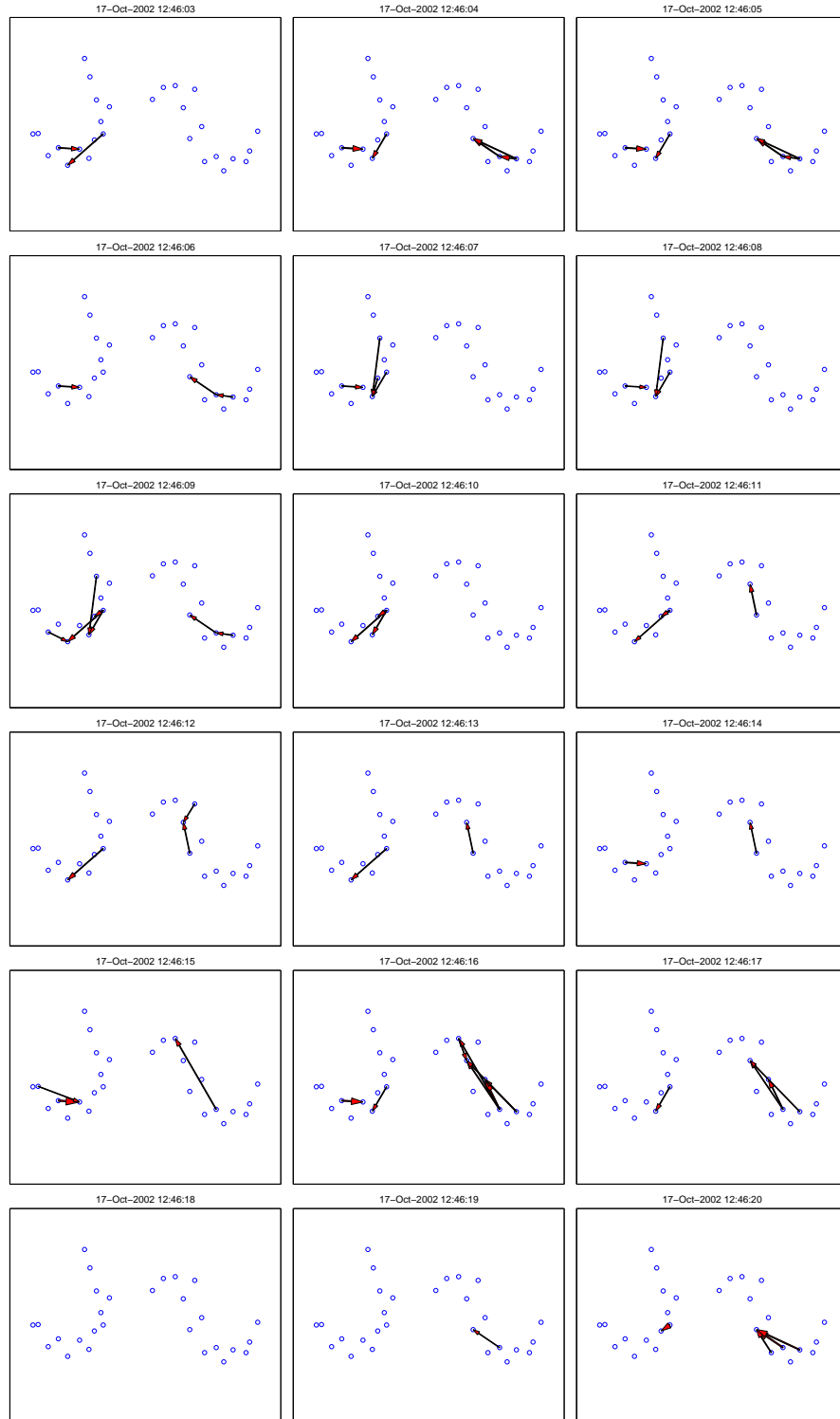
Figure 5.25 (b): 12:46:03 - 12:46:20
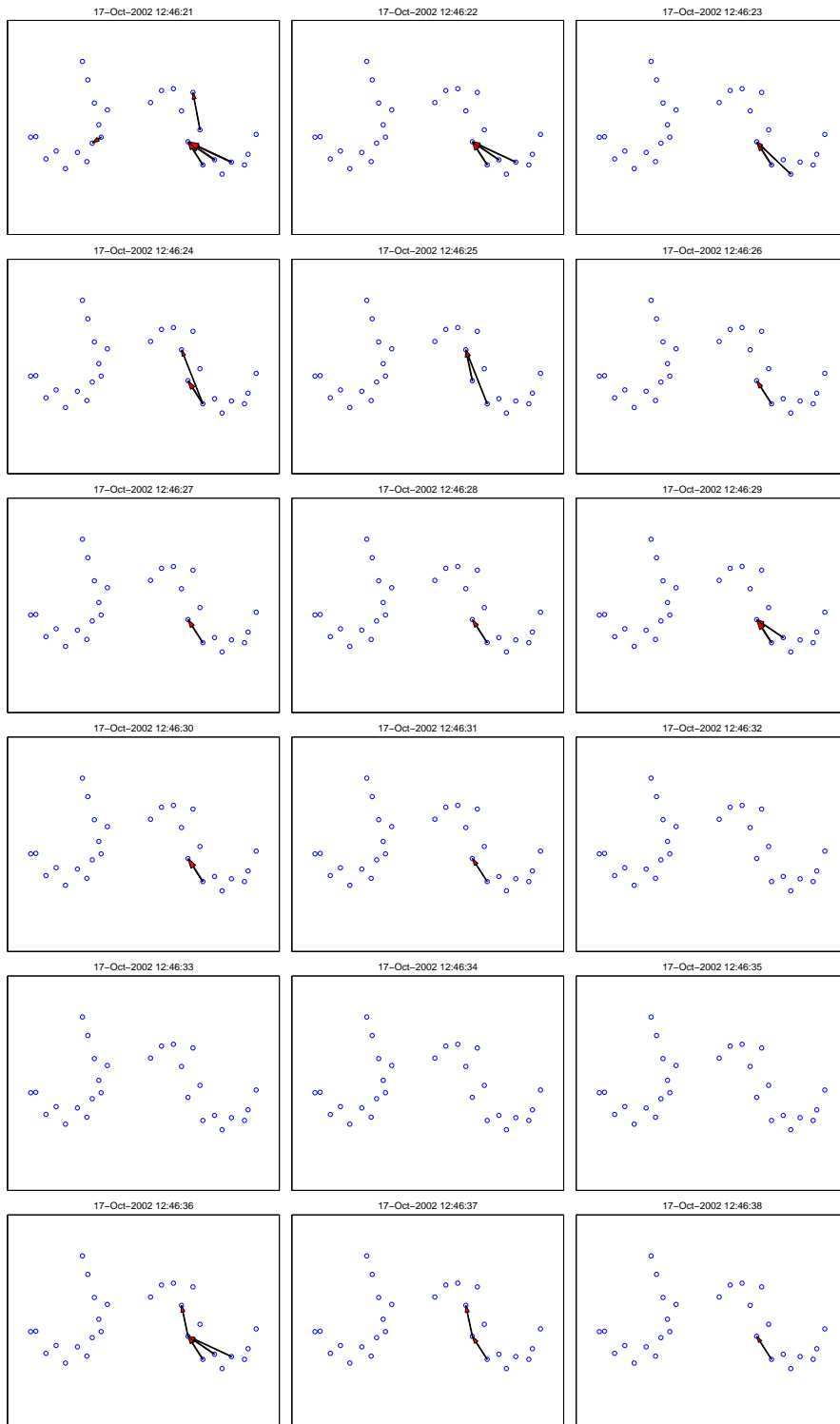
Figure 5.25 (c): 12:46:21 - 12:46:38
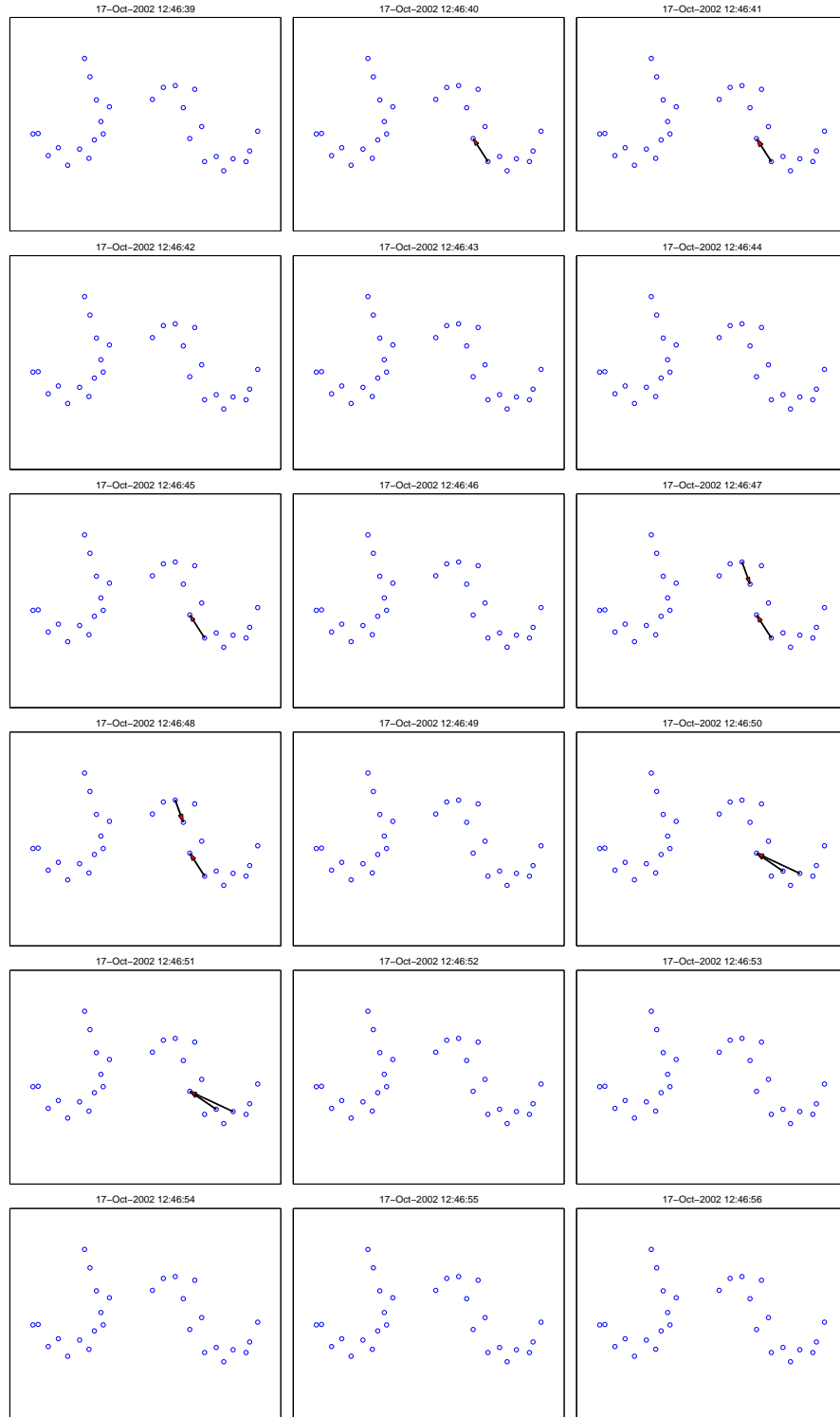
Figure 5.25 (d): 12:46:39 - 12:46:56
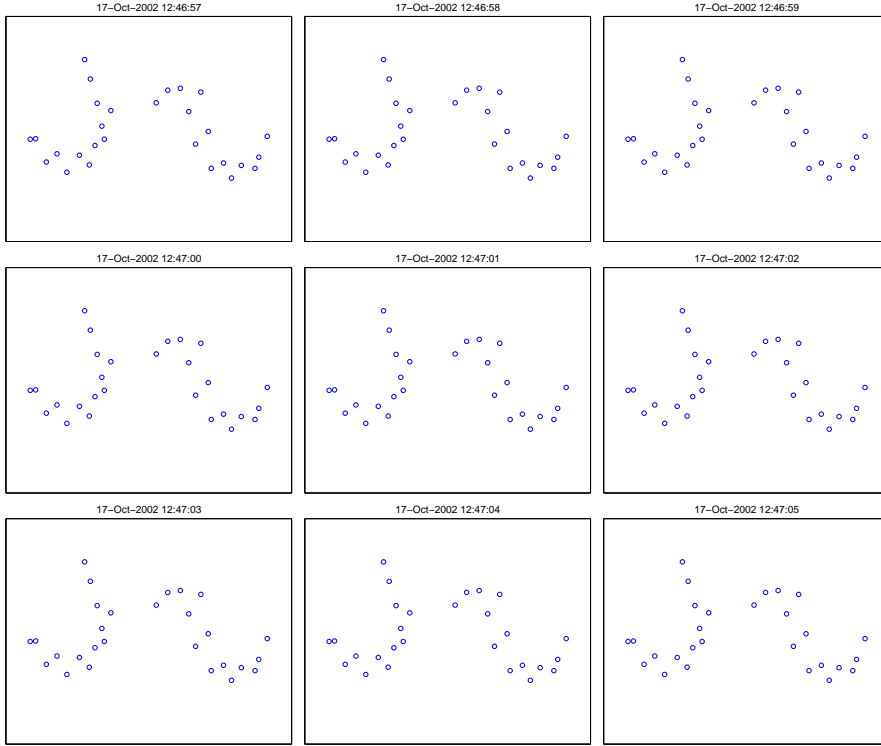
Figure 5.25 (e): 12:46:57 - 12:47:05

Figure 5.25: ***Spatio-temporal map of seizure propagation.*** *Figures 5.25 (a) - (e) track the spatio-temporal seizure propagation in steps of one second: perfect accordance with findings of clinicians.*

The propagation of the epileptic seizure presented in figure 5.25 (a) - (e) is in perfect accordance with the clinicians' findings, as given in section 5.1.

At the very end, we allow ourselves to add two final remarks:

1. As we have a temporal resolution of one second, we – of course – do not show the continuous EIPR stream which he have at our disposition.[35]
   In order to profit by the high temporal resolution obtained by means of RLS, we replace the static (printed) spatio-temporal map by a dynamic representation. This "video" continuously shows the evolution of the epileptic seizure focus on the screen.[36]

2. Despite the satisfying results note, however, that setting the threshold is not obvious. Whatever threshold we choose, we have a trade-off between over- and under-interpretation of the indicated epileptic activity:

---

[35]As this stream has a sampling frequency of $f_s = 128$Hz, we only represent every 128th sample.

[36]See figure B.1 in annex B for a screenshot.

- A low threshold allows many EIPR-arrows to be plotted. On the one hand this leads to a good visibility in even weakly developed periods of the seizure, but might also indicate epileptic activity outside the seizure focus on the other hand.

- A high threshold rejects lots of EIPR-arrows and only allows the very strong ones to be plotted. Therefore we get a very concentrated picture, but we might "miss" parts of the seizure evolution where epileptic activity is not very distinct.

A consequence of setting the threshold to 2.5 in figure 5.25 is that we "miss" the end of the epileptic seizure (which is characterized by low epileptic activity), which doctors see at 12:47:00 at electrodes B4 and B5. If we decreased, for example, the threshold to 2.0, the algorithm would indicate epileptic activity at 12:47:00, but also preictally.[37]

Further investigation is needed for elaborating a meaningful (and ideally automatic) algorithm for threshold determination.

5.5.4.4   MMSE regression with dead time

Note that we could also perform the MMSE regression with a dead time of $d = 2$. In this case, the optimal maximal lag order is determined to be $p = 4$, yielding $\mathbb{S} = \mathbb{Q} = [3, 4]$.[38]

Although mathematical properties of the MMSE model with dead time are very poor,[39] the resulting spatio-temporal map is extremely similar to the one obtained by means of RLS in figure 5.25. It is therefore in perfect accordance with the clinicians' findings.

The interested reader is referred to annex A for details, where we present the spatio-temporal map in figure A.2 and mathematical properties of the model in tables A.4, A.5 and A.6.

---

[37] We especially encounter this problem when plotting the EIPR obtained by regression without dead time.

[38] Figure A.1 in annex A shows the histogram of optimal lag orders.

[39] Even without dead time we have high autocorrelation of the residual errors, as discussed in section 5.2.

Chapter 6

Conclusion and Outlook

We want to use this last chapter for a short overview of the topics we have dealt with in this diploma thesis: We sum up established results and address unresolved problems. Furthermore, we give an outlook on potential enhancements in the future.

6.1 Conclusion

In this diploma thesis we presented a novel method for epileptic seizure propagation analysis, which is based on linear spatio-temporal regression and allows to track the spatio-temporal evolution of the seizure focus.

Using adaptive model coefficient estimation by means of recursive-least-squares (RLS), we were able to cope with the instationarity of the biosignals. An important feature of our method was the use of a channel selection algorithm which determines the optimal spatial neighborhood for each channel, before the regression is performed. This approach reduces the complexity of the system and helps to handle the highly correlated signals.

Based on these approaches we introduced a novel dependency measure in the time-domain termed extrinsic-to-intrinsic-power ratio (EIPR). Its good correlation with epileptic activity revealed its physiologically meaningful character.

Our experiments were performed with ECoG recordings consisting of 28 channels from patients suffering from temporal lobe epilepsy. By applying our method to these data, we obtained results which are in excellent agreement with the findings of medical experts: The prediction of the propagation of epileptic activity shows a good spatial and temporal resolution. Furthermore, our algorithm can be efficiently implemented, as it is based on autoregressive models which benefit from numerical simplicity.

Therefore we are convinced that our approach has potential for the computer-assisted evaluation of ECoG recordings of epileptic seizures. This would be an important step to support clinicians in the pre-surgical examination phase and

to help to treat patients sufferings from epilepsy in a better and more efficient way.

6.2   Outlook

Despite the accordance of our indication of epileptic activity with clinicians' findings, further investigation is needed to ameliorate this novel method of epileptic seizure propagation analysis.

First of all, the consequences of the introduction of dead time have to be analyzed exhaustively. It would be particularly important not to use any form of dead time, as results obtained by means of RLS regression without dead time have better statistical properties.

Secondly, at the moment the EIPR threshold for spatio-temporal maps has to be determined manually. An automatic adaption of this threshold delivering a clear and precise indication of epileptic activity is being strongly pursued. This algorithm would probably have to take the density of flashes into consideration – that is what we are doing visually right now.

The exact physiological signification of EIPR needs further investigation. As it is a directed measure (explaining synchronization influence from one channel to another), we display it in form of flashes. However, the direction of these flashes has to be examined and linked to physiological processes.

Another important point is the definition of EIPR itself, which does not take physiological properties of synchronization effects into consideration. One could think of improving EIPR to operate in the frequency domain as well.

Furthermore, results based on EIPR would also have to be compared with indications given by other measures defined in the frequency domain which are commonly used in literature, like Direct Transfer Function (DTF).

We also want to mention that the channel selection algorithm of the autoregressive model currently works with a fixed temporal lag order. We consequently over- or underestimate the order of the ECoG signal, depending on the sampling position and the channel. A possible improvement would be an iterated optimization choosing channels and lag orders. Furthermore, the selection algorithm might use information about the anatomy (e.g. on which hemesphere the specific electrode is located).

Last but not least we would like to state that work done in this diploma thesis is a "proof of concept". As we are speaking about future tasks, we consider application of the proposed method to ECoG data of other patients to be of highest priority. Some tests with recordings of two supplementary patients have already been performed and showed promising results. However, exhaustive examinations have to reveal the general aptitude of our method for epileptic seizure propagation analysis.

Appendix A

Results of MMSE regression

A.1 MMSE regression without dead time

The following tables detail the results of the MMSE regression (without dead time), which we described in section 5.2.

Note that channel 6 is always left out as it is the reference electrode.

A.1.1 Regression fit

Table A.1 details the average values of R_k^2 per channel.[1]

k	R_k^2	k	R_k^2	k	R_k^2	k	R_k^2
1	0.9684	8	0.9787	15	0.9520	22	0.9660
2	0.9746	9	0.9681	16	0.9636	23	0.9650
3	0.9710	10	0.9159	17	0.9412	24	0.9529
4	0.9732	11	0.9160	18	0.9585	25	0.9544
5	0.9747	12	0.9645	19	0.9660	26	0.9447
6	-	13	0.9798	20	0.9748	27	0.9638
7	0.9717	14	0.9925	21	0.9739	28	0.9737

Table A.1: *Average values of R_k^2 (MMSE)*

A.1.2 Autocorrelation

Table A.2 on the next page contains the average values of the Durbin-Watson statistic DW_k per channel.[2]

---

[1]See figure 5.5 for the evolution of R_k^2 of channels 1, 11 and 16.

[2]See figure 5.6 for the evolution of the Durbin-Watson statistic of channels 1, 11 and 16.

k	DW_k	k	DW_k	k	DW_k	k	DW_k
1	1.6268	8	1.6667	15	1.7518	22	1.7300
2	1.7048	9	1.6704	16	1.7307	23	1.7184
3	1.6811	10	1.7022	17	1.7547	24	1.8036
4	1.6664	11	1.5784	18	1.7514	25	1.6982
5	1.5808	12	1.6040	19	1.7320	26	1.6377
6	-	13	1.5800	20	1.7403	27	1.6549
7	1.6845	14	1.5226	21	1.6659	28	1.7013

Table A.2: *Average values of DW_k per channel (MMSE)*

A.1.3   Extrinsic channel set

Table A.3 details the average size of each extrinsic channel set $\mathbb{L}_k$. For comparison, the results of BIC and AIC as information criterion in the channel selection algorithm are given.[3]

k	$\#\mathbb{L}_k$		k	$\#\mathbb{L}_k$		k	$\#\mathbb{L}_k$		k	$\#\mathbb{L}_k$	
	BIC	AIC		BIC	AIC		BIC	AIC		BIC	AIC
1	2.2	9.2	8	2.0	9.3	15	1.8	10.8	22	1.7	10.3
2	1.6	8.7	9	2.1	10.2	16	2.0	11.1	23	2.3	11.0
3	1.8	8.4	10	2.5	9.9	17	2.1	10.9	24	2.2	11.7
4	1.4	7.5	11	2.5	9.8	18	2.1	11.7	25	2.4	11.8
5	1.3	7.5	12	2.4	10.0	19	2.0	10.9	26	2.5	10.7
6	-	-	13	2.1	9.0	20	1.9	11.3	27	2.0	10.2
7	2.0	8.1	14	2.0	8.6	21	1.6	9.1	28	1.9	10.4

Table A.3: *Average size of extrinsic channel sets (MMSE)*

---

[3]See figure 5.4 for the evolution of the extrinsic channels sets of channels 1, 11 and 16.

A.2 MMSE regression with dead time

The following section summarizes results MMSE regression with dead time, which we shortly mentioned in subsection 5.5.4.

Note that channel 6 is always left out as it is the reference electrode.

A.2.1 Optimal lag order

Figure A.1 gives a histogram of the optimal lag order in the case of dead time.
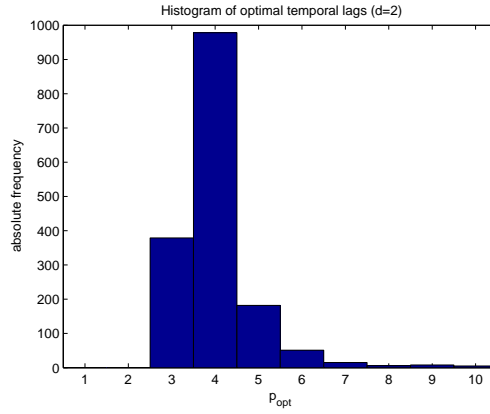
Figure A.1: *Optimal lag order (MMSE with dead time).*

A.2.2 Regression fit

Table A.4 details the average values of R_k^2 per channel.

k	R_k^2	k	R_k^2	k	R_k^2	k	R_k^2
1	0.9242	8	0.9147	15	0.8474	22	0.9321
2	0.9368	9	0.9136	16	0.9250	23	0.9140
3	0.9577	10	0.7089	17	0.8404	24	0.9063
4	0.9569	11	0.6917	18	0.9023	25	0.8880
5	0.8343	12	0.8562	19	0.9308	26	0.7956
6	-	13	0.9067	20	0.9478	27	0.8539
7	0.8826	14	0.9265	21	0.8931	28	0.9339

Table A.4: *Average values of R_k^2 (MMSE with dead time)*

A.2.3   Autocorrelation

Table A.5 contains the average values of the Durbin-Watson statistic DW_k per channel.

k	DW_k	k	DW_k	k	DW_k	k	DW_k
1	1.0756	8	0.8463	15	0.9350	22	1.2092
2	1.0048	9	1.0731	16	1.2681	23	1.2201
3	1.2050	10	1.0013	17	1.1120	24	1.1264
4	1.2045	11	0.7832	18	1.1933	25	1.0193
5	0.5726	12	0.8935	19	1.1596	26	1.0109
6	-	13	0.7830	20	1.1248	27	0.9758
7	0.8132	14	0.5778	21	0.8791	28	1.0134

Table A.5: *Average values of DW_k per channel (MMSE with dead time)*

A.2.4   Extrinsic channel set

Table A.5 details the average size of each extrinsic channel set $\mathbb{L}_k$.

k	$\#\mathbb{L}_k$	k	$\#\mathbb{L}_k$	k	$\#\mathbb{L}_k$	k	$\#\mathbb{L}_k$
1	4.8	8	4.4	15	5.3	22	4.3
2	4.4	9	4.9	16	5.6	23	5.2
3	3.8	10	5.5	17	5.0	24	5.2
4	3.3	11	5.7	18	5.3	25	6.1
5	4.2	12	5.8	19	4.4	26	4.5
6	-	13	4.7	20	4.0	27	4.4
7	4.3	14	3.2	21	4.1	28	5.0

Table A.6: *Average size of extrinsic channel sets (MMSE with dead time)*

A.2.5   Spatio-temporal map

Figure A.2 on the next pages shows the spatio-temporal map of MMSE regression with dead time. Note that due to the window design parameters the temporal resolution is two seconds.[4]
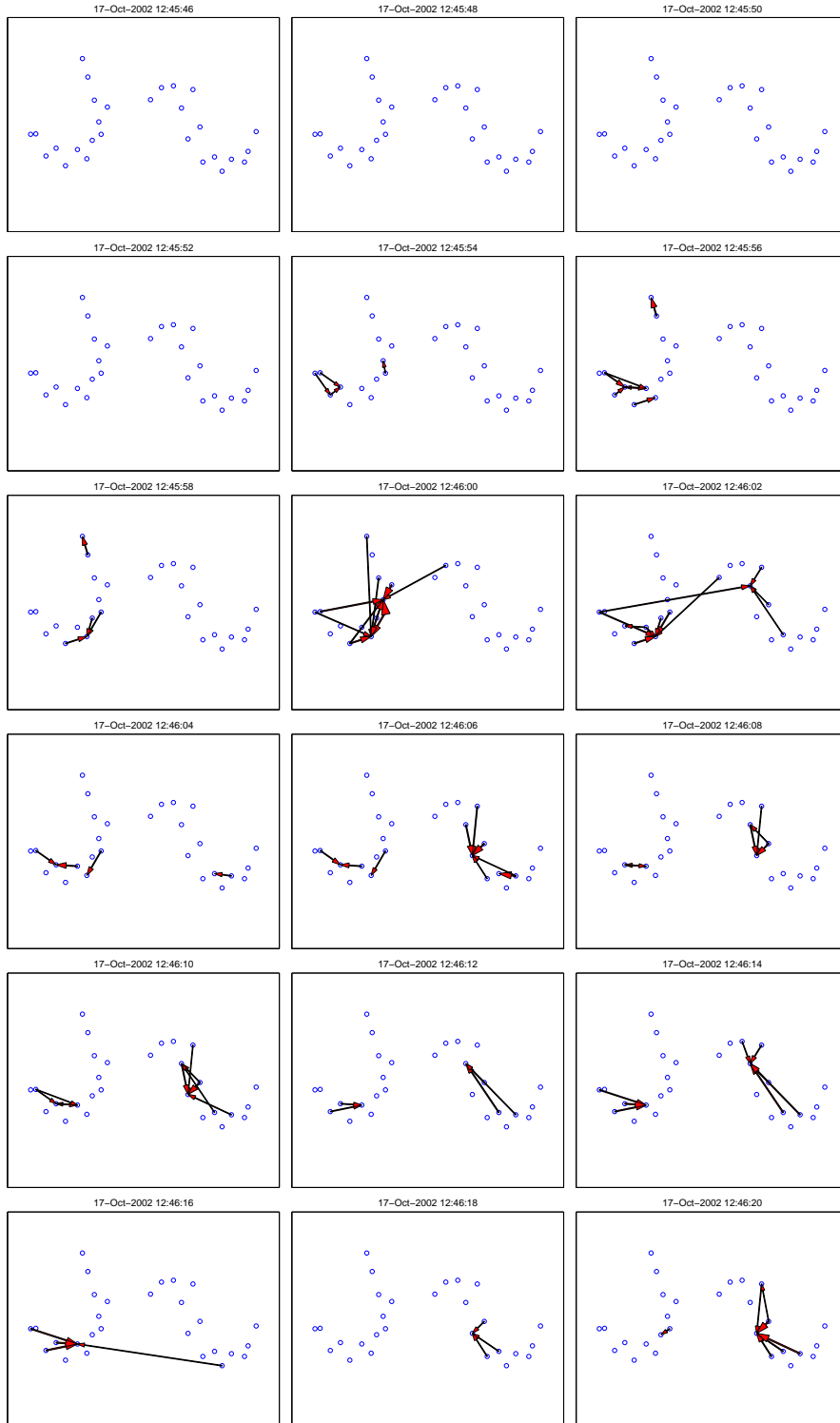

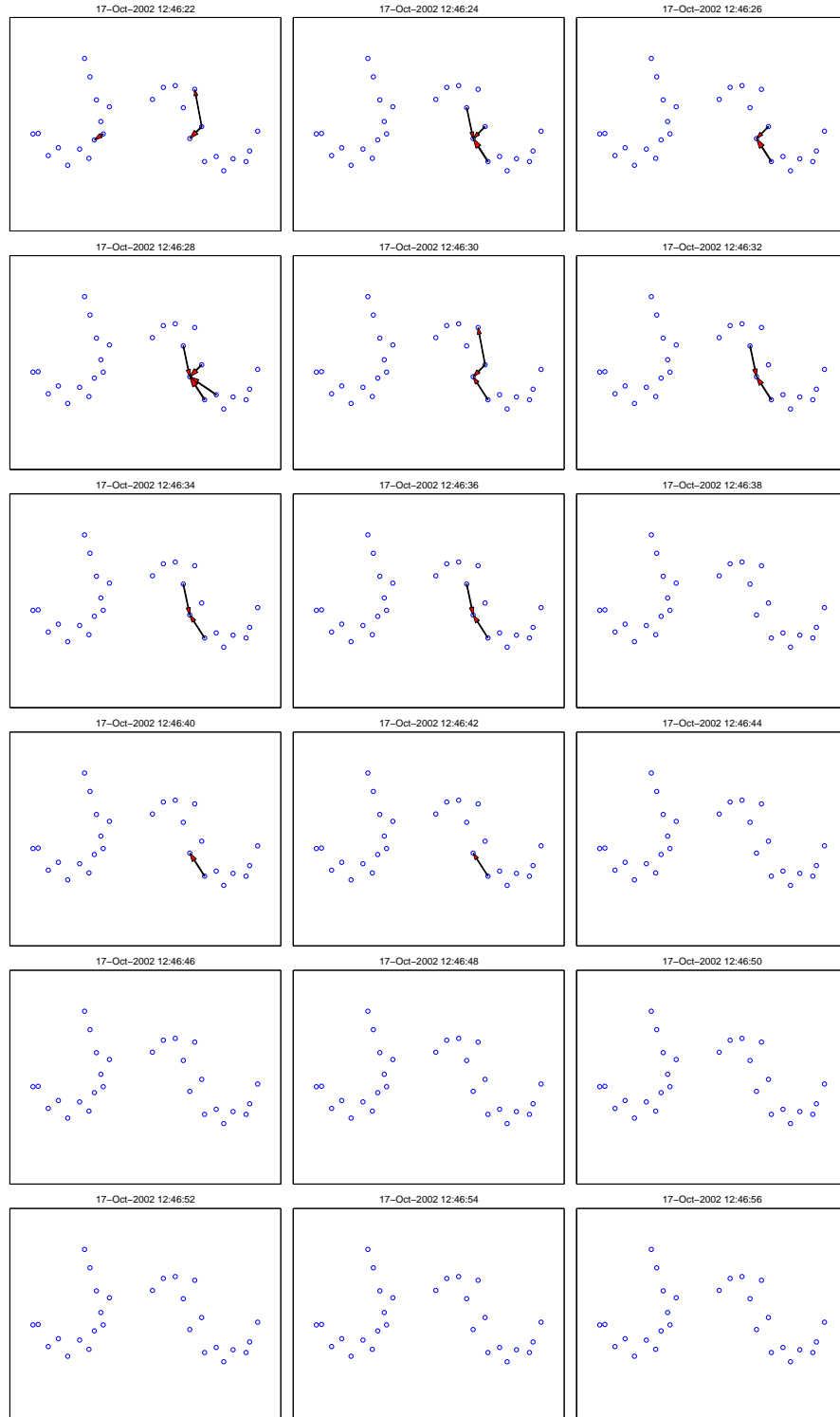[4]Compare subsection 4.1.1.

Figure A.2 (a): 12:45:46 - 12:46:20

Figure A.2 (b): 12:46:22 - 12:46:56
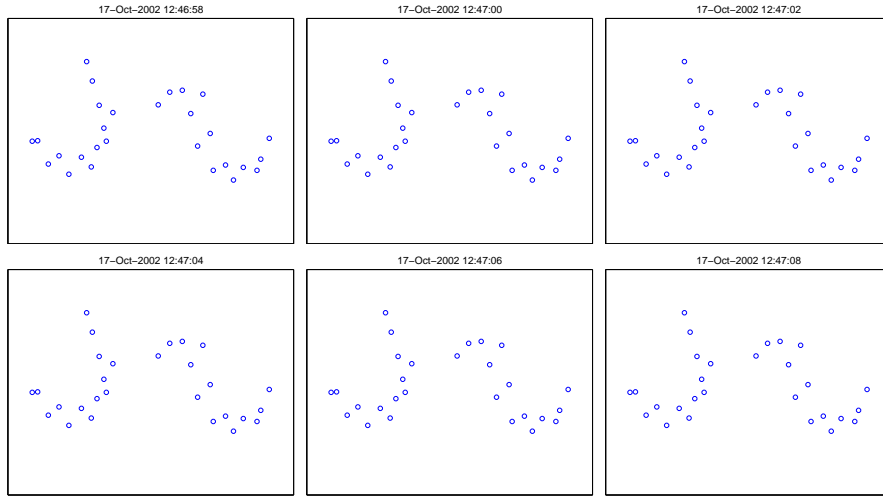
Figure A.2 (c): 12:46:58 - 12:47:08

Figure A.2: ***Spatio-temporal map (MMSE with dead time).*** *Figures A.2 (a) - (c) track the spatio-temporal seizure propagation in steps of two seconds: perfect accordance with findings of clinicians.*

Appendix B

Results of RLS regression

B.1 RLS regression without dead time

The following tables detail the results of the RLS regression (without dead time), which we described in section 5.5.

Note that channel 6 is always left out as it is the reference electrode.

B.1.1 Regression fit

Table B.1 details the average values of the coefficient of determination per channel. Hereby, the in-sample correlation coefficient is denoted by R_k^2 and the out-of-sample correlation coefficient by $\widetilde{R}_k^2$.[1]

k	R_k^2	$\widetilde{R}_k^2$	k	R_k^2	$\widetilde{R}_k^2$	k	R_k^2	$\widetilde{R}_k^2$	k	R_k^2	$\widetilde{R}_k^2$
1	0.9708	0.9516	8	0.9788	0.9612	15	0.9648	0.9566	22	0.9655	0.9238
2	0.9763	0.9483	9	0.9709	0.9485	16	0.9682	0.9360	23	0.9667	0.9460
3	0.9714	0.9451	10	0.9521	0.9207	17	0.9536	0.9105	24	0.9636	0.9502
4	0.9763	0.9304	11	0.9535	0.9373	18	0.9654	0.9204	25	0.9693	0.9535
5	0.9737	0.9675	12	0.9703	0.9317	19	0.9708	0.9593	26	0.9606	0.9529
6	-	-	13	0.9810	0.9352	20	0.9783	0.9699	27	0.9725	0.9674
7	0.9711	0.9395	14	0.9937	0.9885	21	0.9759	0.8791	28	0.9750	0.9690

Table B.1: *Average values of R_k^2 and $\widetilde{R}_k^2$ (RLS)*

B.1.2 Autocorrelation

Table B.2 contains the average values of the Durbin-Watson statistic DW_k per channel.[2]

---

[1]See figure 5.16 for the evolution of R_k^2 and $\widetilde{R}_k^2$ of channels 1, 11 and 16.

[2]See figure 5.17 for the evolution of the Durbin-Watson statistic of channels 1, 11 and 16.

k	DW_k	k	DW_k	k	DW_k	k	DW_k
1	1.9745	8	1.9943	15	1.9881	22	1.9783
2	1.9869	9	1.9819	16	1.9958	23	1.9792
3	2.0013	10	1.9503	17	1.9730	24	1.9913
4	1.9913	11	1.9683	18	1.9858	25	1.9997
5	2.0011	12	1.9657	19	1.9853	26	1.9866
6	-	13	1.9761	20	1.9843	27	1.9933
7	1.9811	14	1.9985	21	1.9639	28	1.9993

Table B.2: *Average values of DW_k per channel (RLS)*

B.1.3   Extrinsic channel set

Table B.3 details the average size of each extrinsic channel set $\mathbb{L}_k$.[3]

k	$\#\mathbb{L}_k$	k	$\#\mathbb{L}_k$	k	$\#\mathbb{L}_k$	k	$\#\mathbb{L}_k$
1	0.9	8	1.0	15	1.4	22	1.0
2	1.2	9	1.0	16	1.1	23	0.9
3	0.9	10	1.8	17	1.3	24	1.6
4	0.9	11	1.7	18	1.3	25	1.3
5	0.8	12	1.2	19	1.3	26	1.2
6	-	13	0.9	20	1.4	27	1.4
7	0.9	14	0.7	21	1.1	28	1.1

Table B.3: *Average size of extrinsic channel sets (RLS)*

---

[3]See figure 5.15 for the evolution of the extrinsic channels sets of channels 1, 11 and 16.

B.2 RLS regression with dead time

The following tables detail the results of the RLS regression with dead time, which we quickly described in subsection 5.5.4.4.

Note that channel 6 is always left out as it is the reference electrode.

B.2.1 Regression fit

Table B.4 details the average values of the coefficient of determination per channel. Hereby, the in-sample correlation coefficient is denoted by R_k^2 and the out-of-sample correlation coefficient by $\widetilde{R}_k^2$.

k	R_k^2	$\widetilde{R}_k^2$	k	R_k^2	$\widetilde{R}_k^2$	k	R_k^2	$\widetilde{R}_k^2$	k	R_k^2	$\widetilde{R}_k^2$
1	0.940	0.9177	8	0.9460	0.9036	15	0.9433	0.9068	22	0.9432	0.9187
2	0.9536	0.9366	9	0.9380	0.9116	16	0.9490	0.9297	23	0.9450	0.9250
3	0.9555	0.9418	10	0.9113	0.8293	17	0.9257	0.8922	24	0.9509	0.8954
4	0.9546	0.9399	11	0.9037	0.8235	18	0.9447	0.9235	25	0.9475	0.9017
5	0.9168	0.8681	12	0.9247	0.8842	19	0.9646	0.9316	26	0.9086	0.8751
6	-	-	13	0.9368	0.9080	20	0.9688	0.9407	27	0.9347	0.9025
7	0.9091	0.8722	14	0.9566	0.9282	21	0.9354	0.9057	28	0.9626	0.9389

Table B.4: *Average values of R_k^2 and $\widetilde{R}_k^2$ (RLS with dead time)*

B.2.2 Autocorrelation

Table B.5 on the next page contains the average values of the Durbin-Watson statistic DW_k per channel.[4]

k	DW_k	k	DW_k	k	DW_k	k	DW_k
1	1.3523	8	1.0953	15	1.1817	22	1.4109
2	1.2669	9	1.2813	16	1.5595	23	1.5061
3	1.5576	10	1.1830	17	1.3167	24	1.3627
4	1.4798	11	0.9934	18	1.4520	25	1.3426
5	0.8042	12	1.0799	19	1.4317	26	1.2962
6	-	13	0.9951	20	1.4094	27	1.2675
7	1.0065	14	0.8193	21	1.1145	28	1.3021

Table B.5: *Average values of DW_k per channel (RLS with dead time)*

---

[4]See figure 5.23 for the evolution of the Durbin-Watson statistic of channels 1, 11 and 16.

B.2.3   Extrinsic channel set

Table B.6 details the average size of each extrinsic channel set $\mathbb{L}_k$.

k	$\#\mathbb{L}_k$	k	$\#\mathbb{L}_k$	k	$\#\mathbb{L}_k$	k	$\#\mathbb{L}_k$
1	4.3	8	6.6	15	6.1	22	4.3
2	4.9	9	4.9	16	4.9	23	4.1
3	3.4	10	6.1	17	4.7	24	4.8
4	3.4	11	6.3	18	4.9	25	5.0
5	6.5	12	6.7	19	5.0	26	4.0
6	-	13	5.9	20	4.8	27	4.7
7	5.5	14	5.4	21	5.2	28	4.7

Table B.6: *Average size of extrinsic channel sets (RLS with dead time)*

B.2.4   Screenshot

We finally give a screenshot of the program which plays the evolution of the epileptic seizure status in form of a "video". Figure B.1 shows the graphical user interface of this program at 12:46:04.
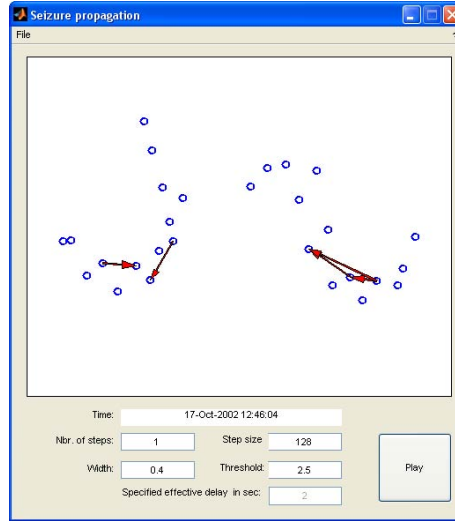
Figure B.1: *Screenshot of the seizure focus propagation "video".*
Epileptic activity indicated on the left and right hemispheres at 12:46:04.

Bibliography

[AG89]   H. An and L. Gu, *Fast stepwise procedures of selection of variables by using AIC and BIC criteria*, Acta mathematicae applicatae Sinica **5** (1989), no. 1, 60–67.

[Aka74]   H. Akaike, *A New Look at the Statistical Model Identification*, IEEE Transactions on Automatic Control **19** (1974), no. 6, 716–723.

[Bau01]   C. Baumgartner (ed.), *Handbuch der Epilepsien: Klinik, Diagnostik, Therapie und psychosoziale Aspekte*, Springer, 2001.

[BD91]   P. Brockwell and R. Davis, *Time Series: Theory and Methods*, Springer, 1991.

[BP70]   G. Box and D. Pierce, *Distribution of Residual Autocorrelations in Autoregressive-Integrated Moving Average Time Series Models*, Journal of the American Statistical Association **65** (1970), no. 332, 1509–1526.

[BS01]   L. Baccala and K. Sameshima, *Partial directed coherence: a new concept in neural structure determination*, Biological Cybernetics **84** (2001), 463–474.

[Dah00]   R. Dahlhaus, *Graphical interaction models for multivariate time series*, Metrika **51** (2000), 157–172.

[DE03]   R. Dahlhaus and M. Eichler, *Causality and graphical models in time series analysis*, Highly structured stochastic systems (P. Green, N. Hjort, and S. Richardson, eds.), Oxford University Press, 2003, pp. 115–137.

[DF79]   D. Dickey and W. Fuller, *Distribution of the Estimators for Autoregressive Time Series with a Unit Root*, Journal of the American Statistical Association **74** (1979), 427–431.

[DH05]   M. Deistler and E. Harmann, *Identification of Factor Models for Forecasting Returns*, Journal of financial econometrics **3** (2005), 256–281.

[Dob01]   G. Doblinger, *MATLAB-Programmierung in der digitalen Signalverarbeitung*, J. Schembach Fachverlag, 2001.

[EH02]   M. Ebe and I. Homma, *Leitfaden für die EEG-Praxis. Ein Bildkom-pendium*, 3 ed., Urban & Fischer, 2002.

[Eic06]   M. Eichler, *Graphical modeling of dynamic relationships in multi-variate time series*, Handbook of time series analysis (B. Schelter, M. Winterhalder, and J. Timmer, eds.), Wiley-VCH, 2006, pp. 335–372.

[FBK85]   P. Franaszczuk, K. Blinowska, and M. Kowalczyk, *The Application of Parametric Multichannel Spectral Estimates in the Study of Elec-trical Brain Activity*, Biological Cybernetics **51** (1985), 239–247.

[Gra69]   C. Granger, *Investigating causal relations by econometric models and cross-spectral methods*, Econometrica **37** (1969), 424–438.

[Gru04]   *Pschyrembel Klinisches Wörterbuch*, 261 ed., de Gruyter, 2004.

[Hac05]   P. Hackl, *Einführung in die Ökonometrie*, Pearson Studium, 2005.

[Hay02]   S. Haykin, *Adaptive filter theory*, 4th ed., Prentice Hall Information and System Sciences Series, Prentice Hall, 2002.

[HD88]   E. Hannan and M. Deistler, *The Statistical Theory of Linear Sys-tems*, John Wiley, 1988.

[Her99]   S. Hermann, *Epilepsien: Diagnose und Behandlung*, 3rd ed., Thieme, 1999.

[HK07]   M. Hartmann and T. Kluge, *A Novel Method for the Characteri-zation of Synchronization and Coupling in Multichannel EEG and ECoG*, ARC Report, 2007.

[JB76]   G. Jjung and G. Box, *On a measure of lack of fit in time series models*, Biometrika **65** (1976), no. 2, 297–303.

[Kay93]   S. Kay, *Fundamentals of Statistical Signal Processing: Estimation Theory*, Prentice Hall Signal Processing Series, vol. 1, Prentice Hall, 1993.

[KB91]   M. Kaminski and K. Blinowska, *A new method of the description of the information flow in the brain structures*, Biological Cybernetics **65** (1991), 203–210.

[KDTB01]   M. Kaminski, M. Ding, W. Truccolo, and S. Bressler, *Evaluating causal relations in neural systems: Granger causality, directed trans-fer function and statistical assessment of significance*, Biological Cy-bernetics **85** (2001), 145–157.

[KKB04]   R. Kus, M. Kaminski, and K. Blinowska, *Determination of EEG Ac-tivity Propagation: Pair-Wise Versus Multichannel Estimate*, IEEE Tansactions on Biomedical Engineering **51** (2004), no. 9, 1501–1510.

[KMK⁺03] A. Korzeniewska, M. Manczak, M. Kaminski, K. Blinowska, and S. Kasicki, *Determination of information flow direction among brain structures by a modified directed transfer function (dDTF) method*, Journal of Neuroscience Methods **125** (2003), 195–207.

[KPSS92] D. Kwiatkowski, P. Phillips, P. Schmidt, and Y. Shin, *Testing the null hypothesis of stationarity against the alternative of a unit root*, Journal of Econometrics **54** (1992), 159–178.

[Lüd92] H. Lüders, *Epilepsy Surgery*, Raven Press, 1992.

[Lüt93] H. Lütkepohl, *Introduction to Multiple Time Series Analysis*, 2nd ed., Springer, 1993.

[Mar87] S. Marple, *Digital spectral analysis with applications*, Prentice Hall, 1987.

[MSAW01] E. Möller, B. Schack, M. Arnold, and H. Witte, *Instantaneous multivariate EEG coherence analysis by means of adaptive high-dimensional autoregressive models*, Journal of Neuroscience Methods **105** (2001), 143–158.

[NMW02] J. Nicholls, A. Martin, and B. Wallace, *Vom Neuron zum Gehirn*, Spektrum Akademischer Verlag, 2002.

[NS01] A. Neumaier and T. Schneider, *Estimation of parameters and eigenmodes of multivariate autoregressive models*, ACM Transactions on Mathematical Software **27** (2001), no. 1, 27–57.

[PP04] R. Putz and R. Pabst (eds.), *Sobotta: Atlas der Anatomie des Menschen*, 21 ed., Elsevier, 2004.

[Sch78] G. Schwarz, *Estimating the dimension of a model*, The Annals of Statistics **6** (1978), no. 2, 461–464.

[SD84] E. Said and D. Dickey, *Testing for unit roots in autoregressive moving average models of unknown order*, Biometrika **71** (1984), 599–607.

[Smi99] S. Smith, *The Scientist and Engineer's Guide to Digital Signal Processing*, 2nd ed., California Technical Publishing, 1999.

[SN01] T. Schneider and A. Neumaier, *Algorithm 808: ARFIT - A Matlab package for the estimation of parameters and eigenmodes of multivariate autoregressive models*, ACM Transactions on Mathematical Software **27** (2001), no. 1, 58–65.

[SWH⁺06] B. Schelter, M. Winterhalder, B. Hellwig, B. Guschlbauer, C. Lücking, and J. Timmer, *Direct oder indirect? Graphical model for neural oscillators*, Journal of Physiology **99** (2006), 37–46.

[TB81]   G. Tiao and E. Box, *Modeling Multiple Time Series with Applications*, Journal of the American Statistical Association **76** (1981), no. 376, 802–816.

[THRK08]   W. Tatum, A. Husain, S. Renbadis, and P. Kaplan, *Handbook of EEG Interpretation*, Demos Medical Publishing, 2008.

[Vai08]   P. Vaidyanathan, *The Theory of Linear Prediction*, Synthesis Lectures of Signal Processing, Morgan & Claypool Publishers, 2008.

[Wol05]   *Stedman's Medical Dictionary for the Health Professions & Nursing*, 28 ed., Wolters Kluwer, 2005.